Effects of Leptin Receptor, C-C Chemokine Receptor 2 and Complement Factor 5 Deficiency on Mouse Immunometabolism

By

Dario A. Gutierrez

Dissertation

Submitted to the Faculty of the Graduate School

of Vanderbilt University in Partial Fulfillment of the

Requirements for the Degree of

DOCTOR OF PHILOSOPHY

in

Molecular Physiology and Biophysics

May, 2012

Nashville, Tennessee

Approved:

Professor Richard O'Brien

Professor Owen McGuinness

Assistant Professor Amy Major

Assistant Professor Kate Ellacott

Para mi familia, especialmente mi mama Deysi, mi mama Carmen y mi papa Mundo. Ustedes hicieron el hombre que soy ahora y este logro es el resultado tanto de mi esfuerzo como el de ustedes

And Rachel who has become my closest family member in the past four years

ACKNOWLEDGEMENTS

First, I would like to thank my mentor Alyssa Hasty. I do not think that there are words to describe the effect that she has had in my life both academically and personally. I never get tired of telling people over and over that she is the best mentor not only at Vanderbilt but in the world. She identified my strengths early in my graduate career, strengthened them, and encouraged me to use them to have a successful scientific career. Personally she became one of my great friends here in Nashville and a third mother figure. I plan to continue to have her be part of my scientific and personal life and look forward to making her proud in the years to come.

Second, I would like to thank my thesis committee members: Dr. Richard O'brien, Dr. Owen McGuinness, Dr. Amy Major and Dr. Kate Ellacott. I am certain that I have developed a close relationship with all my committee members that will last a life time. Richard has been essential for my success in graduate school and has been a great committee member chair. I am sure that his guidance and letters of recommendation played a big role in my success during my postdoctoral search process. Owen has always been my mentor if I ever had a metabolism question, and I knew that I would be getting the best advice possible. His door has always been open and just a few steps away. Amy has been instrumental in providing immunology expertise for this dissertation. She has always been open to any collaboration or experimental advice since I joined

the Hasty laboratory. Additionally, I have thoroughly enjoyed all of our joint lab meetings. Dr. Kate Ellacot always made me think outside the box and made me remain sharp with my knowledge of techniques and alternatives to my hypotheses. She has also taken the time to provide me with career advice when it came to choosing a post-doctoral laboratory and my big move to Europe.

Third, I would like to thank all my present and past lab mates. Each of them has impacted my life in so many different ways and has contributed to the best work environment that I could have hoped for.

Additionally, I would like to express my gratitude to my family and my best friend Rachel Lippert. My family has always given me incredible support since I was a child, and I know that they are very proud of all my accomplishments. Rachel Lippert has been my best friend the last 4 years and has been instrumental in all of my successes and the best traveling partner ever.

Last, I would like to acknowledge the funding for this research. Funds for this research have been obtained through the NIH grant (HL809466) and American Diabetes Association Career Development Award (1-07-CD-10) to Dr. Alyssa Hasty. I have been supported by a Molecular Endocrinology Training Grant (NIH grant number DK07563-23), a supplement to NIH grant (HL809466), and pre-doctoral NIH National Research Service Award F31DK091128.

TABLE OF CONTENTS

LIST OF FIGURES

Figure **Page**

LIST OF TABLES

Table **Page**

LIST OF ABBREVIATIONS

1) AT: adipose tissue

2) IR: insulin resistance

3) T2DM: type 2 diabetes mellitus

4) HFD: high fat diet

5) LFD: low fat diet

6) CD: chow diet

7) RT-PCR: reverse transcriptase polymerase chain reaction

8) ELISA: enzyme-linked immunosorbent assay

9) SVF: stromal vascular fraction

10) SVC: stromal vascular cell

11) INSR: insulin receptor

12) LepR: leptin receptor

13) CCR2: CC-chemokine receptor 2

14) TBO: Toluidine Blue O

15) BM: bone marrow

16) SEM: standard error of the mean

17) WT: wild-type

18) C5D: complement factor 5 deficient

19) DAPI: 4,6-diamidino-2-phenyllindole

20) GTT: glucose tolerance test

21) ITT: insulin tolerance test

22) ER: endoplasmic reticulum

23) MCP-1: monocyte chemoattractant protein 1

24) MIP-1α: macrophage inflammatory protein 1α

25) IL-#: interleukin-#

26) H & E: hematoxylin and eosin

27) ATM: adipose tissue macrophage

28) IRS: insulin receptor substrate.

CHAPTER I

INTRODUCTION

The Obesity Pandemic

Obesity is a pandemic affecting developed and developing countries. Current reports show that over 33% of adults in the United States are obese (defined as having a body mass index [BMI] ≥ 30.0 kg/m^2) (1). A Center for Disease Control publication reports that people who are obese incurred $1,429 more in medical costs per year than people of normal weight, making the nation's total medical cost of obesity $147 billion in the year 2008 alone (2). Even more concerning, the prevalence of obesity is on the rise in children and adolescents. The percentage of obese children and adolescents tripled in the United States from 1980 to 2008 (3). This is alarming because studies have shown that children and adolescents that are obese have an 80% greater likelihood of being overweight or obese as adults (4).

Obesity is a complex disease that involves both genetic and environmental factors (1), with the exception of some rare single gene mutations (5, 6). Obesity increases the risk of mortality by all causes, and people with a BMI higher than 35 have a significantly greater risk of dying from a wide range of diseases (Figure 1.1) (7). Several health problems are associated with obesity, including sleep apnea, osteoarthritis, hypertension, cancer, dyslipidemia, insulin resistance (IR), type 2 diabetes mellitus (T2DM), and cardiovascular disease (CVD) (4). In fact,

the relative risk for the latter four is over threefold higher in obese compared to lean individuals.

Insulin Resistance and Type 2 Diabetes

Obesity significantly raises the risk for developing T2DM (4). According to Center for Disease Control statistics, approximately 1 out of 9 adults in the United States are diabetic, and 1 out of 3 adults are pre-diabetic, a state also known as IR. In general, people with T2DM have a life span that is 5 to 10 years shorter than people without this disease. The most common long-term effect of T2DM is damage to the cardiovascular system, which includes macrovascular complications (atherosclerosis and amputations) and microvascular complications (retinopathy, nephropathy, and neuropathy) (8).

During the insulin resistant pre-diabetic stage, there is a reduction in insulin-stimulated glucose uptake; however, the pancreatic islets respond to this state by enhancing their mass and insulin secretion. After a certain period of IR, the expansion and increased secretory activity of β-cells fails to compensate for the increasing degree of IR, a state known as β-cell failure, which corresponds to the onset of T2DM (9). The leading mechanisms for IR and β-cell failure include oxidative stress, endoplasmic reticulum stress (ER stress), ectopic lipid storage in the muscle, liver and pancreas, lipotoxicity and glucotoxicity. These mechanisms are also associated with obesity and AT inflammation (10, 11), as described below.

Insulin Signaling

In order to understand the molecular mechanism of IR, it is imperative to first define the insulin signaling pathway. Insulin signals through its tyrosine kinase insulin receptor (INSR). After INSR autophosphorylation, this receptor catalyzes the tyrosine phosphorylation of the insulin receptor substrates (IRS-1, -2). Tyrosine phosphorylated IRS then binds to the Src-homology (SH)-2 site of the regulatory domain of phosphatidylinositol 3-kinase (PI3K). This leads to the activation of the catalytic subunit of PI3K, which catalyzes the production of the second messenger PIP3. PIP3 binds 3-phophoinositide-dependent protein kinase-1 (PDK-1), which phosphorylates and activates AKT, also known as PKB. This serine/threonine kinase mediates the activation/inactivation of many downstream mediators including FOXO1 and small GTPases. FOXO1 mediates transcriptional regulation and small GTPases lead to the translocation of the insulin sensitive glucose transporter-4 to the cell membrane, leading to transporter-mediated glucose uptake (12) (Figure 1.2).

Mechanisms of Insulin Resistance

AT inflammation during obesity is a key event that leads to the production of inflammatory mediators that have been shown to promote IR. These inflammatory factors include free fatty acids and cytokines. Signaling downstream of cytokines and free fatty acids through cytokine receptors or toll-like receptors, respectively, lead to the activation of serine kinases such as JUN N-terminal kinase (JNK) and IKB Kinase (IKK). These kinases catalyze the serine

phosphorylation of IRS's, making them less sensitive to tyrosine phosphorylation, thus, decreasing insulin signaling (13). In addition, signaling downstream of cytokines such as interleukin 6 (IL-6) can lead to the activation of suppressors of cytokine signaling (SOCS), which can block the interactions between the INSR and IRS (14) (Figure 1.2). Many of the inflammatory mediators produced in AT during obesity are discussed in detail below.

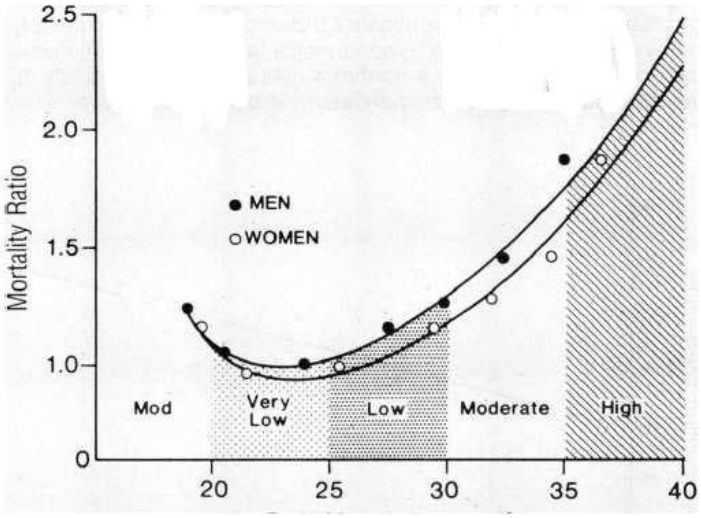

Figure 1.1 Risk of mortality in both men and women increases with increases in body mass index. Adapted from Bray *et al.* West J Med 1988; 149:429-41(7).

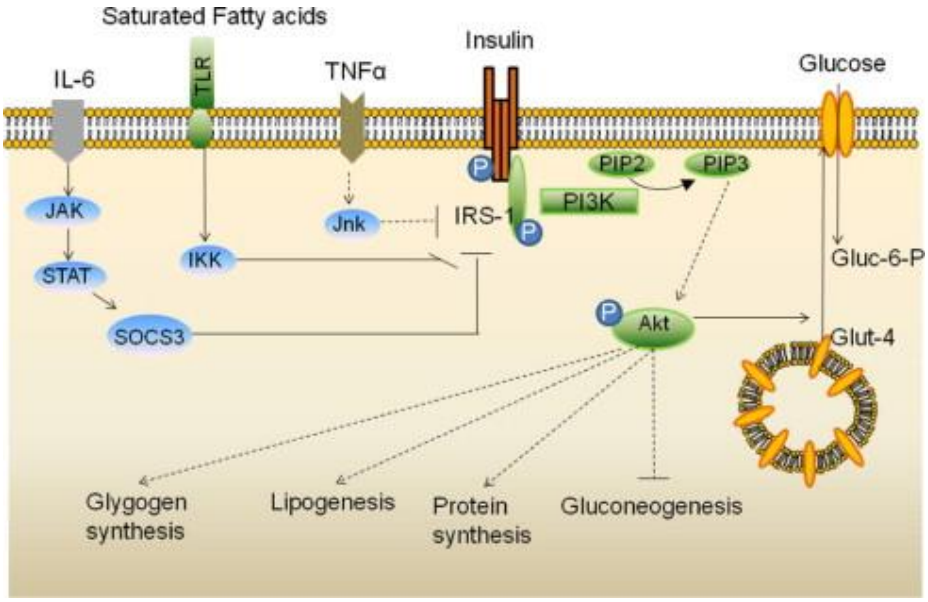

Figure 1.2 Insulin Signaling and Insulin Resistance Pathways. From Kalupahana *et al.* Mol Aspects of Medicine 33 (2012) 26-34 (15).

Adipose Tissue as an Endocrine Organ

AT consists of two fractions, the adipocyte fraction where most fat storage occurs, and the stromal vascular fraction (SVF), which contains endothelial cells, fibroblasts, and several immune cell types. All the different cell types contribute to the secretion of hormones, cytokines and adipokines that act in other tissues directly involved in systemic glucose metabolism such as the liver and muscle, and centrally in the brain. The most studied adipokine to this date is leptin (16, 17); the circulating levels of this adipokine have a strong association with obesity and its associated co-morbidities.

Additionally, the secretion of several other inflammatory AT factors is increased with obesity; these include tumor necrosis factor –α (TNF-α), resistin, IL-6, IL-1β and monocyte chemoattractant protein 1 (MCP-1). The factors secreted by AT during obesity that are relevant to this dissertation are shown in Figure 1.3. There is a strong temporal correlation between the infiltration of macrophages into AT and onset of IR in this tissue (18, 19). Additionally, macrophage infiltration into AT is correlated with AT dysfunction and subsequent onset of IR in the liver and muscle possibly due to ectopic lipid accumulation and increased inflammation.

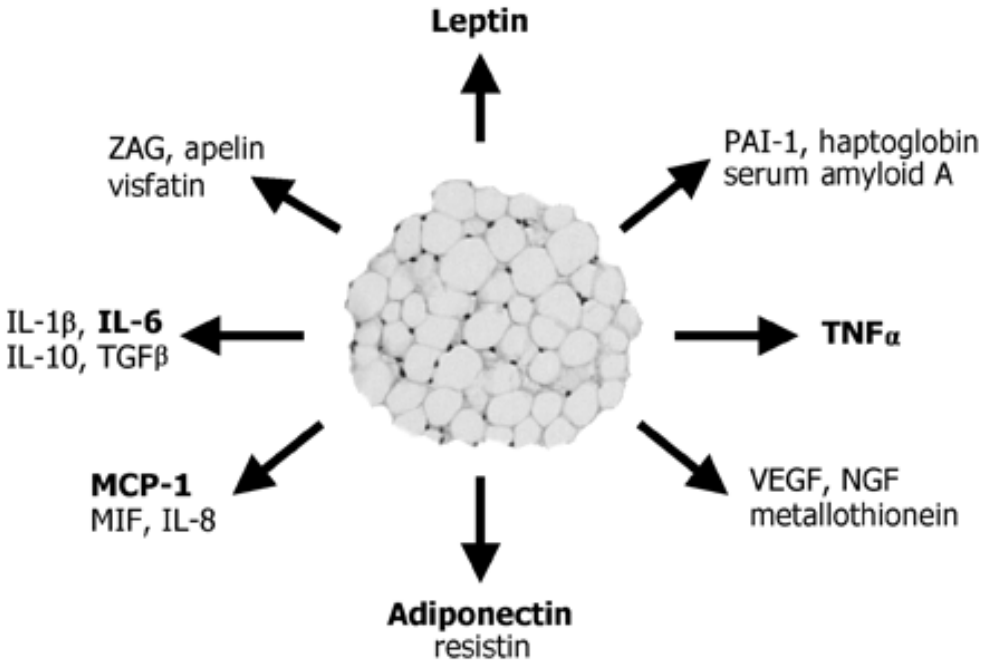

Figure 1.3 Hormones, Cytokines and Adipokines Produced in AT. From Trayhurn *et al.* (20).

Adipose Tissue Inflammation

A large part of this section on AT inflammation was published in my review for *Current Diabetes Reports* (21). Early studies on obesity showed that there was increased expression of the inflammatory mediator TNF-α in the AT of obese humans and rodents when compared to their lean counterparts (18, 22, 23). Studies published a decade later clearly demonstrated that the presence of macrophages in AT increases in obesity and that most of the production of inflammatory factors was mediated by the immune cells in the SVF, mainly the macrophages (19, 24). Since discovering a link between obesity and increased AT macrophages (ATMs), different genetic and diet-induced obese mouse models have been used to study the nature of AT inflammation. Importantly, much focus has been placed on investigating the factors that lead to the increased accumulation of ATMs in obese AT (25).

Mechanisms of macrophage recruitment to AT

Extensive research has been performed to understand the factors that initiate macrophage infiltration into AT. Many possible AT-specific cells and molecules can contribute to the macrophage infiltration of AT, including apoptosis of adipocytes due to hypoxia and increased production of chemokines.

Adipocyte apoptosis

During AT expansion, hypoxia can occur due to reduced delivery of oxygen to the hypertrophic adipocytes (26). This hypoxia can cause an increase in

inflammatory cytokine production from adipocytes and can also lead to adipocyte cell death (27). As a part of their natural role in innate immunity, macrophages can be attracted to AT to phagocytose these dead adipocytes. Cinti *et al.* (28) and Strissel *et al.* (29) used electron microscopy and immunohistochemical techniques to show that the macrophages in AT are often localized to crown-like structures surrounding adipocytes that are believed to be dead or dying. These adipocytes are thought to have increased inflammatory cytokine and chemokine secretion that may also contribute to further macrophage recruitment, as described below.

Chemokines

Several groups have reported that macrophage chemokines are upregulated in AT during obesity (30-32). Furthermore, our laboratory has shown that Western diet-fed Agouti yellow mice have a dramatic increase in MCP-1 and MIP-1α expression in AT compared with lean controls (33). Increased chemokine expression in obese AT is also found in humans. A study by Huber *et al.* (34) found an increase in the expression of MCP-1 and its receptor, CCR2, in AT of obese patients (BMI, 53.1 kg/m^2) when compared with AT of individuals with an average BMI of 25.9 kg/m^2. They also found that expression of two different chemokines, CCL3 (MIP-1α) and CCL5 (RANTES) positively correlated with fasting plasma insulin levels in obese individuals.

Evidence also exists that manipulating the chemokine system can alter ATM accumulation. Weisberg *et al.* (35) found that obese mice lacking CCR2 had

reduced macrophage recruitment, decreased proinflammatory gene expression, and improved insulin sensitivity when compared with obese wild-type mice after long periods of HFD feeding. Kanda *et al.* (30) tested three different conditions: overexpression of MCP-1 in AT, global disruption of the MCP-1 gene, and expression of a dominant-negative MCP-1 mutant. Their results showed that MCP-1 overexpression increased macrophage infiltration and promoted IR, whereas silencing of the MCP-1 gene or expression of a dominant-negative mutant reduced ATM recruitment and improved insulin sensitivity. Together, these data would suggest that chemokine expression in AT plays an important role in macrophage recruitment to AT; however, since the publications of these studies several conflicting findings have been made, including the studies described in Chapter III and IV of this dissertation (36, 37).

In addition, other groups have demonstrated that deficiency of these and other chemokines and their receptors does not affect macrophage accumulation in AT (32, 38-41). These opposing findings suggest that the role of MCP-1 and other chemokines in macrophage recruitment to AT is complex and that many other factors may contribute to this process, including macrophage turnover as described in Chapter VI of this dissertation. Alternatively, these findings suggest that active chemokine-mediated macrophage recruitment to AT may not be an important factor in their accumulation in this tissue.

When this dissertation work was initiated there was much interest in the potentially key role of leptin in macrophage recruitment to AT (21, 42). Our laboratory had shown that leptin was a potent monocyte chemoattractant *in vitro* (43). Additionally, Curat *et al.* had demonstrated that leptin was important in the diapedesis of monocytes into AT. Both of these studies led to the speculation that leptin could be an important player in macrophage recruitment to AT *in vivo*. In fact, several review papers were written highlighting the importance of leptin in this process (21, 44, 45). Chapter III of this document investigated this hypothesis *in vivo* and it is the seminal project of this dissertation.

Adipose Tissue Macrophage Phenotype

ATMs have been classified into two simplified primary phenotypes: M1 “classically activated” and M2 “alternatively activated.” *In vitro*, M1 macrophages are polarized and activated in response to stimulation by bacterial lipopolysaccharide and by interferon-γ. These cells have a “pro-inflammatory” phenotype, specialized in fighting bacterial infections. Conversely, M2 macrophages have been defined *in vitro*, as cells stimulated with the Th2 cytokines IL-4 and/or IL-13, and are characterized by the increased expression of arginase-1, IL-10 and mannose receptor. M2 macrophages have a predominantly anti-inflammatory phenotype (46).

Lumeng et al. (47, 48) were among the first to propose a differential activation of ATMs depending on the degree of adiposity. They found that ATMs

from lean and CCR2$^{-/-}$ obese mice express many genes characteristic of M2 macrophages, including Ym1, arginase 1, and IL-10. Studies by Wu *et al.* and my own work described in Chapter IV of this dissertation, have shown that the prevalence of an M2 phenotype in the macrophages of CCR2$^{-/-}$ mice is likely due to the increased number of eosinophils that secrete the T_H2 cytokine IL-4 in this tissue (49).

Conversely, diet-induced obesity in wild-type mice decreased the expression of M2 genes and increased the expression of pro-inflammatory M1 genes, such as TNF-α, IL-6, and inducible nitric oxide synthase (iNOS). Thus, diet-induced obesity leads to a shift in macrophage phenotype from an anti-inflammatory M2 type to a pro-inflammatory M1 type, and CCR2 appears to play an important role in this phenotypic switch ((50) and Chapter IV of this dissertation).

The role of M1 versus M2 ATMs in controlling inflammation and IR in AT has been delineated by recent studies demonstrating that peroxisome proliferator-activated receptor (PPAR)-γ and PPAR-δ are integral for induction of M2 macrophages. First, an increase in M2 markers is induced upon the activation of PPAR-γ with rosiglitazone (51). Second, macrophage deficiency of PPAR-γ or PPAR-δ results in a reduction of M2 macrophages in the AT, leading to an increase in IR, possibly due to the reduced presence of protective M2 macrophages (52, 53). Taken together, these results indicate that a higher degree of adiposity is positively correlated with increased numbers of M1

macrophages and a heightened state of inflammation and IR. Whereas a lower degree of adiposity is strongly correlated with an increased number of M2 macrophages and dampened inflammation leading to improved insulin sensitivity.

Other Immune Cells in AT

Since the initial discovery of the infiltration of macrophages into AT, several other immune cells have been shown to play a role in AT inflammation, including $CD8^+$ T cells, $CD4^+$ T_H1, T_H2 and T_H17 cells, $CD4^+CD25^+FOXP3^+$ regulatory T cells, NKT cells, neutrophils, mast cells, B cells and eosinophils (Reviewed in (54, 55)). All of these cell types and their roles have become important in paving the road to understanding the regulation of AT function and inflammation in lean and obese humans and rodents. A comprehensive analysis of the effects of these cells on AT function is provided below and summarized in Table 1.1 and Figure 1.4 at the end of this section.

$CD8^+$ T cells

$CD8^+$ effector T cells have been shown to infiltrate AT during obesity. These cells play an important role in promoting AT inflammation and systemic IR (56-58). Two studies have shown that infiltration of AT by $CD8^+$ T cells precedes the infiltration of macrophages, and that in fact these cells are important contributors to macrophage recruitment into AT. Ablation of $CD8^+$ T cells led to decreased levels of macrophages in AT and improved insulin sensitivity. Conversely,

adoptive transfer experiments of $CD8^+$ T cells into wild-type mice led to increased AT inflammation and worsened IR (56, 57) (Table 1.1 & Figure 1.4).

$CD4^+$ T_H1, T_H2 and T_H17 Cells

Interferon-gamma (IFN-γ) producing CD4+ T_H1 cells have been shown to be increased in AT during obesity and ablation of these cells has been shown to improve AT inflammation and decrease IR (56-59). Similarly, obesity leads to the expansion of the pools of T_H17 T cells in AT, promoting inflammation (60). In contrast, CD4+ T_H2 cells have been shown to be decreased with the progression of obesity, and adaptive transfer of these cells leads to improvements in inflammation and IR (59, 61) (Table 1.1 & Figure 1.4).

CD4+CD25+$FOXP3^+$ T_{regs}

T regulatory cells are important players in controlling autoimmunity, allergic responses, inflammation and other types of immune responses (55). They usually make up about 5-20% of the $CD4^+$ T cell population (62). Importantly, these cells have been shown to be one of the key regulators of inflammation in AT, as they have the power to control the immune response regulated by all cells of the innate and adaptive immune system (63). T_{regs} are a major source of IL-10 in lean AT. Levels of T_{regs} have been found to be higher in lean mice and humans and the percentage of these cells are decreased with weight gain (56, 59, 63). Selective ablation of AT T_{regs} leads to increased inflammation and worsened IR (61, 63) (Table 1.1 & Figure 1.4).

B cells, Mast cells and NKT cells

B cells, mast cells and NKT cells have all been shown to be increased in AT during obesity. Furthermore, their increased numbers are known to promote AT inflammation and systemic IR. Conversely, the selective ablation of these cells leads to decreased inflammation and improved insulin sensitivity (64-66) (Table 1.1 & Figure 1.4).

Eosinophils

Eosinophils are the newest player added to the milieu of immune cells in the AT. Eosinophils, similar to “M2” polarized macrophages, have traditionally been known to play an important role in host protection against parasites. However, recently these cells have been shown to play important roles in asthma, allergy and the regulation of the innate and adaptive immune system (67). Studies by Wu *et al.* have made important contributions to understanding the role of eosinophils in AT inflammation and the systemic metabolic effects, as well as their regulation with respect to HFD (49). Eosinophils have been found to support the alternative activation of macrophages in AT by producing and secreting IL4; therefore, their ablation leads to increased inflammation and worsened IR. Additionally, just like other anti-inflammatory cells in AT, their numbers decrease with increasing adiposity (49) (Table 1.1 & Figure 1.4). Chapter IV of this dissertation describes the discovery of increased numbers of eosinophils in the AT of $CCR2^{-/-}$ mice. Additionally, these data made important contributions to

understanding the regulation of eosinophils in AT during obesity (discussed in detail in Chapter IV).

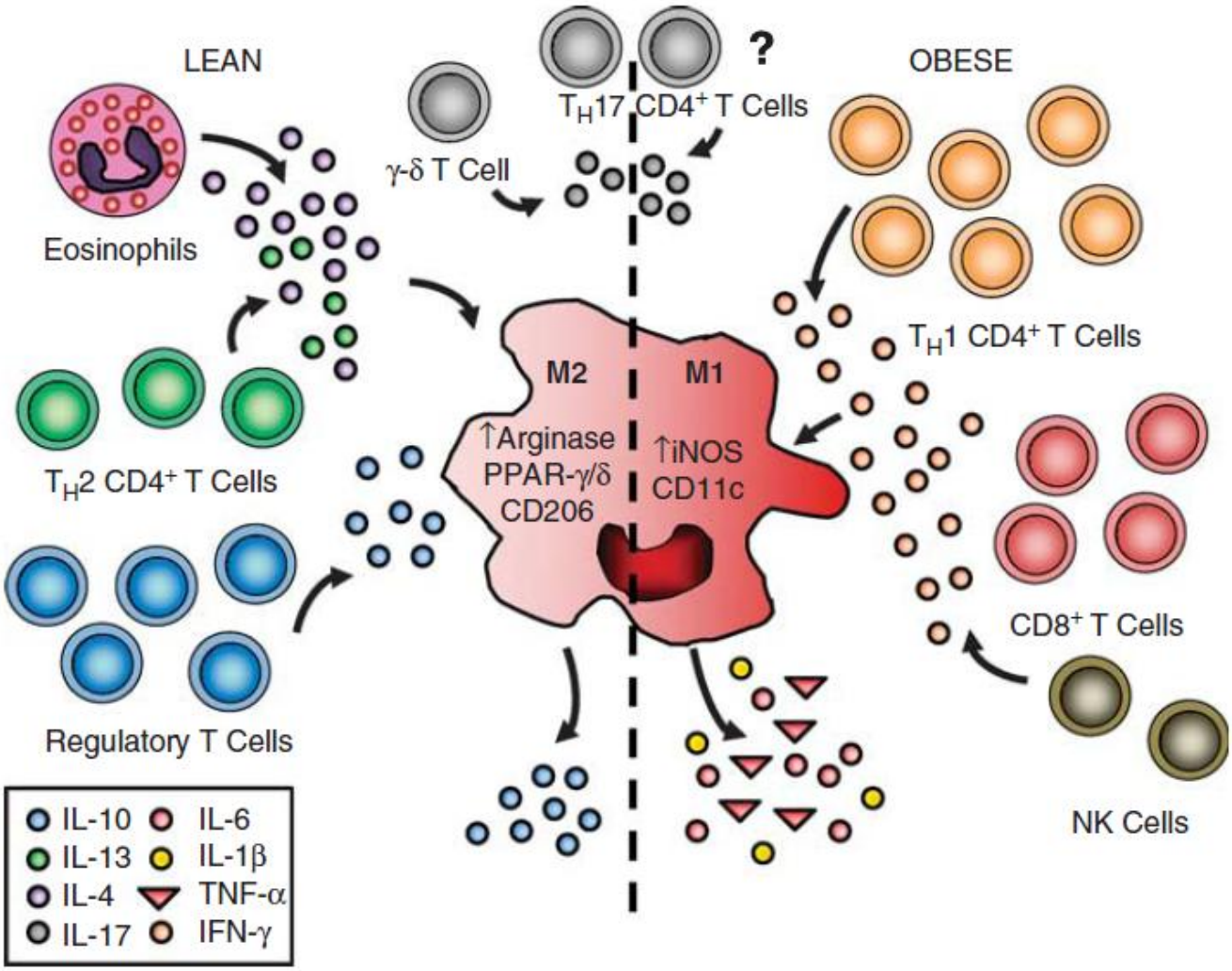

Figure 1.4 Adipose Tissue Immune Cells. From Winer *et al.* Immunology and Cell Biology 2012: 1-8 (54). Obesity leads to a macrophage phenotypic switch from M2 to M1. Additionally obesity leads to a decrease in the anti-inflammatory: eosinophils, T_H2 CD4+ T cells and regulatory T cells. In contrast, the levels of B cells, mast cells, CD8+ T cells, NK cells and T_H1 CD4+ T cells are increased with obesity.

Table 1.1 Immune cells in Adipose Tissue

Cell Type	Inflammation	Obesity Effect	Citation
"M1" Macrophages	↑	↑	(19, 24, 47, 50)
"M2" Macrophages	↓	↓	(47, 50)
$CD8^+$ T cells	↑	↑	(56, 57)
$CD4^+$ T_H1 Cells	↑	↑	(58, 59)
$CD4^+$ T_H2 Cells	↓	↓	(57-59)
$CD4^+$ T_H17 Cells	↑	↑	(60)
$CD4^+CD25^+FOXP3^+$ T_{Regs}	↓	↓	(56, 59, 63)
B Cells	↑	↑	(64)
NKT Cells	↑	↑	(66)
Mast Cells	↑	↑	(65)
Eosinophils	↓	↓	(49)

Molecules Studied in This Dissertation

This dissertation investigated the effects of deficiency of the leptin receptor, CCR2 and complement 5 on AT inflammation and Immunometabolism. The first goal of this dissertation was to test whether **leptin** was an important macrophage chemoattractant *in vitro* and *in vivo.* Chapter III provides a detailed analysis of the results obtained from this project. While performing the *in vivo* portion of project 1, **CCR2** deficient mice were used as a positive control, which led to the discovery of a previously unknown immune cell population in the AT of the mice deficient for this receptor. The results from these studies are presented in Chapter IV. In the process of performing the *in vitro* section of project 1, **complement factor 5a (C5a)** was used as a positive control for macrophage migration studies. The results obtained led to the generation of the hypothesis for project 3; the findings from this project are presented in Chapter V of this dissertation.

Leptin and Leptin Receptor

Leptin is a 16 kDa soluble protein encoded by the *Ob* gene and is expressed primarily by white AT (16, 33). In lean humans, total plasma leptin concentrations average 1.6-16 ng/ml (68). Obese individuals are known for having central leptin resistance and increased circulating levels of leptin due to the expansion of white AT (69). The circulating plasma levels of leptin for obese humans have been shown to be > 80 ng/ml (68).

Leptin acts through the long form of the leptin receptor (LepR) and plays an important role in weight regulation through its action in the hypothalamus (70). The LepR belongs to the IL-6 class I family of cytokine receptors. LepR does not contain intrinsic enzymatic activity, but instead signals through its non-covalent association with the tyrosine kinase, Janus Kinase 2 (JAK2). The activation by tyrosine phosphorylation of LepR triggers several tyrosine kinase signaling cascades that carry out multiple cellular functions (71). Mice that lack either leptin or the LepR are characterized by severe hyperphagia and morbid obesity, as well as other hormonal abnormalities (72).

Our laboratory showed that leptin is a potent monocyte chemoattractant, and that LepR signaling is required for this chemotaxis *in vitro* (43). Given that leptin is primarily secreted from AT and that its circulating levels are positively correlated with increases in macrophage infiltration (33), we hypothesized that leptin could act as a monocyte chemoattractant that regulates macrophage recruitment to AT *in vivo*. In Chapter III of this dissertation I tested this hypothesis and found that LepR deficiency does not affect macrophage recruitment to AT.

CC-Chemokine Receptor 2

CCR2 is the functional receptor for the chemokines CCL2 (MCP-1), CCL7 and CCL8 (35). CCR2 is expressed in myeloid, lymphoid and stromal cells (73). $CCR2^{-/-}$ mice were found to have an immune deficiency in Th1 responses

characterized by low levels of IFNγ production and delayed macrophage recruitment to sites of inflammation (74). Since that initial study, $CCR2^{-/-}$ mice have been shown to have reduced recruitment of monocytes in several inflammatory disease models including auto immune encephalitis (75), peritonitis (74), atherosclerosis (76) and tuberculosis (77). In Chapter IV of this dissertation, I show that CCR2 not only plays an important role in monocyte/macrophage migration to AT; its deficiency leads to the accumulation of eosinophils in this tissue, which has a large impact on systemic insulin sensitivity.

Complement Factor 5

The complement system is a vital component of innate and adaptive immune responses and is conserved across a wide range of species. Three different complement activation pathways have been discovered: the classical, alternative, and lectin binding pathways. The classical pathway is activated by antigen-antibody complexes. The alternative pathway is initiated by surface molecules containing carbohydrates or lipids. The lectin-binding pathway is activated by the binding of mannose-binding lectin protein (58) to bacterial carbohydrate structures. In the alternative pathway, circulating complement 3 is continuously hydrolyzed to C3-H_2O. C3-H_2O binds to factor B (FB) to form C3-H_2OB, which can be cleaved by factor D to form C3 convertase (C3-H_2OBb), resulting in cleavage of C3 to C3a and C3b. C3b binds factor B to form C3bB and form the alternative pathway's C5 convertase, C3b3bBb, which cleaves complement 5 into C5a and C5b (61) (Figure 1.5); the known functions of both of these clevage products are described in detail below. The role of complement in

the immune response has been recognized since the early 1900's; however its role in AT biology is just beginning to be elucidated. In the early 1990's, the discovery that a product of the C3a anaphylatoxin (C3a des-Arg or acetylation stimulating protein) allegedly induced triglyceride synthesis and accumulation in adipocytes, has led several investigators to study the role of this system in AT physiology (78-80). This prompted the discovery of the expression of other proteins involved in the alternative activation pathway in AT, including C3, Factor B and Adipsin (factorD) (78), suggesting that this pathway is active in AT. High expression of complement components has also been shown in the omental AT of obese humans (81).

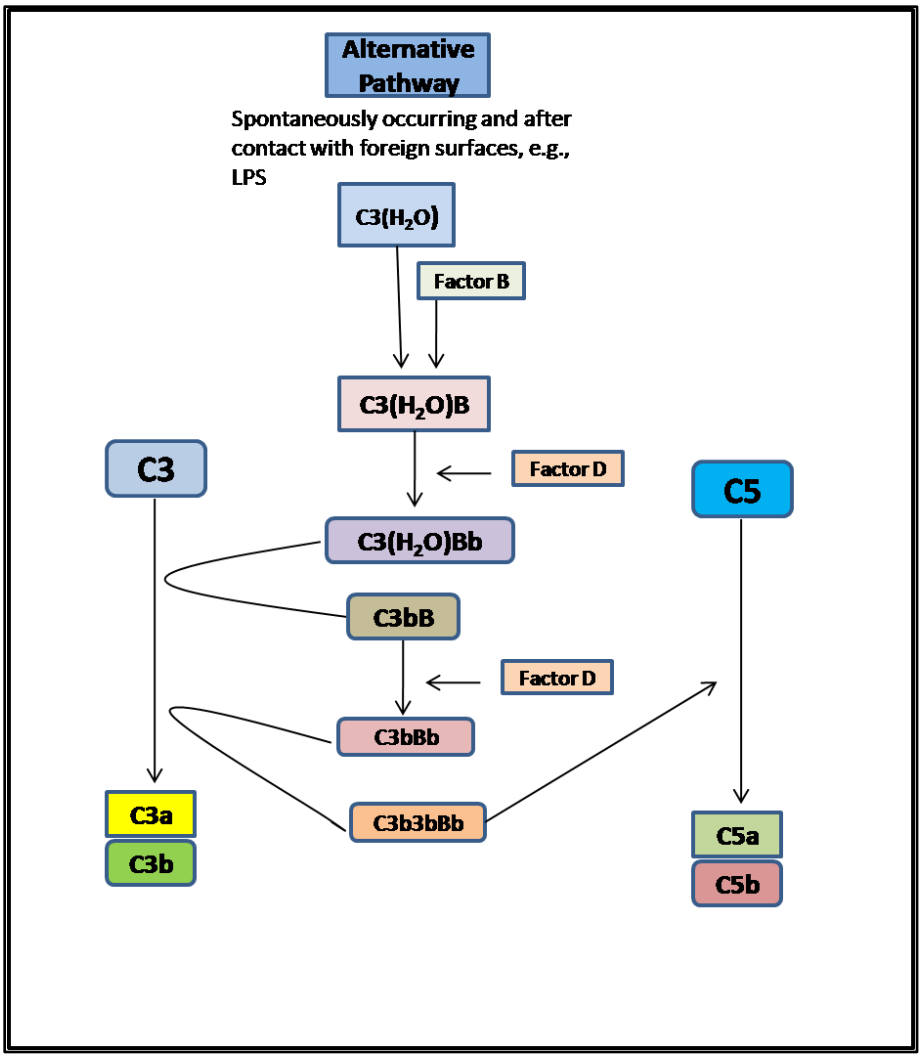

Figure 1.5 Alternative Complement Activation Pathway. Adapted from Guo, R. F. *et al. Annu. Rev, Immunol.* 2005 (61).

C5a

C5a has recently been implicated in the pathogenesis of several inflammatory diseases, including sepsis (61), rheumatoid arthritis (82), ischemia-reperfusion injury and atherosclerosis (83). C5a is a pleitropic peptide and the most potent anaphylatoxin of the complement cascade. It has many functions in the immune system: it is a strong chemoattractant for all cells of the myeloid lineage and some cells of the lymphoid lineage (84), it has been shown to be involved in the modulation of cytokine expression in different cell types (85), and it upregulates adhesion molecules in neutrophils, monocytes and epithelial cells (86).

C5b

C5b is the seminal component of the membrane attack complex (MAC or C5b-9), which also consists of C6, C7, C8 and C9. The MAC inserts into the membrane of target cells directly inducing cell lysis and necrosis (87). Sublethal amounts of C5b-9 activate immune cells and endothelium by upregulating adhesion molecules and promoting the release of reactive oxygen species, arachidonic acid metabolites and cytokines (83, 88, 89). The C5b-9 complex has been shown to play an important role in many diseases, including renal-reperfusion injury (83) and partial lipodystrophy (90).

This project was designed to study the role of complement factor 5 in AT inflammation and systemic IR. In Chapter V of this dissertation, I show that C5 deficiency leads to severe systemic IR in mice, this IR is inflammation

independent, and it is due to reduced insulin receptor message and protein expression.

Significance

Obesity is closely linked to many metabolic diseases such as IR, T2DM, and cardiovascular disease (91). In the past decade, it has been established that immune cells are recruited to AT triggering an inflammatory response characterized by abnormal cytokine production and activation of inflammatory signaling pathways that are temporally associated with IR (19, 24). Nonetheless, there is a gap in our understanding of what triggers and regulates this inflammatory response. Consequently, there are no effective treatments to ameliorate the pathogenesis of this disease. This dissertation covered several aspects involved with AT dysfunction, inflammation and IR during obesity. This work has contributed to the field of Immunometabolism by investigating LepR, CCR2 and C5 deficiency *in vivo*. The studies performed in this dissertation led to the identification of specific roles for all these molecules in either macrophage recruitment to AT, macrophage polarization, regulation of other immune cells in AT, and inflammation-independent regulation of glucose metabolism.

CHAPTER II

MATERIALS AND METHODS

Mice and Diets

All animal care and experimental procedures were performed with approval from the Institutional Animal Care and Use Committee of Vanderbilt University. All studies were performed with 8 week old male mice. In addition, in all studies mice were fed *ad libitum* and given free access to water.

Chapter III: The $LepR^{+/+}$, $LepR^{-/-}$ and $CCR2^{-/-}$ mice were purchased from Jackson Laboratories (Bar Harbor, Maine) and were on a C57BL/6 background. DKO ($LepR^{-/-}$; $CCR2^{-/-}$) donor mice were generated by crossing $CCR2^{-/-}$ with $LepR^{+/-}$ mice. Mice were kept on antibiotic water for 1 week prior to bone marrow transplant (BMT) until 4 weeks post-BMT. Mice were then placed on a 60% fat diet from Research Diets, Inc. (D12492) with a caloric density of 5.24 kcal/g; starting at 4 weeks post-BMT for a total of 6 or 12 weeks (Figure 2.1).

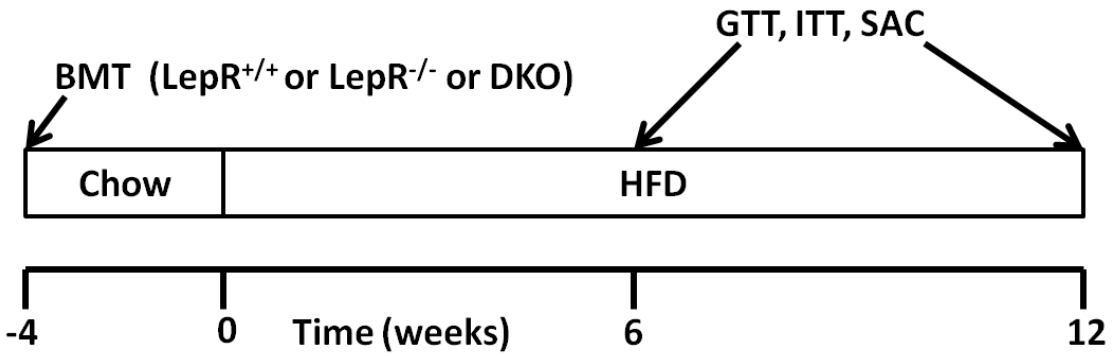

Figure 2.1 Chapter III Study Design.

C57BL/6 mice were transplanted with either $LepR^{+/+}$, $LepR^{-/-}$ or DKO ($LepR^{-/-}$; $CCR2^{-/-}$) bone marrow at 8 weeks of age. After 4 weeks mice were placed on a 60% diet (HFD) for 6 or 12 weeks (n = 10 per group). GTTs and ITTs were performed after 6 and 12 weeks. Mice were sacrificed after the 6 or 12 week period for analysis of AT macrophage infiltration and inflammation.

Chapter IV: The $CCR2^{-/-}$ and $CCR2^{+/+}$ mice used for this study were originally purchased from Jackson Laboratories, are on a C57BL/6 background, and have been propagated in our animal facility. In the BMT study mice were kept on antibiotic water from 1 week prior to BMT through 4 weeks post-BMT. BMT and non-BMT mice were then placed on a 60% fat diet from (Research Diets, Inc., New Brunswick, NJ) for varying periods of time.

Chapter V: C57BL/6, B10.D2-*Hc*^{0} *H2*^{d} *H2-T18*^{c}/oSnJ (C5 deficient and referred to as C5D in this dissertation), C57BL/10SnJ (WT controls $H2^{b}$ haplotype), and B10.D2-*Hc*^{1}*H2*^{d} *H2-T18*^{c}/oSnJ (WT controls $H2^{d}$ haplotype) mice were purchased from The Jackson Laboratory (Bar Harbor, Maine). Eight-week-old C57BL/6 mice were placed on a 10%, 45% or 60% fat diet (Research Diets, Inc., New

Brunswick, NJ) for 16 weeks. C5D and WT mice were placed on either a 10% or 60% fat diet for 12 weeks.

Bone Marrow Transplantation

Chapter III: Bone marrow cells were collected from $LepR^{+/+}$, $LepR^{-/-}$ and DKO ($LepR^{-/-}$; $CCR2^{-/-}$) donor mice and were injected into the retro-orbital venous plexus of lethally irradiated recipient WT mice. Complete reconstitution of the desired bone marrow was confirmed by PCR of splenic cells using primers specific for the *db* allele (forward primer: 5'-AGA ACG GAC ACT CTT TGA AGT CTC-3'; reverse WT: 5'-AAC CAT AGT TTA GGT TTG TTT C-3'; reverse db: 5'-CAA TTC AGT GTA AAC CAT AGT TTA GGT TTG TTT A-3'). This generates a band of 129 base-pairs for the WT allele and 141 base-pairs for the *db* allele (Figure 2.2)

Chapter IV: Bone marrow cells were collected from $CCR2^{+/+}$ or $CCR2^{-/-}$ donor mice and were injected into the retro-orbital venous plexus of lethally irradiated recipient $CCR2^{+/+}$ mice as previously described (92). The efficiency of bone marrow reconstitution was confirmed by PCR using DNA isolated from the spleens of the recipient mice using primers specific for the *Neo* cassette insertion (forward primer: 5'-CTT GGG TGG AGA GGC TAT TC-3'; reverse primer: AGG 5'-TGA GAT GAC AGG AGA TC-3') in the $CCR2^{-/-}$ deficient mice (Figure 2.3).

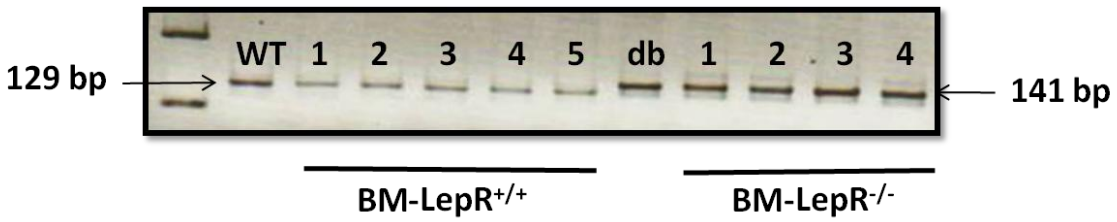

Figure 2.2 Genotyping of splenocytes from BM-LepR$^{+/+}$ and BM-LepR$^{-/-}$ mice.

Confirmation of the reconstitution of the desired bone marrow was performed by isolating DNA from splenocytes of the recipient mice at the end of the study. The 129 base-pair band corresponds to the amplification of the wild-type allele. The 141 base-pair band corresponds to the amplification of the *db* allele. Representative blot, WT: wild-type control DNA; db: db/db control DNA.

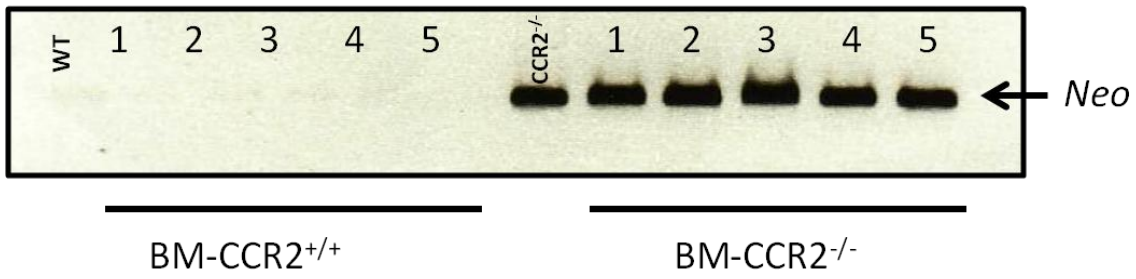

Figure 2.3 Genotyping of splenocytes from BM-CCR2$^{+/+}$ and BM-CCR2$^{-/-}$ mice.

The confirmation of the reconstitution of the desired bone marrow was performed by isolating DNA from splenocytes of the recipient mice at the end of the study. Band corresponds to *Neo* cassette amplification. CCR2$^{-/-}$ mice have a targeted insertion of the *Neo* gene. Representative blot; WT: wild-type (CCR2$^{+/+}$) control DNA; CCR2$^{-/-}$ control DNA.

***Body weight, Body Composition and Food Intake*.**

In all studies, body weight and food intake were measured weekly for the duration of the study. Total lean, fat, and free fluid mass were measured by nuclear magnetic resonance (NMR) using a Bruker Minispec (Woodlands Texas) in the Vanderbilt Mouse Metabolic Phenotyping Center (MMPC) at baseline, 6 and 12 weeks after placement on either a LFD or HFD.

Insulin and Glucose Tolerance Tests.

Mice were fasted for 5 h and baseline glucose levels were measured using a LifeScan One Touch Ultra glucometer (Johnson & Johnson, Northridge, CA) via the tail vein.

Chapter III & IV: Mice were injected intraperitoneally with either 0.4 U (6 weeks of HFD) and 0.5 U (12 weeks of HFD) insulin per Kg of lean mass; or 2 g (6 weeks of HFD) and 1 g (12 weeks of HFD) dextrose per kg of lean mass. Glucose levels were then assessed at 15, 30, 45, 60, 90 and 150 min post-injection.

Chapter V: Mice were then injected with 1g of glucose per kg of lean body mass. Glucose levels were assessed at 15, 30, 45, 60, 90, 120 and 150 min after glucose injection.

Plasma Collection and Measurements

In all studies mice were fasted for 5 h and bled from the retro-orbital venous plexus using heparinized collection tubes. Plasma was separated by centrifugation and stored at -80 ºC. Plasma insulin levels were measured using an ELISA kit from Millipore, Inc (Billerica, MA). Leptin levels were assessed at the Vanderbilt University Hormone Core.

Real-time RT-PCR

In all studies, RNA extraction was performed with an RNeasy kit (Qiagen, Valencia, CA) according to the manufacturer's instructions. The iScript cDNA synthesis kit (BioRad, Hercules, CA) was used for reverse transcriptase reactions. Real-time RT-PCR experiments were performed using an iQ5 thermal cycler. The reactions were carried out using IQ Supermix (BioRad) and FAM conjugated Assay-on-Demand (Applied Biosystems, Foster City, California) primer/probe sets normalized to *18S* or *Gapdh*.

Chapter III: The following genes were assessed: *18S* (4352930E), *Emr1* (Mm00802530_m1), *Arg1* (Mm01190441_g1), *Cd68* (Mm00839636_g1), *Tnf* (Mm00443258_m1), *Nos2* (Mm00440502_m1), *Cd163* (Mm0118511), *Mgl1* (Mm00546125_g1), *Mgl2* (Mm00460844_m1), *Il6* (Mm00446190_m1), and *Il1b* (Mm9999061_mH). Data were presented as expression relative to the BM-LepR$^{+/+}$ controls at each respective time point.

Chapter IV: The following genes were assessed: *Gapdh* (Mm99999915_g1), *Emr1* (Mm00802530_m1), *Arg1* (Mm01190441_g1), *Cd68* (Mm00839636_g1), *Tnf* (Mm00443258_m1), *Nos2* (Mm00440502_m1), *Itgam* (Mm00434455_m1), *Itgax* (Mm00498698_m1), *Mpo* (Mm00447886_m1), *Cxcl1* (Mm04207460), *Cxcl2* (Mm00436450_m1), *Il8rb* (Mm00438258_m1), *Ccl2* (Mm004411242), *Ccl3* (Mm00441258), *Cd163* (Mm0118511), *Mgl1* (Mm00546125_g1), *Mgl2* (Mm00460844_m1), *Il10* (Mm00439614_m1), *Csf3* (Mm00438354_m1), *Ccl5* (Mm01302428_m1), *Il6* (Mm00446190_m1), *Mmp9* (Mm00442991_m1), *Il1b* (Mm9999061_mH), *Csf1* (Mm00432686_,1) *and Csf1r* (Mm01266652_m1), *Il5* (Mm00439646_m1). Data were presented as expression relative to the BM-CCR2$^{+/+}$ or CCR2$^{+/+}$ controls at each respective time point.

Chapter V: The following genes were assessed: *Gapdh* (Mm99999915_g1), *Emr1* (Mm00802530_m1), *Arg1* (Mm01190441_g1), *Tnf* (Mm00443258_m1), *Nos2* (Mm00440502_m1), *Ccl2* (Mm004411242), *Il10* (Mm00439614_m1), *Il1b* (Mm9999061_mH), *C3*ε (Mm00599683_m1), *Insr* (Mm01211875_m1), *Irs1* (Mm01278327_m1), *Hc* (Mm00439275_m1), *C3* (Mm01232779_m1), *C6* (Mm00489521_m1), C*fb* (Mm04333909_m1), *Irs2* (Mm03028438_m1), *Igfbp3* (Mm0051515156 _m1), *Igf1* (Mm00439560_m1), *Igf1r* (Mm00802831_m1), *G6pc* (Mm00839363_m1), *Pck1* (Mm01247058_m1), *Gck* (Mm00439129_m1), *Acacb* (Mm01204578_m1), *Acox1* (Mm00443579_m1). Data were presented as expression relative to the WT 10% fat diet controls at each respective time point.

In all studies, the data were analyzed using the Pfaffl method (93) and presented as relative expression.

Histology

Epididymal AT was harvested from mice, weighed, and a portion was fixed overnight in 10% (v/v) formalin, transferred to 70% (v/v) ethanol, and paraffin embedded.

Chapter III & IV: Tissue was cut into 7μm sections and stained with 0.1% (w/v) toluidine blue O solution (TBO) (Newcomer Supply, Middleton, Wisconsin) as previously described (33).

Chapter IV: $CD11b^{lo}F4/80^{lo}$ and $CD11b^{hi}F4/80^{hi}$ sorted cells were cytospun onto glass slides and stained with hematoxylin and eosin (H&E).

Chapter V: Liver and pancreata samples were collected and frozen in OCT solution, and stored at -80° C. AT samples were fixed in 10% formalin overnight and paraffin embedded. Seven micrometer sections of liver and AT were cut using a cryostat and microtome, respectively. H&E staining was performed as previously described. The pancreata were cut and stained by the Vanderbilt Histology and Immunohistochemistry Core.

In all studies, images were captured using an Olympus BX51 microscope (Tokyo, Japan).

Peritoneal Macrophage Collection

Chapter IV: Mice were injected intraperitoneally with 3 ml of 3% thioglycollate to induce sterile inflammation. After 3 days, the peritoneal cells were collected by lavage with 10 ml of PBS with 0.5% BSA, washed and counted before used for flow cytometric analysis.

Stromal Vascular Fraction (SVF) Separation

Chapter II & IV: Epididymal AT pads were excised and minced in 3 ml of 0.5% (w/v) BSA in PBS and placed on ice. Subsequently, 3 ml of 2 mg/ml collagenase was added to the minced fat and incubated at 37°C for 20 min with shaking. The cell suspension was filtered through a 100-μm filter and then spun at 300 *g* for 10 min to separate floating adipocytes from the SVF pellet. The SVF pellet was then resuspended in 3 ml of ACK lysis buffer and incubated at RT for 5 min to lyse red blood cell, followed by dilution in 10 ml of PBS. The cells were then washed twice with PBS.

Flow Cytometry

For all studies, stromal vascular, bone marrow, peritoneal and white blood cells were first incubated with Fc block for 5 min at RT, followed by incubation for 20 min at 4 ºC with fluorophore-conjugated antibodies. All conjugated antibodies were used at a 1:100 dilution unless otherwise indicated.

Chapter III: F4/80-APC (eBioscience), Ly6C-FITC (BD Biosciences), Ly6G-PE (1:200) (BD Biosciences), CD11b-APC-Cy7 (BD Bioscience).

Chapter IV: F4/80-APC (eBioscience), Ly6C-FITC (BD Biosciences), CD11b-APC-Cy7 (BD Biosciences), CD11c-PeCy7 (BD Biosciences) and Ly6G-PE (1:200) (BD Bioscience), Siglec-F PE (BD Biosciences), IgG2aκ PE isotype control (BD Biosciences), CCR3 PE (1:10) (R&D Biosystems).

Chapter V: CD19 APC, CD11b APC-Cy7, Ly6G PE, Ly6C FITC, TCRβ APC, CD4 A700 (1:50), and CD8 Pe-Cy7 (BD Biosciences, Franklin Lakes, NJ).

In all studies, 4,6-diamidino-2-phenyllindole (DAPI) (0.2 μg/ml) was added to each sample as a viability stain 10 min before flow cytometry analysis. Cells were processed using a 5 Laser LSRII machine in the Vanderbilt Flow Cytometry Core. All data were analyzed using FlowJo software version 7.6.1.

AT Lysates

Chapter IV & V: The epididymal fat pads were collected at the end of the study, flash frozen and kept at -80 ºC until utilized. Approximately 50 mg of AT were homogenized in 250 μl of lysis buffer (20 mM Tris HCl, 150 mM NaCl, 1 mM EDTA, 1 mM EGTA, 0.5% NP-40, 2.5 mM sodium pyrophosphate, 1 mM sodium orthovanadate and 1 mM PMSF). The protein concentration in the lysate was quantified using the Lowry method (94) with samples diluted in 0.1N NaOH, 0.1% SDS.

IFNγ and IL4 ELISA

IFNγ and IL4 ELISAs were performed on AT lysates using BD Biosciences OptEIA ELISA kits according to the manufacturer's instructions; 50 µg of total protein per well was used.

Cell sorting

Cells were collected and stained as described above for the flow cytometry section. The cells were sorted using a FACS Aria I sorter at the Vanderbilt Flow Cytometry Core. The $CD11b^{lo}F4/80^{lo}$ and $CD11b^{hi}F4/80^{hi}$ populations were isolated for RNA expression and histological analysis.

Western Blot Analysis

Protein samples were collected by homogenizing c.a. 50 mg of liver, gastroctnemius muscle and/or AT in 750 µl, 500 µl and 250 µl of lysis buffer, respectively. Protein concentration was measured using the Lowry method. Western blot analysis was conducted as previously described (95).

Glycosidase Assay

Chapter V: A glycosidase assay was performed according to the manufacturer's instructions (New England Biolabs Inc., Ipswich, MA). Briefly, aliquots of 20 µg of

protein extracts from livers of WT and C5D mice were incubated with 1 µl of 10X glycoprotein denaturing buffer. The protein was then denatured by heating reaction at 100 ºC for 10 min. Subsequently, 2 µl of 10X G7 reaction buffer, 2µl of N-glycosidase F enzyme and H_2O up to a total volume of 20 µl were added. The reaction was incubated at 37 ºC for 1 h prior to performing Western blot analysis as previously described.

Statistical Analysis

GraphPad Prism 4.0 software was used for all statistical analyses. Data was analyzed using two-tailed unpaired t-tests to determine differences between two groups with 1 variable; one way ANOVA when more than two measurements were compared and two way ANOVA to compare measurements with two different variables (i.e. GTTs, Diet versus Genotype Effects). Outliers were excluded from the data for each individual parameter if outside the range of the mean ±2SD, and $P \leq 0.05$ was considered significant.

CHAPTER III

HEMATOPOIETIC LEPTIN RECEPTOR DEFICIENCY DOES NOT AFFECT MACROPHAGE ACCUMULATION IN ADIPOSE TISSUE OR SYSTEMIC INSULIN RESISTANCE

(Adapted from Gutierrez *et al. J. Endocrinol.* 2012; **212**, 343-351)

INTRODUCTION

Accumulation of inflammatory macrophages in AT during obesity has been shown to correlate with AT inflammation and subsequent IR (19, 24). In addition, the polarization of the infiltrating macrophages is known to be an important factor in the inflammatory state of AT (47, 93, 96). Thus, understanding the mechanism(s) of macrophage recruitment to AT could lead to the development of therapies against IR and T2DM. Adipokines, which are hormones secreted from AT, could act as chemoattractants and contribute to macrophage recruitment into AT. The adipokine leptin has emerged as a strong candidate given its known role in immune regulation (97). Leptin is a 16 kDa soluble protein encoded by the *Ob* gene and is expressed primarily by white AT, such that circulating levels of leptin are positively correlated with levels of adiposity and AT macrophage accumulation (16, 33).

Leptin acts primarily through the long form of the leptin receptor (LepR) and plays an important role in weight regulation through its action in the hypothalamus (70). Mice that lack either leptin or the LepR are characterized by

severe hyperphagia and morbid obesity, as well as other hormonal abnormalities (72).

Previous studies have shown that leptin promotes neutrophil and monocyte chemotaxis; as well as the activation of monocytes/macrophages leading to secretion of pro-inflammatory cytokines and the upregulation of inducible nitric oxide synthase (iNOS) (43, 98, 99). We have shown that leptin is a potent monocyte chemoattractant *in vitro* and that this chemotaxis is LepR-dependent (43). In addition, we have shown that expression of *Emr1* (the gene for F4/80) in AT, which is an indicator of macrophage infiltration, is positively correlated with circulating levels of leptin during obesity (Figure 3.1) ($r^2 = 0.6973$; $P<0.0001$) (33). Given that leptin is primarily secreted from AT and that its circulating levels are positively correlated with increases in macrophage infiltration, we hypothesized that leptin could act as a monocyte chemoattractant that regulates macrophage recruitment to AT during obesity.

We designed a bone marrow transplant study to determine if hematopoietic deficiency of the functional long-form of the LepR would lead to decreases in macrophage recruitment to AT during HFD feeding. We transplanted bone marrow from $LepR^{-/-}$ and DKO ($LepR^{-/-}$; $CCR2^{-/-}$) mice into wild type (WT) recipients and placed these mice on a HFD for 6 or 12 weeks. These time points were chosen because of previously shown kinetics of macrophage recruitment to AT (56). We examined macrophage infiltration to AT by flow cytometry, histology and real-time RT-PCR. Our data provides evidence that

hematopoietic deficiency of the LepR does not affect macrophage recruitment to AT or insulin sensitivity during HFD-induced obesity.

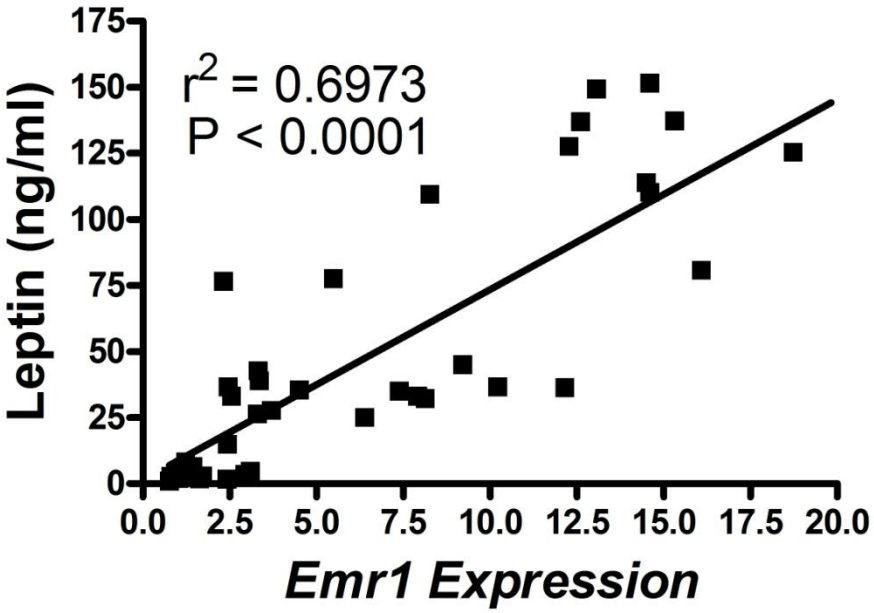

Figure 3.1 *Emr1* expression in AT is positively correlated to plasma leptin levels.

Data from Coenen *et al.* (33) previously published by our group was re-analyzed and plotted as *Emr1* expression (arbitrary units) versus plasma leptin levels (ng/ml). (n = 41 mice).

RESULTS

C57BL/6 mice were transplanted with either $LepR^{+/+}$, $LepR^{-/-}$ or DKO ($LepR^{-/-}$; $CCR2^{-/-}$) bone marrow at 8 weeks of age. Four weeks after transplant mice were placed on a 60% diet (HFD) for 6 or 12 weeks (Figure 2.1). The BM-$LepR^{+/+}$ controls in this study were also used as negative controls for the study performed simultaneously and presented in Chapter IV of this dissertation. Recipients of $CCR2^{-/-}$ marrow (BM-$CCR2^{-/-}$) were included in Chapter IV as well. There were no significant differences in any parameter studied between the BM-$CCR2^{-/-}$ and BM-DKO ($LepR^{-/-}$; $CCR2^{-/-}$) mice. Thus, only the BM-DKO mice are shown in this chapter.

Metabolic Profile

There were no differences in body weight (Figure 3.2A) or food intake (data not shown) between the groups at any point during the study. Likewise, there were no differences in adiposity among genotypes at any time, although all groups increased in adiposity after 6 and 12 weeks of HFD feeding (Figure 3.2B). Epididymal fat pad weight (Figure 3.2C) and circulating leptin levels (Figure 3.2D) were not different among genotypes at any time point. In accordance with the NMR adiposity data, epididymal AT weight and leptin levels were generally elevated between the 6 and 12 week time points for each group (Figure 3.2C-D). Glucose and insulin tolerance tests were performed after 6 (Figure 3.3A & C) and 12 (Figure 3.3B & D) weeks of HFD feeding. All groups responded similarly to the intraperitoneal glucose and insulin challenges after both periods of HFD feeding.

In general, fasting insulin levels were increased for all groups between the baseline measurements and 12 weeks of HFD feeding (Figure 3.3E). Fasting glucose levels were significantly increased ($P<0.001$) in all groups between the pre-HFD and both the 6 and 12 week time points (Figure 3.3F).

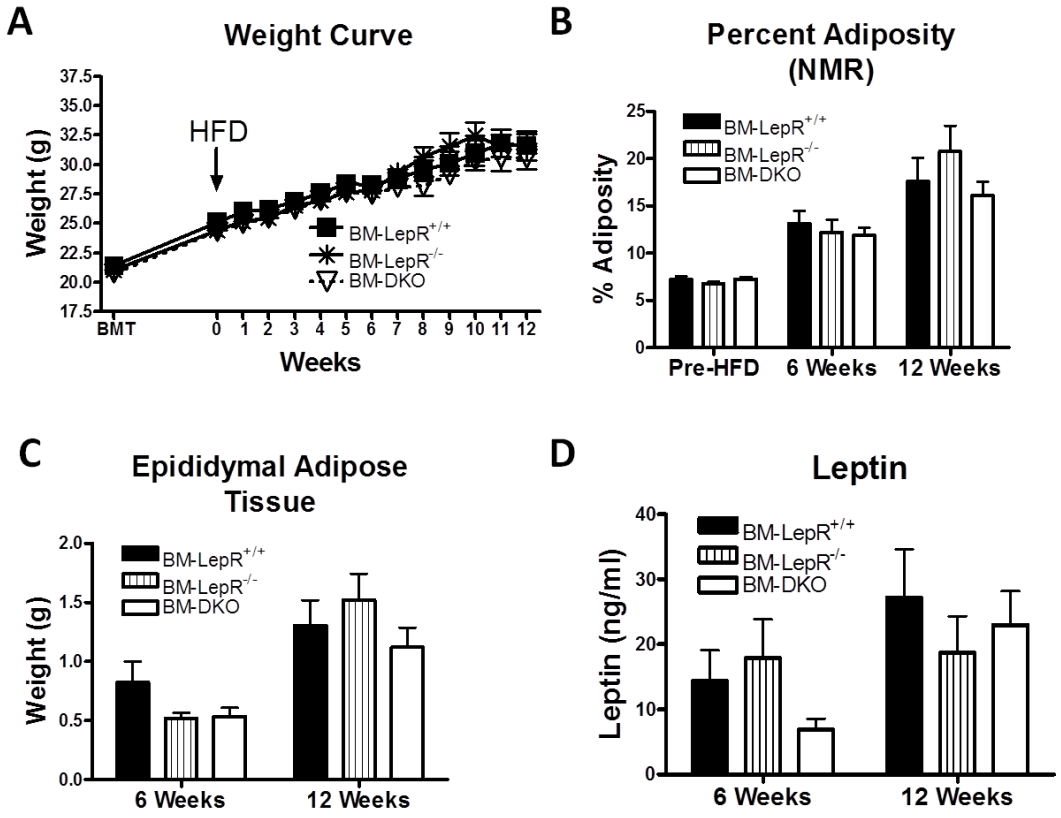

Figure 3.2 Metabolic Phenotyping.

A) Average weekly body weight of BM-LepR$^{+/+}$, BM-LepR$^{-/-}$ and BM-DKO mice pre- and post-HFD. B) Percent adiposity (total fat tissue divided by total body weight) determined by nuclear magnetic resonance. C) Epididymal AT weight. D) Circulating plasma leptin levels assessed by ELISA. Data are presented as mean ± SEM. For pre-HFD up to 6 weeks post-HFD, n=20 mice per group. For 12 weeks post-HFD, n=9-10 mice per group.

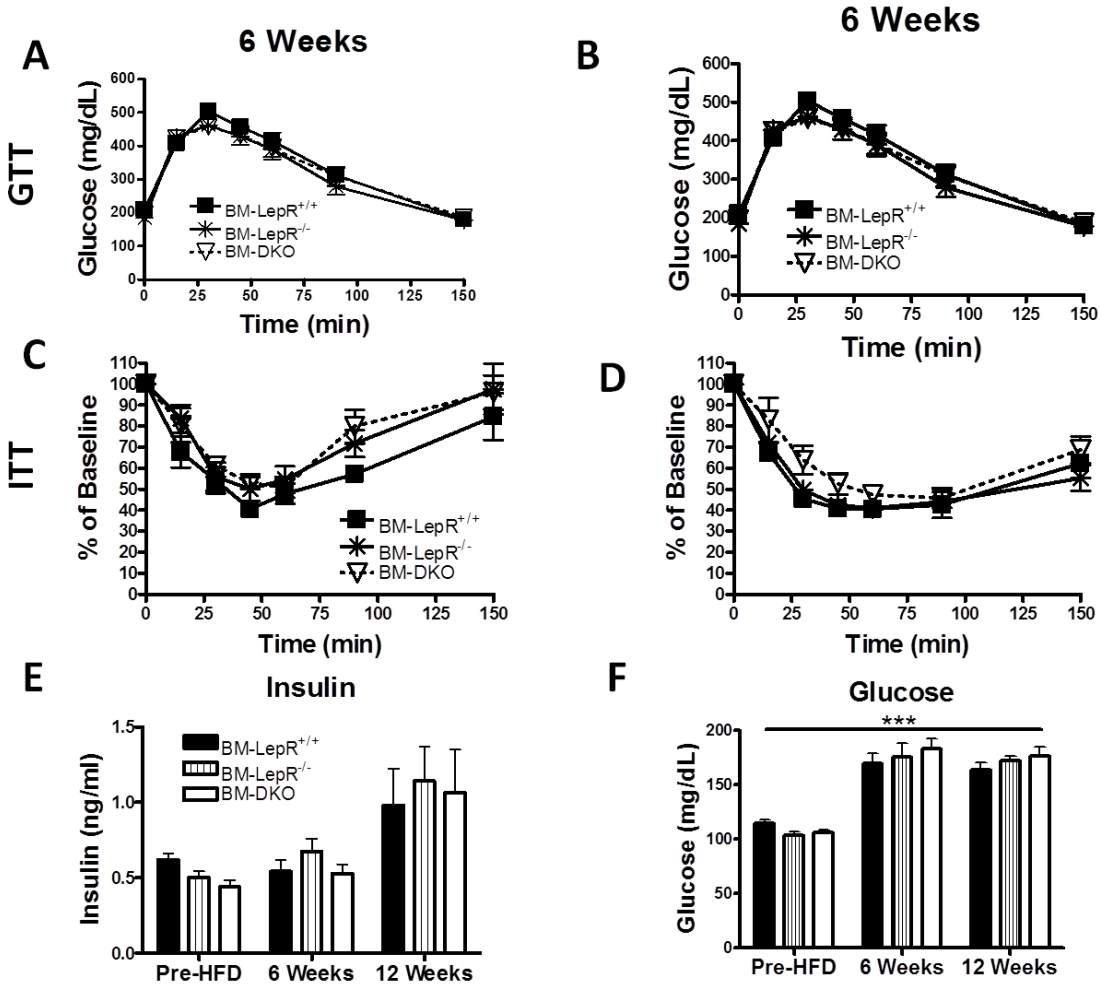

Figure 3.3 All groups have similar glucose and insulin tolerance. Glucose tolerance tests were performed by injecting mice intraperitoneally with dextrose at a concentration of 2g (6 weeks) or 1g (12 weeks) per kilogram of lean mass after a 5 h morning fast. Glucose tolerance curves for all groups after A) 6 weeks and B) 12 weeks of HFD feeding. Insulin tolerance tests were performed by injecting mice intraperitoneally with 0.4 U (6 weeks) or 0.5 U (12 weeks) human insulin per kilogram of lean mass after a 5 h morning fast. Insulin tolerance curves for all groups after C) 6 weeks and D) 12 weeks of HFD feeding. E) Fasting insulin levels were measured by ELISA at the pre-HFD, 6 and 12 weeks time points. F) Fasting glucose levels were assessed at the pre-HFD, 6 and 12 weeks time points. Data are presented as mean ± SEM. For GTT and ITT data, n=9-10 mice per group for 6 week data and n=5 mice per group for 12 week data. For fasting insulin and glucose data, n= 8-10 per group.

*** P<0.001 for all groups between Pre-HFD and 6 or 12 weeks

Blood Monocytes

Two phenotypic and functional subsets of mature blood monocytes have been described: Ly6C^{lo} and Ly6C^{hi} (100). The Ly6C^{hi} circulating monocyte subset is thought to be the source of recruited inflammatory macrophages to inflamed tissues. The circulating levels of blood monocytes and neutrophils were assessed by flow cytometry after 12 weeks of HFD feeding by first gating on all live CD11b^{+} cells. The BM-LepR$^{-/-}$ mice had a ~40% ($P<0.05$) reduction in circulating Ly6C^{hi} monocytes, and BM-DKO mice a ~90% ($P<0.001$) reduction, when compared to the BM-LepR$^{+/+}$ controls (Figure 3.4A-D). No differences were observed in the Ly6C^{lo} monocyte subset or the percentage of circulating neutrophils between groups (Figure 3.4E-F).

Macrophage Accumulation in AT

The accumulation of macrophages in AT after 6 and 12 weeks of HFD feeding was evaluated by histology, real-time RT-PCR and flow cytometry. TBO staining showed that there were no overt differences in overall immune infiltration between groups after either period of HFD feeding (Figure 3.5A-F). Real-time RT-PCR gene expression analysis in total AT for the macrophage markers *Emr1* and *Cd68* showed no differences between groups after 6 (Figure 3.5G) or 12 weeks (Figure 3.5H) of HFD feeding.

The stromal vascular fraction (SVF) was separated from the adipocytes of the epididymal AT by collagenase digestion. Macrophages from the SVF were

quantified by flow cytometry using an antibody against F4/80. The representative histograms illustrate the percentage of live F4/80^{hi} cells in the SVF after 6 (Figure 3.6A-C) and 12 weeks (Figure 3.6D-F) of HFD feeding. Quantification of the percentage of F4/80^{hi} cells in the SVF showed a significant decrease ($P<0.05$) in the BM-DKO group when compared to the BM-LepR$^{+/+}$ and BM-LepR$^{-/-}$ groups after 6 weeks of HFD feeding (Figure 6G). There were no differences in the percentage of F4/80^{hi} cells in the AT of any group after 12 weeks of HFD feeding (Figure 6H). The BM-DKO mice had an increase in a discrete F4/80^{lo} myeloid population (Figure 3.6C, arrow) which is due to the deficiency in hematopoietic CCR2, as I have reported in Chapter IV of this dissertation (37).

AT inflammatory State

The inflammatory state of total AT was determined by assessing the gene expression of several pro- and anti-inflammatory markers by real-time RT-PCR. Analysis of the expression of the inflammatory markers *Tnf* and *Nos2* showed no differences in these genes among groups after 6 weeks on the HFD (Figure 3.7A). There was a significant decrease ($P<0.001$) in *Nos2* expression in the BM-DKO group when compared to the BM-LepR$^{+/+}$ and BM-LepR$^{-/-}$ groups at the 12 week time point (Figure 3.7B). Additionally, assessment of the anti-inflammatory "M2" markers *Arg1*, *Mgl1* and *Mgl2* showed that there was a significant increase ($P<0.05$) in *Arg* 1 expression in the BM-DKO mice in comparison to the BM-LepR$^{+/+}$ mice after 6 weeks of HFD feeding (Figure 3.7A). *Arg1*, *Mgl1* and *Mgl2*

were all significantly increased ($P<0.05$) in the BM-DKO group in comparison to the BM-LepR$^{+/+}$ and/or BM-LepR$^{-/-}$ groups after 12 weeks of HFD (Figure 3.7B). Bone marrow LepR deficiency alone did not impact anti-inflammatory gene expression in AT.

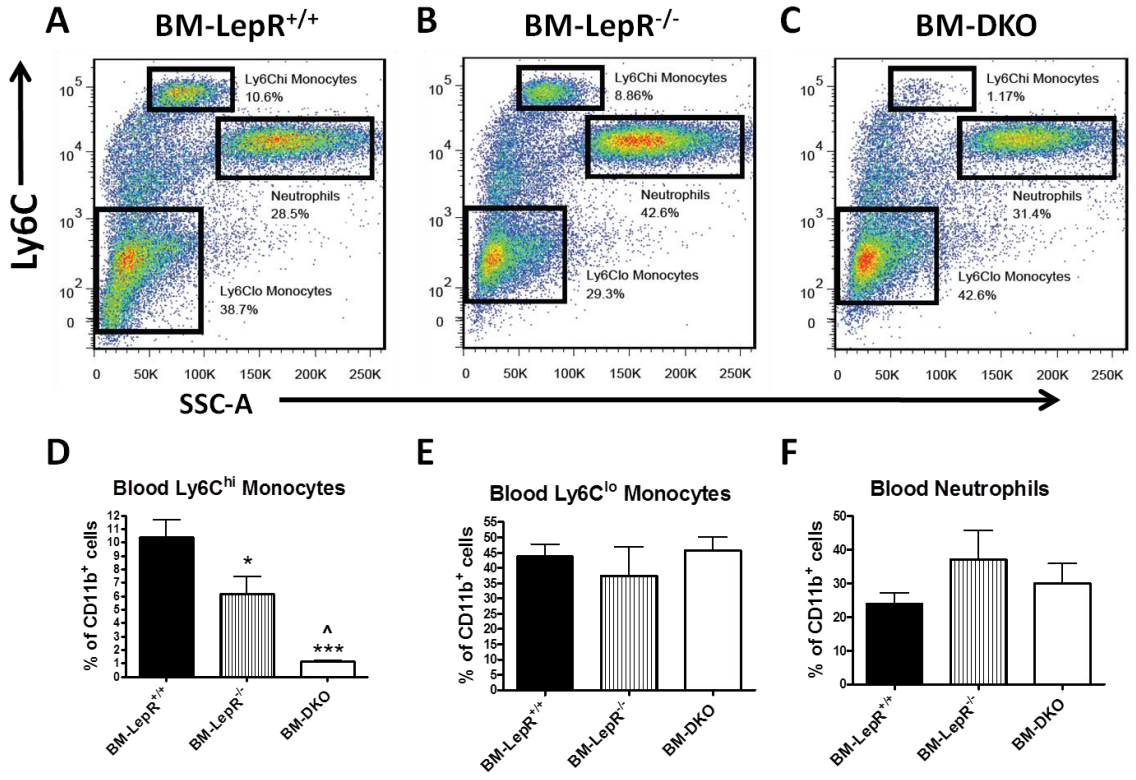

Figure 3.4 BM-LepR$^{-/-}$ mice have decreased circulating inflammatory monocytes.

Blood cells were isolated from 12 week HFD fed recipient mice and analyzed by flow cytometry. Representative plots showing expression of Ly6C after gating on all CD11b+ live cells. A) BM-LepR$^{+/+}$ B) BM-LepR$^{-/-}$ C) BM-DKO. Quantification of the percentage of D) CD11b^{+}Ly6C^{hi}, E) CD11b^{+}Ly6C^{lo} and CD11b^{+}Ly6G^{hi} cells in all groups (mean ± SEM; n = 4-5 mice per group).

* P<0.05 between BM-LepR$^{+/+}$ and BM-LepR$^{-/-}$ mice

*** P<0.001 between BM-LepR$^{+/+}$ and BM-DKO mice

^ P<0.05 between BM-LepR$^{-/-}$ and BM-DKO mice.

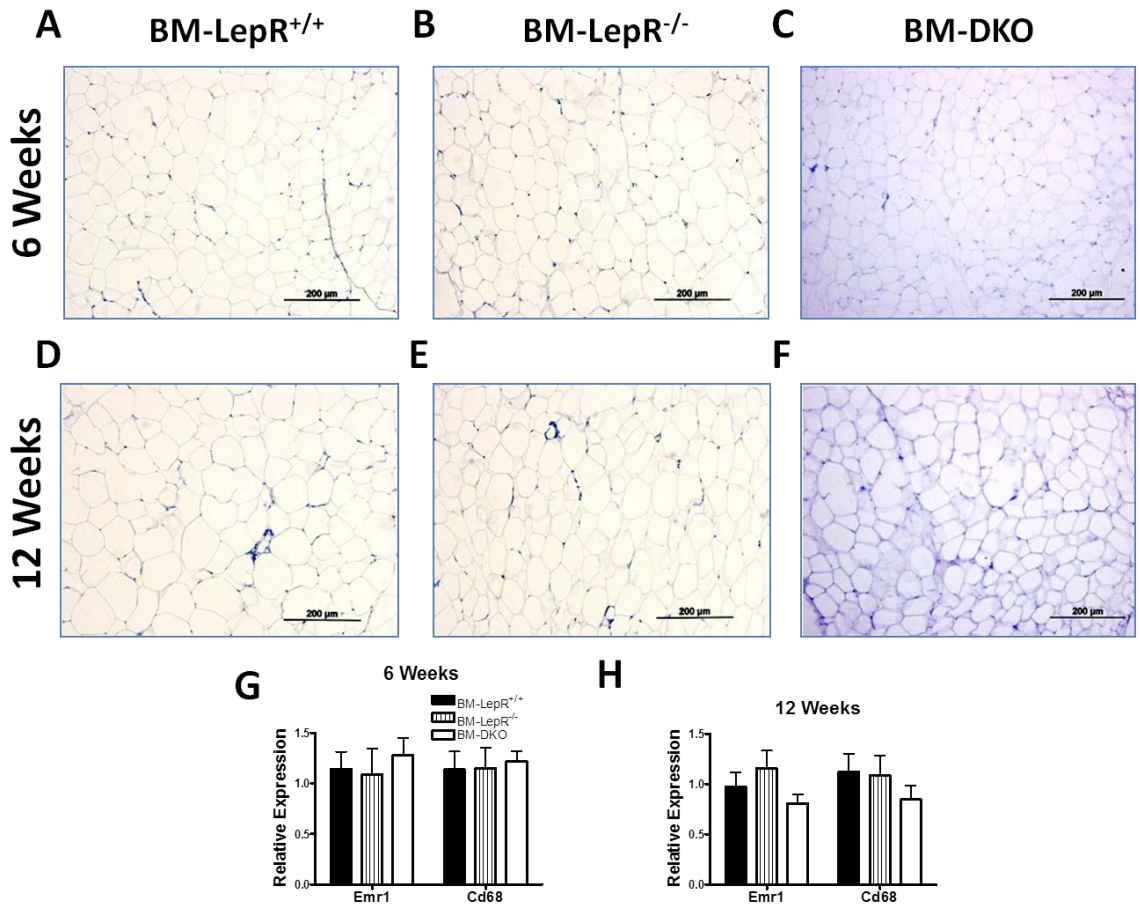

Figure 3.5 Histology and real-time RT-PCR analysis of F4/80^{+} cells in AT.

Representative AT TBO images of A) BM-LepR$^{+/+}$, B) BM-LepR$^{-/-}$ and C) BM-DKO mice after 6 weeks of HFD feeding. Representative AT TBO images of D) BM-LepR$^{+/+}$, E) BM-LepR$^{-/-}$ and F) BM-DKO mice after 12 weeks of HFD feeding. Real-time RT-PCR gene expression analysis of *Emr1* (F4/80 and *Cd68* in total AT after G) 6 and H) 12 weeks of HFD feeding (mean ± SEM; n = 10 mice per group).

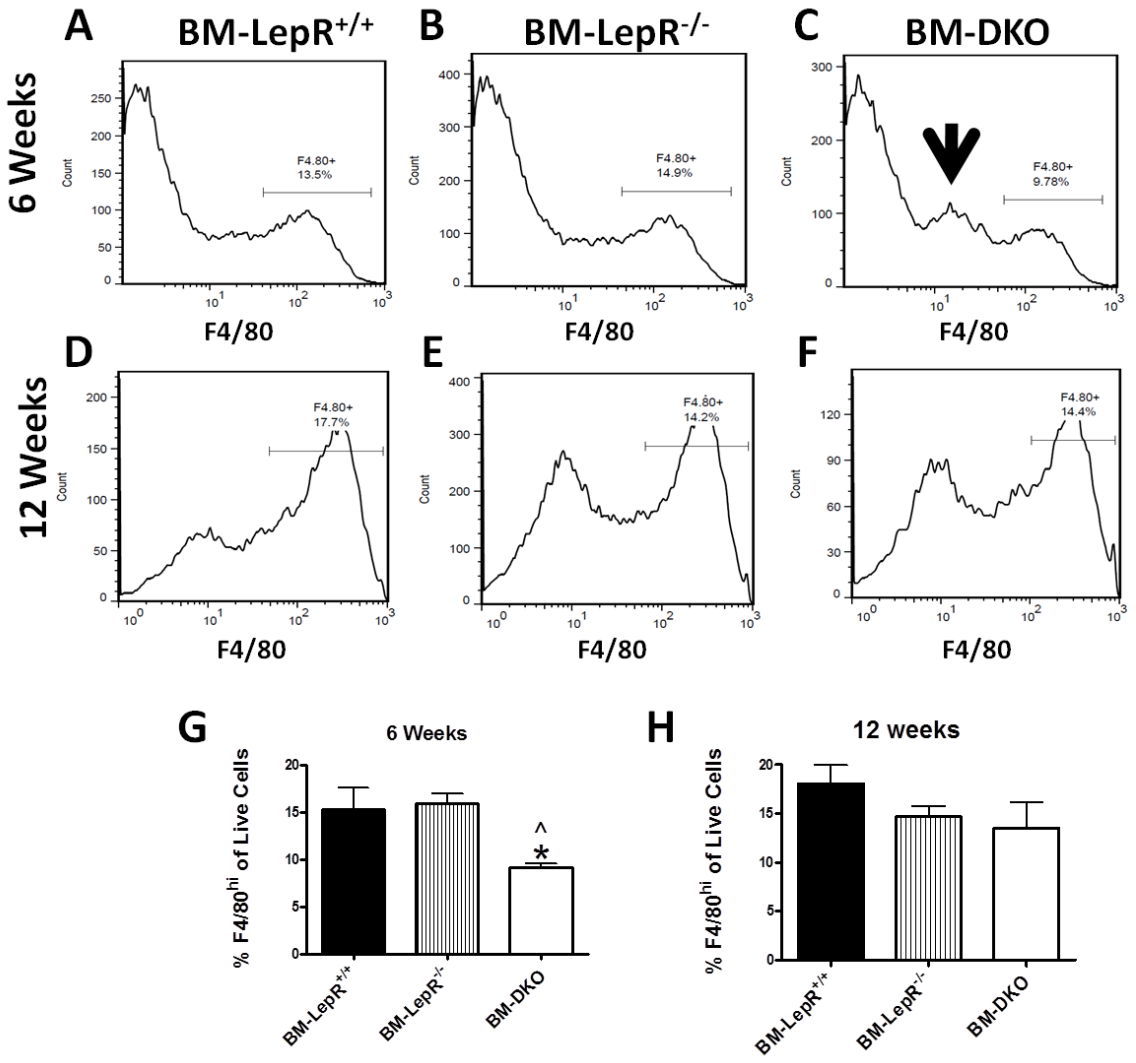

Figure 3.6 Flow cytometry analysis of stromal vascular cells

Stromal vascular cells were isolated and the percentage of live F4/80^{+} cells was quantified. Representative histograms of F4/80^{hi} cells for A) BM-LepR$^{+/+}$ B) BM-LepR$^{-/-}$ and C) BM-DKO mice after 6 weeks of HFD feeding; D) BM-LepR$^{+/+}$, E) BM-LepR$^{-/-}$ and F) BM-DKO mice after 12 weeks of HFD feeding. G-H) Quantification of the percentage of F4/80^{hi} live cells in the SVF of all groups after 6 or 12 weeks of HFD feeding. Data presented as mean ± SEM. (n=4-5). Arrow indicates F4/80^{lo} cells found in BM-DKO mice.

* P<0.05 between BM-LepR$^{+/+}$ and BM-DKO mice

^ P<0.05 between BM-LepR$^{-/-}$ and BM-DKO mice

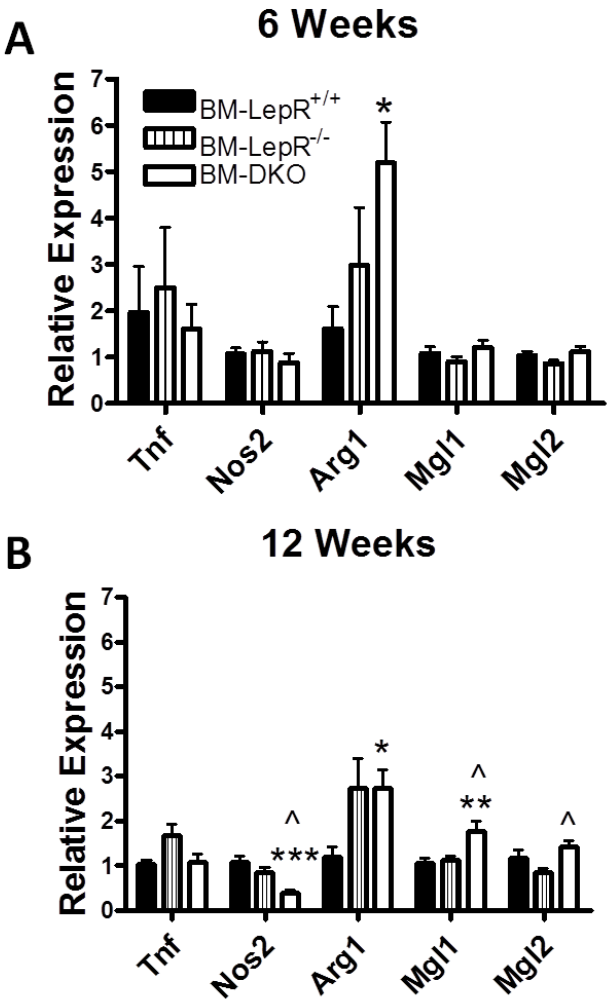

Figure 3.7 Pro- and anti-inflammatory gene expression.

Real-time RT-PCR gene expression analysis of pro- and anti-inflammatory markers was performed on RNA isolated from total AT. Expression of *Tnf*, *Nos2*, *Arg1*, *Mgl1* and *Mgl2* in all groups after A) 6 weeks and B) 12 weeks of HFD feeding (mean ± SEM; n = 10 mice per group).

* P<0.05 between BM-LepR$^{+/+}$ and BM-DKO mice

** P<0.01 between BM-LepR$^{+/+}$ and BM-DKO mice

*** P<0.001 between BM-LepR$^{+/+}$ and BM-DKO mice

^ P<0.05 between BM-LepR$^{-/-}$ and BM-DKO mice

DISCUSSION

Inflammatory macrophage infiltration into AT during obesity has been shown to be temporally correlated with local and systemic inflammation and IR (19, 24, 47, 50). Several genetic models that either disrupt macrophage recruitment to AT (30, 35, 38, 52) or promote an AT macrophage switch towards an “M2” or anti-inflammatory phenotype (52, 101, 102) have been explored. Despite the great progress made in this field in the past decade, methods to actively decrease macrophage recruitment to AT or diminish their inflammatory impact on this tissue are poorly understood.

We and others have shown that the adipokine leptin plays an important role in macrophage chemotaxis *in vitro* directly via its ability to act as a macrophage chemoattractant (43) or indirectly through the upregulation of adhesion molecules on endothelial cells (103). Additionally, leptin has been shown to play a role in eosinophil (104) and neutrophil (105, 106) chemotaxis. These findings have led to the speculation that leptin, which is mainly produced in AT and has potent monocyte chemotactic activity, could be an important mediator of monocyte/macrophage chemotaxis to AT, where this adipokine is mainly produced (21, 42, 44, 45, 107-110). This is of particular interest during the initial stages of inflammatory macrophage accumulation in AT when recruitment is positively correlated with adiposity and circulating leptin levels (Figure 3.1) (33). However, this hypothesis had not been tested *in* vivo. In this study we assessed whether hematopoietic LepR deficiency led to a disruption in

macrophage recruitment to AT during obesity with the hypothesis that BM-LepR$^{-/-}$ chimeras would have reduced macrophage accumulation and improvements in glucose and insulin tolerance. Given that compensation by other cytokines was possible, we generated BM-DKO chimeras that have a hematopoietic deficiency in both LepR and CCR2.

Our results showed that hematopoietic LepR deficiency led to a significant decrease in the percentage circulating Ly6C^{hi} monocytes (Figure 3.4B & D). A similar but more dramatic phenotype has been observed in mice with CCR2 deficiency (37, 111), in which Ly6C^{hi} monocytes fail to egress from the bone marrow. In fact, the BM-DKO mice showed an identical phenotype to that of the BM-CCR2$^{-/-}$ mice in Chapter IV of this document (Figure 3.4C-D), indicating that having both CCR2 and LepR deficiency does not confer an additive or synergistic effect on the decreases in circulating inflammatory monocyte levels. The mechanism responsible for the reduction of Ly6C^{hi} monocytes in BM-LepR$^{-/-}$ mice is unknown; however, because the levels of circulating monocytes in the BM-DKO mice are identical to those of the BM-CCR2$^{-/-}$ mice, it is likely that the BM-LepR$^{-/-}$ mutation is not affecting inflammatory monocyte egress but instead their proliferation and/or differentiation in the bone marrow. This hypothesis remains to be tested.

The main end point of this study was to determine if the deficiency of LepR led to a reduction in macrophage recruitment to AT. Previous studies have shown that the initial process of inflammatory macrophage accumulation in AT occurs between 6 and 12 weeks of HFD feeding (56, 112); thus, we used these

time points to assess macrophage accumulation using multiple approaches. Our histology (Figure 3.5A-F), gene expression (Figure 3.5G-H) and flow cytometry (Figure 3.6) data showed no protective effect of LepR deficiency on macrophage accumulation in AT after 6 or 12 weeks of HFD feeding. There was a significant decrease ($P<0.05$) in the percentage of $F4/80^{hi}$ macrophages in the BM-DKO group after 6 weeks of HFD feeding (Figure 3.6G); however, this can be accounted for by the hematopoietic CCR2 deficiency, which leads to a decrease in $F4/80^{hi}$ cells and the accumulation of $F4/80^{lo}$ cells as I show in Chapter IV of this dissertation. In addition, no changes in glucose or insulin tolerance were observed between the three groups (Figure 3A-D) despite the fact that all mice became hyperglycemic and hyperinsulinemic in response to the HFD feeding (Figure 3E-F). Thus, we can conclude that hematopoietic LepR deficiency alone or in combination with hematopoietic CCR2 deficiency does not affect inflammatory macrophage recruitment to AT or insulin sensitivity after 6 or 12 weeks of HFD feeding.

The negative results are not a consequence of the inability of these mice to have increased macrophage infiltration, become insulin resistant or glucose intolerant during HFD feeding. We performed an additional study in which we show that $LepR^{+/+}$ mice fed a HFD have increased macrophage infiltration ($P<0.01$), glucose intolerance ($P<0.001$) and IR ($P<0.01$) when compared to $LepR^{+/+}$ mice fed a chow diet (Figure 3.8). Thus, within the limits of the sensitivity of our assays, hematopoietic LepR deficiency does not affect macrophage recruitment or insulin sensitivity during obesity.

Similar negative results have been obtained by our group and others when assessing inflammatory macrophage recruitment to AT after deletion of a single chemokine or chemokine receptor (38-41, 113). Accordingly, the current study provides evidence for the redundancy of chemokines and chemokine receptors in the innate immune system. Despite the elimination of two receptors that mediate the function of four different chemokines (leptin, CCL2, CCL7 and CCL8) that are upregulated in the AT during obesity, macrophage infiltration to AT is not disrupted. This redundancy in the chemokine system reflects the importance of leukocyte chemotaxis in normal immune system function and makes it "robust" to naturally occurring mutations (114).

Previously published studies suggest that *in vitro* leptin treatment leads to the activation of monocyte/macrophages and have shown a dose-dependent induction of inflammatory mediators such as IL-6 and TNF-α (98). Macrophages are primarily responsible for AT inflammation during obesity (18, 19, 22); thus, we tested whether hematopoietic LepR deficiency led to changes in the inflammatory state of total AT by real-time RT-PCR. Our results showed no differences in pro- or anti-inflammatory marker gene expression between BM-LepR$^{+/+}$ and BM-LepR$^{-/-}$ mice after any period of HFD feeding (Figure 3.7A-B). Significant differences were observed in the inflammatory gene expression of BM-DKO mice; however, these are similar to the changes in gene expression found in the BM-CCR2$^{-/-}$ mice (Chapter IV). As with macrophage chemotaxis, the effects of leptin on inflammatory gene expression that have been found *in vitro*

are likely compensated *in vivo* by other cytokines found in the AT environment during obesity.

In conclusion, our study provides evidence that despite the potency of leptin as a monocyte/macrophage chemoattractant (43), hematopoietic deficiency of its functional receptor does not affect macrophage accumulation in AT. Our current finding that hematopoietic LepR deficiency decreases the number of circulating Ly6C^{hi} monocyte levels should be further studied as it could provide a novel role for leptin in hematopoiesis and/or myeloid cell migration. Our results do not rule out the possibility that leptin can affect macrophage infiltration into AT through the upregulation of adhesion molecules in the endothelial cells of the SVF, as has been previously suggested by Curat *et al.* (103).

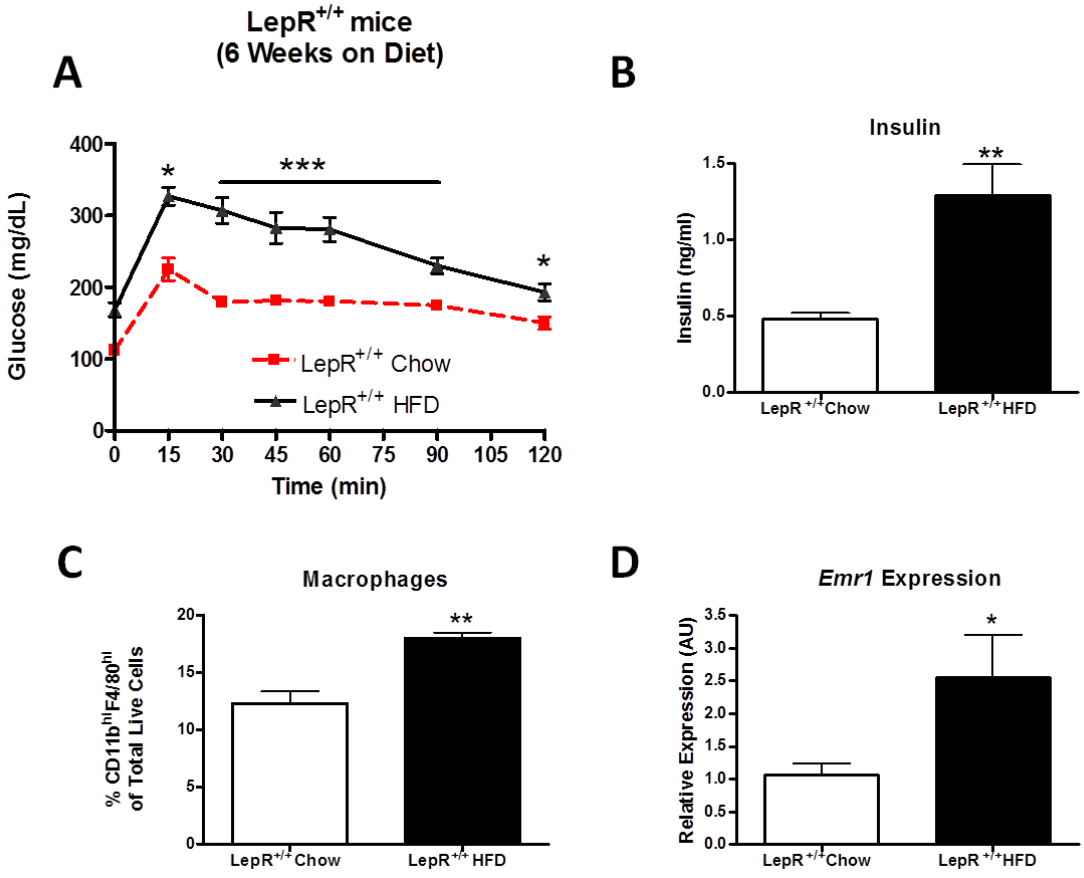

Figure 3.8 LepR$^{+/+}$ mice fed a HFD have increased macrophage infiltration and become glucose intolerant and insulin resistant.

LepR$^{+/+}$ mice were placed on either a chow or high fat diet for 6 weeks. A) Glucose tolerance test, using 1 g of dextrose per kg of lean mass after a 5 hour fast. B) Fasting insulin levels. C) Flow cytometric percentage of CD11b^{hi}F4/80^{hi} cells from all live stromal vascular cells. D) *Emr1* expression in total epididymal AT. Data presented as mean ± SEM (n = 5 per group).

*P<0.05 between diets

**P<0.01 between diets

***P<0.001 between diets

CHAPTER IV

ABERRANT ACCUMULATION OF EOSINOPHILS IN THE ADIPOSE TISSUE OF CCR2 DEFICIENT MICE PROMOTES ALTERNATIVE MACROPHAGE ACTIVATION AND DELAYS IMPROVEMENTS IN INSULIN SENSITIVITY

(Adapted from: Gutierrez *et al. Diabetes* 60: 2820-2829, 2011 and Gutierrez *et al*. Manuscript in Preparation, 2012)

INTRODUCTION

Obesity is an independent risk factor for type 2 diabetes, cardiovascular disease, fatty liver disease, atherosclerosis, and several cancers. Chronic AT inflammation is a cardinal feature of obesity that leads to other health complications such as IR (9, 115, 116). Recruitment of macrophages is an important factor in AT inflammation (24) and has been shown to be temporally associated with IR (50, 117).

CCR2 regulates monocyte chemotaxis through direct interactions with its ligands, monocyte chemoattractant proteins-1 and -3 (MCP-1, and -3) (118). $CCR2^{-/-}$ mice have an immune deficiency in Th1 responses characterized by low levels of IFNγ production and delayed macrophage recruitment to sites of inflammation (74). Studies by Tsou *et al.* found that the $CCR2^{-/-}$ mice have a

defect in the egress of inflammatory monocytes from the bone marrow, resulting in a dramatic reduction of these cells in the circulation (111, 119).

The role of CCR2 and MCP-1 in macrophage recruitment to AT and the liver, and their contribution to IR has been evaluated by various groups (30, 35, 39, 120-122). One study showed that obese $CCR2^{-/-}$ mice have a modest decrease in macrophage marker expression in AT and ATM number after 24 weeks on a 60% fat diet when compared to wild-type controls (35). Additionally, a bone marrow transplant (BMT) study showed that hematopoietic CCR2 deficiency leads to decreased F4/80 expression in the AT of obese ob/ob mice (120). These experiments indicate that substantial obesity (i.e. long periods of HFD feeding and/or a genetically morbidly obese model) is required before differences in macrophage recruitment and improvements in insulin sensitivity are observed in $CCR2^{-/-}$ mice, despite their striking reduction in circulating inflammatory monocytes. We set out to investigate the mechanism responsible for the delayed protection in AT inflammation and macrophage recruitment in global and hematopoietic models of CCR2 deficiency ($CCR2^{-/-}$ and BM-$CCR2^{-/-}$, respectively).

In this study we analyzed the changes in myeloid populations that take place in the AT of $CCR2^{-/-}$ and BM-$CCR2^{-/-}$ mice and contrasted them to changes in $CCR2^{+/+}$ and BM-$CCR2^{+/+}$ controls. Our data showed that global and hematopoietic CCR2 deficiency leads to the accumulation of Siglec-$F^{+}CD11b^{lo}F4/80^{lo}$ eosinophils during early periods of HFD feeding. The AT eosinophilia is associated with increased expression of anti-inflammatory

markers in total AT. Surprisingly no improvements in systemic metabolism are observed until after the eosinophils are no longer found in AT after extended periods of HFD feeding.

RESULTS

Part I: (Gutierrez *et al. Diabetes* 60: 2820-2829, 2011)

Weight and Adiposity.

Four weeks post-BMT, BM-CCR2$^{-/-}$ and BM-CCR2$^{+/+}$ mice were placed on a HFD for 6, 12 or 20 weeks. The recipient groups had similar weight gain, adiposity, and epididymal fat pad weight throughout the study (Figure 4.1). In addition, there were no differences in food intake between groups (data not shown).

Immunophenotype of Circulating Monocytes.

BM-CCR2$^{-/-}$ mice fed a HFD for 12 weeks had a 10-fold reduction in the percentage of circulating Ly6C^{hi} monocytes ($P<0.001$; Figure 4.2A - C) when compared to the BM-CCR2$^{+/+}$ mice. The percentage of Ly6C^{lo} cells was not affected in the BM-CCR2$^{-/-}$ mice (Figure 4.2D). CCR2$^{-/-}$ mice fed a HFD for 12 weeks presented a similar reduction in Ly6C^{hi} monocytes when compared to CCR2$^{+/+}$ controls (Figure 4.3A & D). We also analyzed the expression of CD11c and F4/80 in blood monocytes of CCR2$^{+/+}$ and CCR2$^{-/-}$ mice fed either a HFD or chow diet (CD) for 12 weeks (Figures 4.3 & 4.4). Interestingly, the ly6C^{lo} population from HFD-fed CCR2$^{-/-}$ mice had increased CD11c expression (rightward shift of blue line in Figure 4.3E) compared to the Ly6C^{lo} cells from HFD-fed CCR2$^{+/+}$ mice (Figure 4.4B). In the general interest of assessing the

effects of HFD feeding on the imunophenotype of circulating monocytes we investigated monocytes isolated from HFD and CD-fed $CCR2^{+/+}$ mice. As previously shown (123, 124), a comparison of HFD-fed and CD-fed $CCR2^{+/+}$ mice showed a small increase in expression of CD11c in $Ly6C^{hi}$ monocytes while the expression of CD11c in $Ly6C^{lo}$ monocytes remained unaffected during HFD feeding (Figure 4.4B & F).

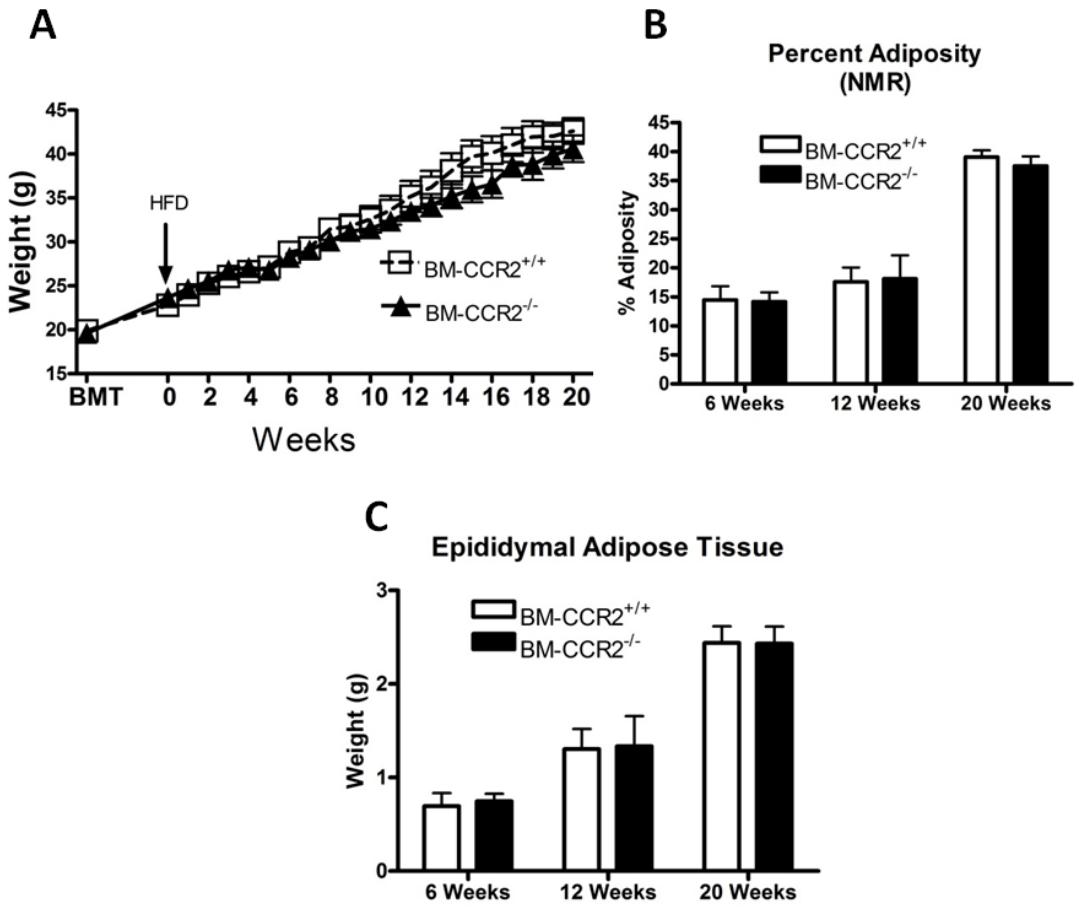

Figure 4.1 BM-CCR2$^{-/-}$ and BM-CCR2$^{+/+}$ mice have similar metabolic Parameters.

A) Weight gain curves of BM-CCR2$^{+/+}$ and BM-CCR2$^{-/-}$ mice during 20 weeks of HFD feeding (mean ± SEM; n = 9 mice per group). B) Percent adiposity in BM-CCR2$^{+/+}$ and BM-CCR2$^{-/-}$ mice after 6, 12 and 20 weeks on a HFD (mean ± SEM; n = 7-10 mice per group). Percent adiposity was calculated by dividing total AT mass, as assessed by NMR, by body weight. C) Epididymal AT pad weight after 6, 12 and 20 weeks on a HFD (mean ± SEM; n = 7-10 mice per group).

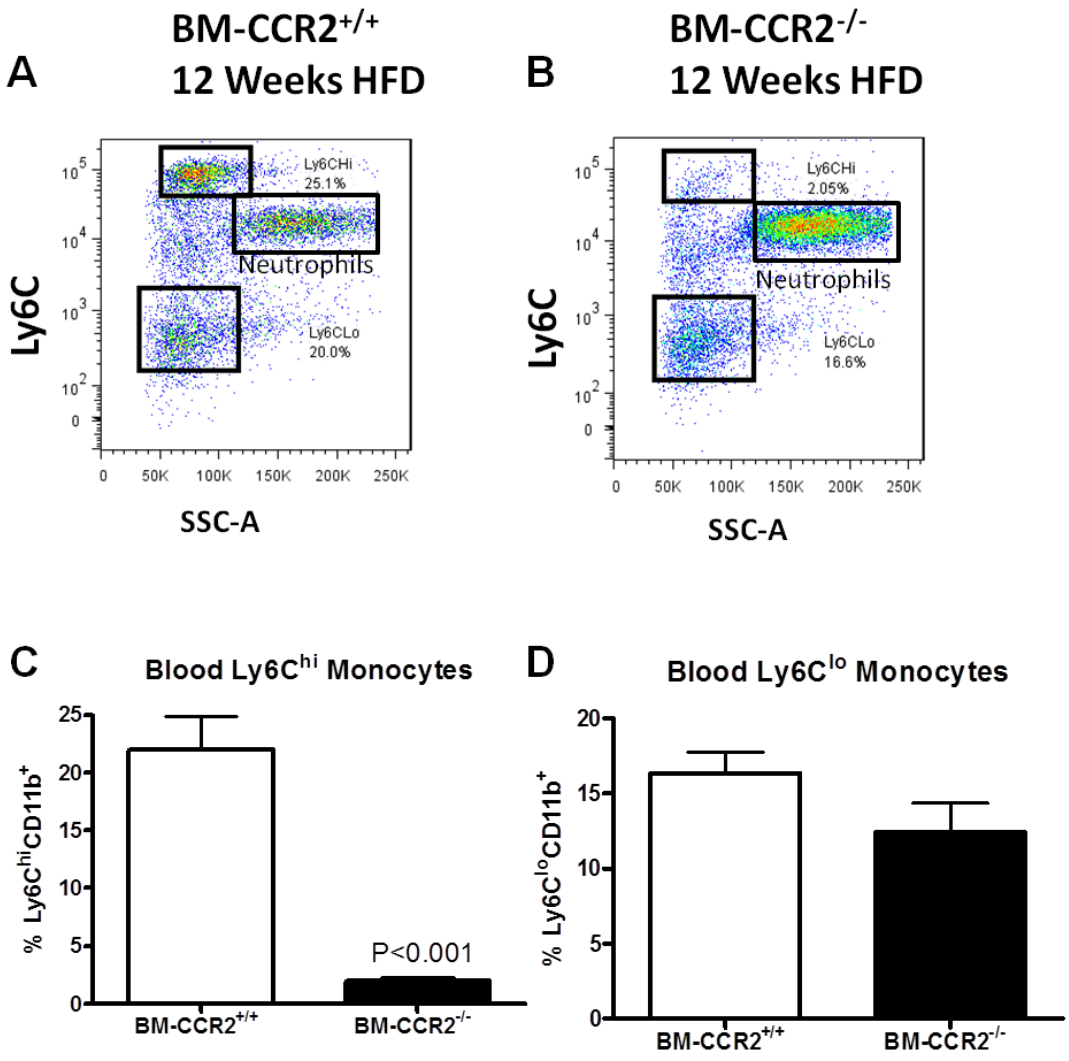

Figure 4.2 BM-CCR2$^{-/-}$ mice have decreased levels of circulating inflammatory monocytes.

White blood cells were isolated from BM-CCR2$^{+/+}$ and BM-CCR2$^{-/-}$ mice fed a HFD for 12 weeks. Circulating monocyte levels were assessed by flow cytometry by first gating on all live CD11b^{+} cells. Representative pseudo-color flow cytometry plot of Ly6C expression in the A) BM-CCR2$^{+/+}$ controls and B) BM-CCR2$^{-/-}$ mice. Quantification of the percentage of circulating C) Ly6C^{hi} monocytes and D) Ly6C^{lo} monocytes in BM-CCR2$^{+/+}$ and BM-CCR2$^{-/-}$ mice (mean ± SEM; n = 4 mice per group).

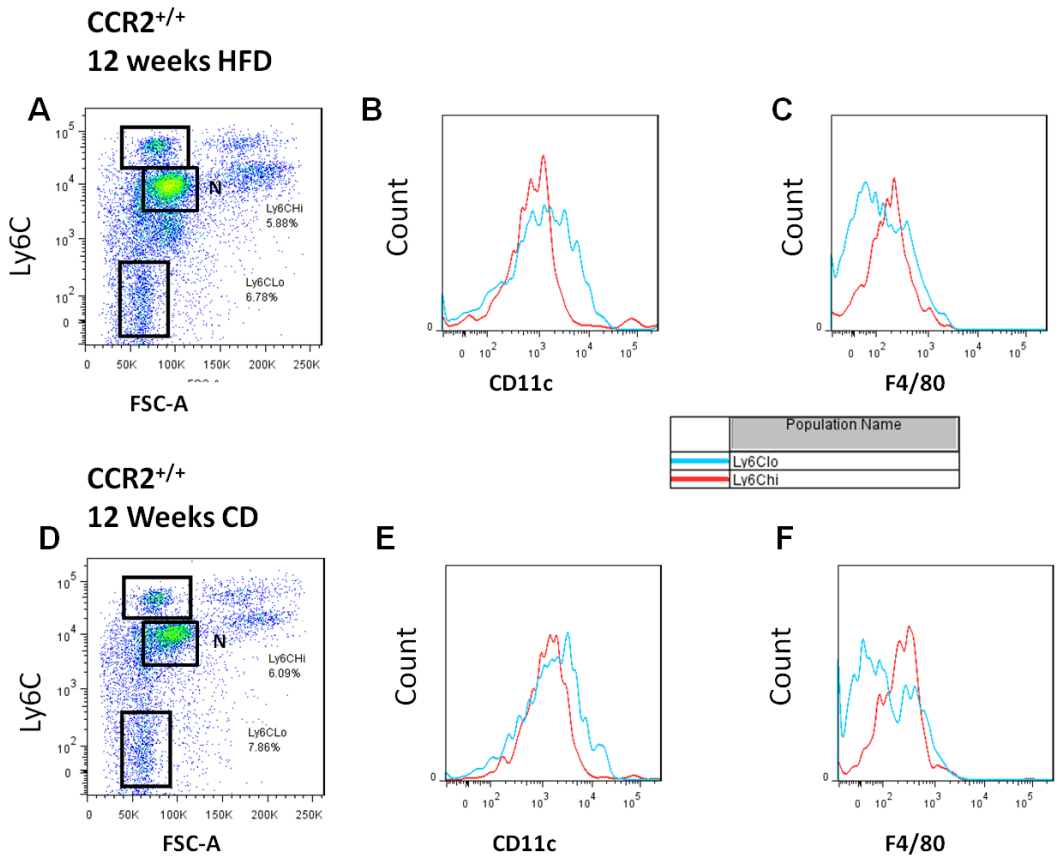

Figure 4.3 CCR2$^{-/-}$ mice have decreased levels of blood Ly6C^{hi} monocytes and increased expression of CD11c in Ly6C^{lo} monocytes.
White blood cells were isolated from CCR2$^{+/+}$ and CCR2$^{-/-}$ mice fed a HFD for 12 weeks. Circulating monocyte levels were assessed by flow cytometry by first gating on all live CD11b^{+} cells. A) Gates on Ly6C^{hi} and ly6C^{lo} populations in CCR2$^{+/+}$ mice. B) Histogram of CD11c expression in Ly6C^{hi} (red line) and Ly6C^{lo} (blue line) monocytes in CCR2$^{+/+}$ mice. C) Histogram of F4/80 expression in Ly6C^{hi} (red line) and Ly6C^{lo} (blue line) monocytes in CCR2$^{+/+}$ mice D) Gates on Ly6C^{hi} and ly6C^{lo} populations in CCR2$^{-/-}$ mice. E) Histogram of CD11c expression in Ly6C^{hi} (red line) and Ly6C^{lo} (blue line) monocytes in CCR2$^{-/-}$ mice. F) Histogram of F4/80 expression in Ly6C^{hi} (red line) and Ly6C^{lo} (blue line) monocytes in CCR2$^{-/-}$ mice. “N” in panels A & D indicate neutrophil populations.

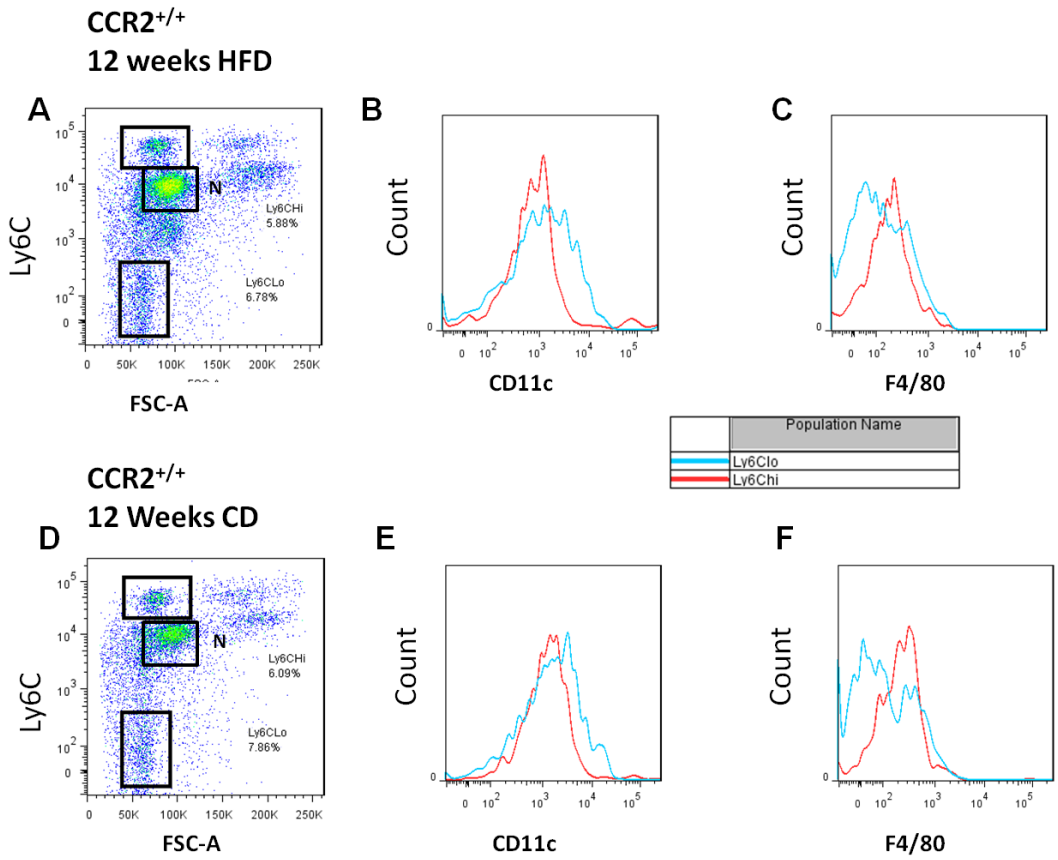

Supplementary Figure 4.4 HFD feeding increases the numbers and the CD11c expression of Ly6C^{hi} monocytes in CCR2$^{+/+}$ mice.
White blood cells were isolated from CCR2$^{+/+}$ mice fed a HFD or CD for 12 weeks. Circulating monocyte levels were assessed by flow cytometry by first gating on all live CD11b^{+} cells. A) Gates on Ly6C^{hi} and ly6C^{lo} populations in HFD fed CCR2$^{+/+}$ mice. B) Histogram of CD11c expression in Ly6C^{hi} (red line) and Ly6C^{lo} (blue line) monocytes in HFD fed CCR2$^{+/+}$ mice. C) Histogram of F4/80 expression in Ly6C^{hi} (red line) and Ly6C^{lo} (blue line) monocytes in HFD fed CCR2$^{+/+}$ mice. D) Gates on Ly6C^{hi} and ly6C^{lo} populations in CD fed CCR2$^{+/+}$ mice. E) Histogram of CD11c expression in Ly6C^{hi} (red line) and Ly6C^{lo} (blue line) monocytes in CD fed CCR2$^{+/+}$ mice. F) Histogram of F4/80 expression in Ly6C^{hi} (red line) and Ly6C^{lo} (blue line) monocytes in CD fed CCR2$^{+/+}$ mice. “N” in panels A & D indicate neutrophil populations.

Glucose Tolerance and Insulin Sensitivity.

To examine the systemic metabolic effects of CCR2 deficiency we performed glucose and insulin tolerance tests. We found no differences in glucose or insulin tolerance between groups at the 6 or 12 week time points (Figure 4.5A-D). However, a modest improvement in glucose tolerance was found in the BM-CCR2$^{-/-}$ mice ($P<0.05$), 15 min post glucose injection, after 20 weeks of HFD feeding (Figure 4.5E). Fasting glucose and insulin levels were not different between groups at any time (Table 4.1). Similar results were obtained in the global CCR2$^{-/-}$ mice in which differences in glucose tolerance were not observed until after 20 weeks of HFD feeding (Figure 4.6A-C). The discrepancy in glucose tolerance between the hematopoietic and global CCR2 deficient models can be attributed the inability of the BMT model to gain weight (125). On average, BM-CCR2$^{-/-}$ mice weighed <40g after 20 weeks of HFD feeding while the CCR2$^{-/-}$ weighed >48g during the same HFD feeding period.

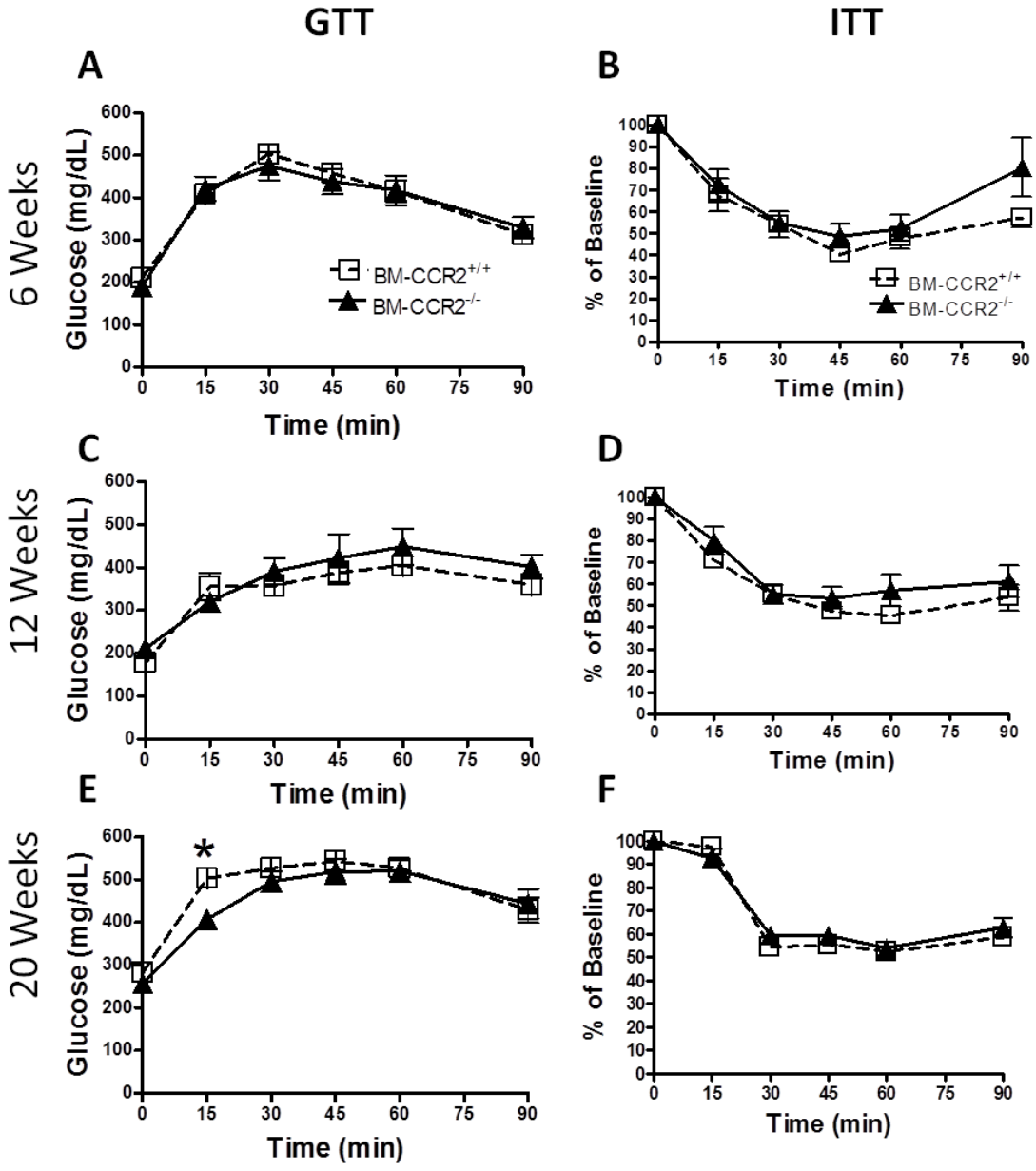

Figure 4.5. BM-CCR2$^{-/-}$ mice have a modest improvement in glucose tolerance after extended periods of HFD feeding. All GTT and ITT experiments were performed by injecting mice with either dextrose (1 g/Kg of lean mass) or insulin 0.5 (U/Kg of leans mass) after a 5 h morning fast. A) GTT after 6 weeks of HFD feeding (mean ± SEM; n = 8-10 mice per group). B) ITT after 6 weeks of HFD feeding (mean ± SEM; n = 4-5 mice per group). C) GTT after 12 weeks of HFD feeding (mean ± SEM; n = 3-5 mice per group). D) ITT after 12 weeks of HFD feeding (mean ± SEM; n = 7-10 mice per group) E) GTT after 20 weeks of HFD feeding (mean ± SEM; n = 8-9 mice per group). F) ITT after 20 weeks on a HFD (mean ± SEM; n = 9 mice per group).
*P<0.05 compared to the BM-CCR2$^{+/+}$ group at the 15 min time point.

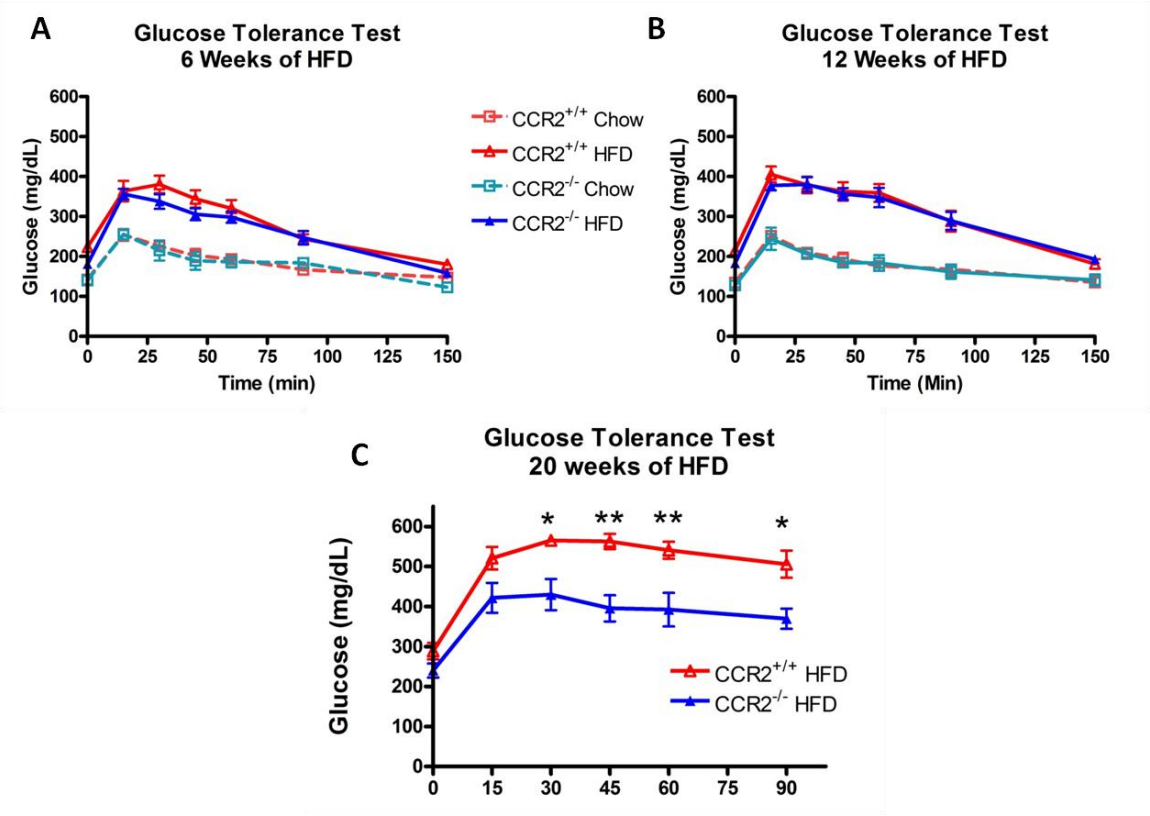

Figure 4.6 HFD fed CCR2$^{-/-}$ mice have delayed improvements in glucose tolerance.

Glucose tolerance curves of mice injected with 1 g of dextrose per kg of lean body mass. A) GTT curve of CCR2$^{+/+}$ and CCR2$^{-/-}$ mice after 6 weeks on either a HFD or CD (mean ± SEM; n = 3-9 mice per group). Both CD groups are significantly more glucose tolerant than both HFD groups (P<0.05). B) GTT curve of CCR2$^{+/+}$ and CCR2$^{-/-}$ mice after 12 weeks on either a HFD or CD (mean ± SEM; n = 2-8 mice per group). Both CD groups are significantly more glucose tolerant than both HFD groups (P<0.05). C) GTT curve of CCR2$^{+/+}$ and CCR2$^{-/-}$ mice after 20 weeks on a HFD (mean ± SEM; n = 4 mice per group). *P<0.05, **P<0.01 compared to CCR2$^{+/+}$ at the 20 week time point.

Table 4.1 No differences in fasting insulin or glucose levels were detected between the BM-CCR2$^{+/+}$ and BM-CCR2$^{-/-}$ mice.

Fasting glucose levels were assessed after a 5 h morning fast. Fasting insulin and were measured by ELISA. (mean ± SEM; n = 7-10 mice per group).

	BM-CCR2$^{+/+}$	**BM-CCR2$^{-/-}$**
Insulin (ng/ml)		
6 wks	0.54 ± 0.24	0.60 ± 0.19
12 wks	0.98 ± 0.76	1.18 ± 1.27
20 wks	1.50 ± 0.33	2.27 ± 0.67
Glucose (mg/dl)		
6 wks	156 ± 29	178 ± 26
12 wks	164 ± 20	180 ± 34
20 wks	282 ± 51	257 ± 30

AT Inflammatory State: Several reports indicate that CCR2$^{-/-}$ mice have deficient Th1 responses characterized by a low number of antigen presenting cells (APCs), resulting in reduced levels of the Th1 cytokine IFNγ (126, 127) and/or elevated IL4 (128). Assessment of IFNγ and IL4 in AT lysates from BM-CCR2$^{-/-}$ and BM-CCR2$^{+/+}$ mice showed no differences in these cytokines levels between groups after any period of HFD feeding (Figure 4.7A-B). Gene expression of the inflammatory genes TNFα (*Tnf*) and iNOS (*Nos2*) was not different between groups at the 6 and 12 week time points (Figure 4.7C & D); however, TNFα expression was significantly lower in the BM-CCR2$^{-/-}$ mice after 20 weeks of HFD feeding ($P<0.05$) (Figure 4.7E). Gene expression of the chemokines MCP-1 (*Ccl2*) and MIP-1α (*Ccl3*) were significantly increased after 6 weeks ($P<0.01$ and $P<0.001$, respectively) and 12 weeks ($P<0.05$ and $P<0.01$, respectively) in the BM-CCR2$^{-/-}$ mice; no differences in the expression of these chemokines were observed in the mice fed a HFD for 20 weeks.

The BM-CCR2$^{-/-}$ mice presented a 3-fold increase in the expression of the anti-inflammatory marker arginase 1 (*Arg1*) at 6 ($P<0.01$) and 12 weeks ($P<0.01$); expression of this gene was not different between groups after 20 weeks of HFD feeding (Figure 4.7C-E). Expression of *Cd163*, *mgl1*, *mgl2* and *Il10* was assessed and these “M2” or anti-inflammatory genes were generally increased in the BM-CCR2$^{-/-}$ mice after 6 and 12 weeks of HFD feeding but not at the 20 week time point, when compared to the BM-CCR2$^{+/+}$ control.

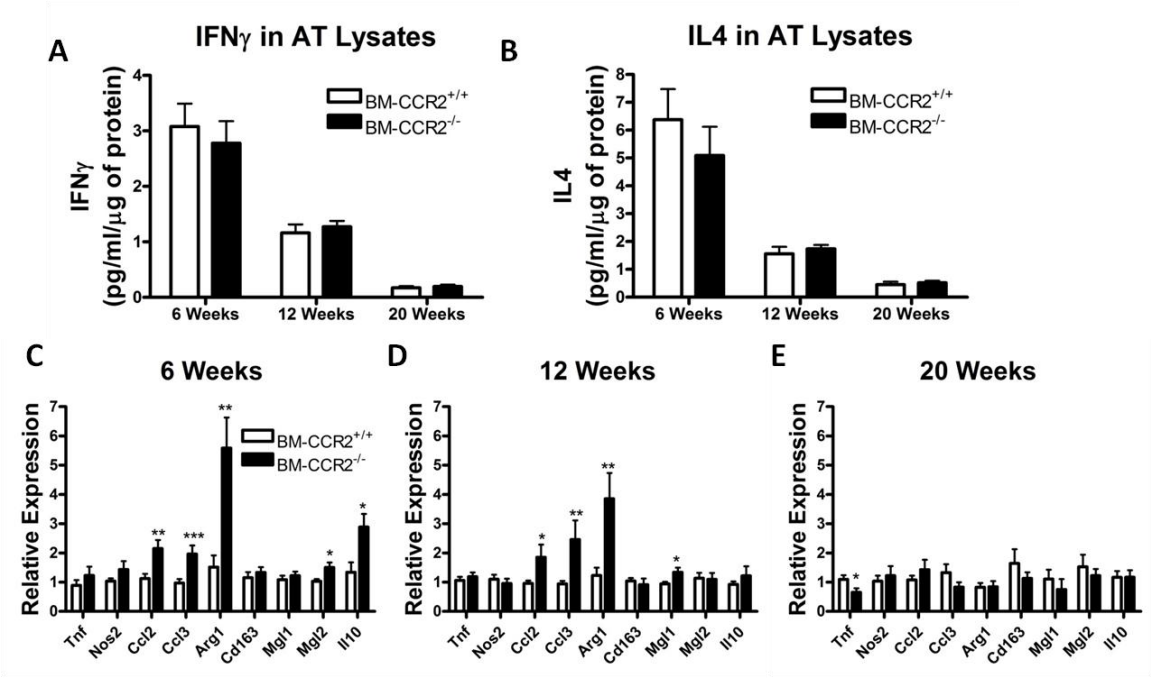

Figure 4.7 BM-CCR2$^{-/-}$ mice have similar levels of IFNγ and IL4 protein in AT to those of BM-CCR2$^{+/+}$ controls after all periods of HFD.

A) Levels of IFNγ protein in AT lysates were measured by ELISA (mean ± SEM; n = 7-10 mice per group). B) Levels of IL4 protein in AT lysates were measured by ELISA (mean ± SEM; n = 6-7 mice per group). C-E) RNA was isolated from AT and used for gene expression analysis by real-time RT-PCR. The mRNA expression of *Tnf*, *Nos2*, *Ccl2*, *Ccl3*, *Arg1*, *Cd163*, *Mgl1*, *Mgl2* and *Il10* was assessed after 6, 12 and 20 weeks of HFD feeding and plotted as expression relative to the BM-CCR2$^{+/+}$ group of each time point (mean ± SEM; n = 7-10 mice per group).

*P<0.05 compared to the BM-CCR2$^{+/+}$ group

**P<0.01 compared to the BM-CCR2$^{+/+}$ group

***P<0.001 compared to the BM-CCR2$^{+/+}$ group

Immune Cell Infiltration into AT: Crown-like structures (CLS), which are an accumulation of immune cells around presumably dead adipocytes, were used to quantify immune cell infiltration in TBO stained sections of AT (Figure 4.8A-F). There were no differences in numbers of CLS between BM-CCR2$^{-/-}$ and BM-CCR2$^{+/+}$ mice after 6 or 12 weeks of HFD feeding (Figure 4.8G). However, there was a significant decrease in CLS in the BM-CCR2$^{-/-}$ mice after 20 weeks of HFD feeding ($P<0.05$) (Figure 4.8E-G). Further analysis of TBO stained AT from mice fed a HFD for 20 weeks showed that the number of CLS is dependent on the body weight of the mouse. There were no differences between weight matched BM-CCR2$^{-/-}$ and BM-CCR2$^{+/+}$ mice under 40g of body weight; conversely, there was a decrease in CLS in the BM-CCR2$^{-/-}$ mice when compared to weight-matched BM-CCR2$^{+/+}$ controls over 45g of body weight (Figure 4.9). In accordance with our histological data, there were no differences in the expression of CD68 (*Cd68*), CD11b (*Itgam*) or CD11c (*Itgax*) in AT of BM-CCR2$^{-/-}$ compared to BM-CCR2$^{+/+}$ mice after 6 or 12 weeks of HFD feeding (Figure 4.8H-I); however, the expression of these genes was significantly lower for the BM-CCR2$^{-/-}$ mice by the 20 week time point when compared to the control group ($P<0.05$; Figure 4.8J). The expression of F4/80 (*Emr1*) in the AT of BM-CCR2$^{-/-}$ mice was significantly increased after 6 weeks ($P<0.05$), unchanged after 12 weeks, and there was a trend towards a decrease after 20 weeks of HFD in comparison to the BM-CCR2$^{+/+}$ controls ($P<0.07$; Figure 4.8H-J).

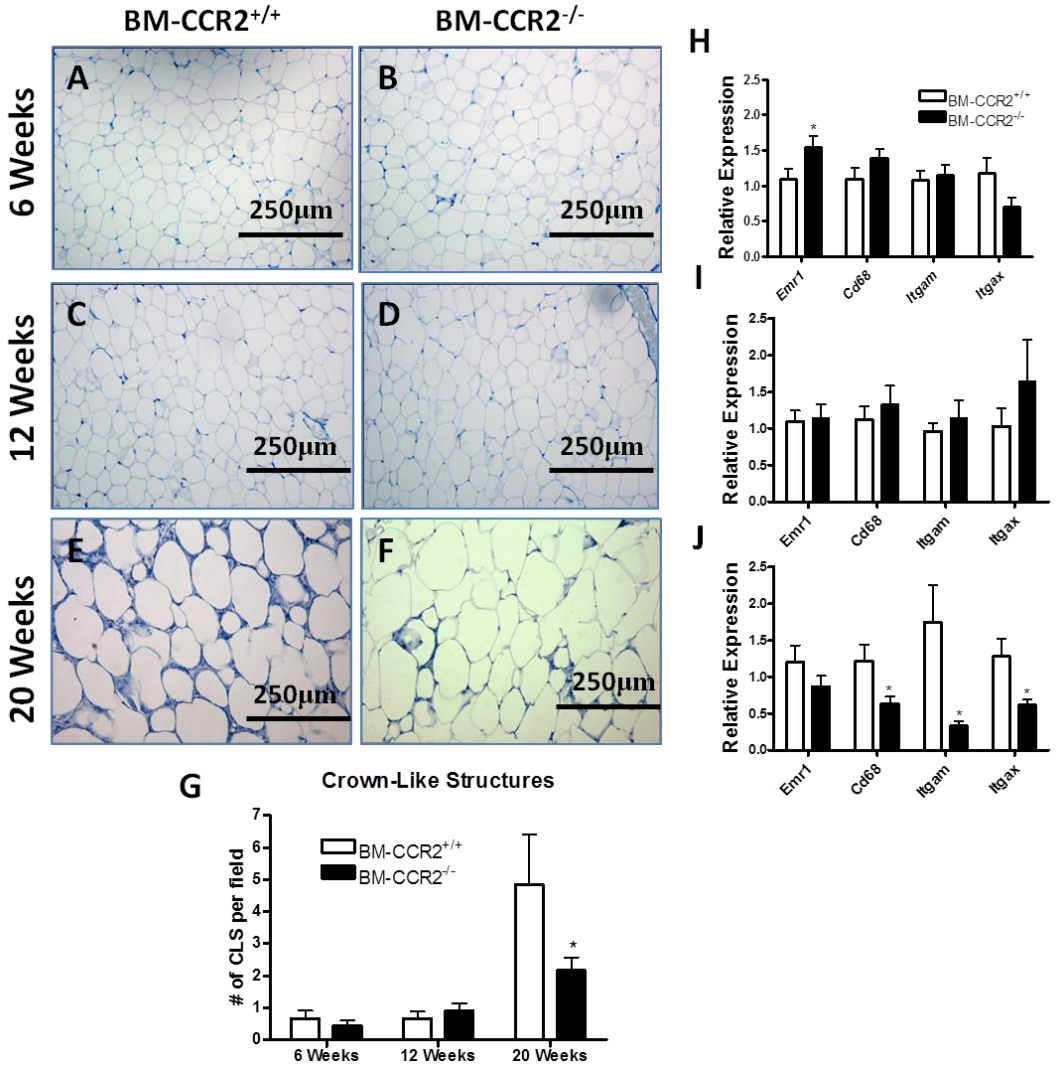

Figure 4.8 BM-CCR2$^{-/-}$ mice have decreased immune infiltration and macrophage marker expression after extended periods of HFD feeding.

AT was collected from BM-CCR2$^{+/+}$ and BM-CCR2$^{-/-}$ mice fed HFD for 6, 12, or 20 weeks and used to assess macrophage infiltration by histological and gene expression analysis. A - F) Representative TBO-stained images from mice as indicated. G) Crown-like structures (CLS) in TBO stained AT sections were quantified from 8 different fields per mouse and presented as number of CLS per field (mean ± SEM; n = 5-7 mice per group). H-J) RNA was isolated from AT and used for gene expression analysis by real-time RT-PCR. The expression of the macrophage markers *Emr1*, *Cd68*, *Itgam,* and *Itgax* was assessed after 6, 12 and 20 weeks of HFD feeding and plotted as expression relative to the BM-CCR2$^{+/+}$ group of each time point (mean ± SEM; n = 7-10 mice per group).

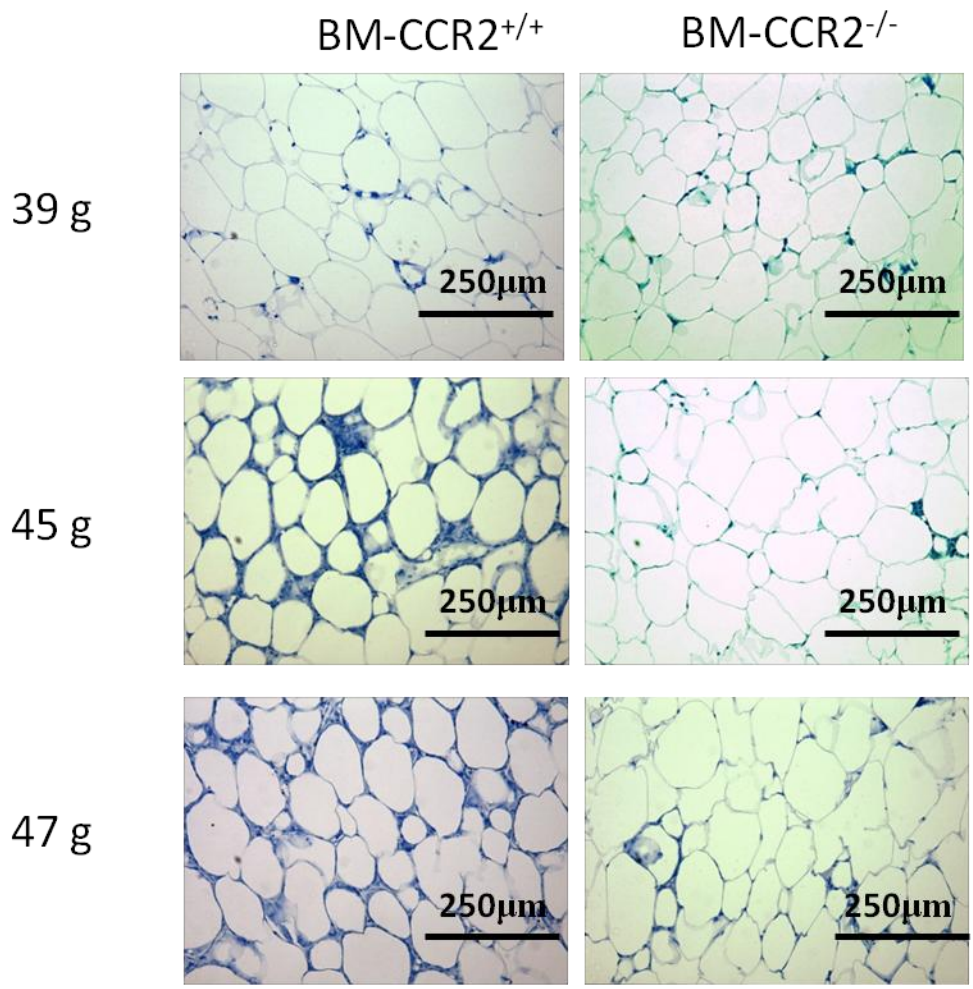

Figure 4.9 BM-CCR2$^{-/-}$ mice have lower immune infiltration than weight-matched BM-CCR2$^{+/+}$ mice.
AT was collected from weight-matched BM-CCR2$^{+/+}$ and BM-CCR2$^{-/-}$ mice fed HFD for 20 weeks and used to assess macrophage infiltration by histological analysis. Representative TBO-stained AT pictures of weight-matched BM-CCR2$^{+/+}$ and BM-CCR2$^{-/-}$ mice are presented.

CCR2 deficiency leads to the aberrant accumulation of F4/80^{lo}cells in AT: Based upon our observation that there were no changes in immune infiltration in AT after 6 and 12 weeks of HFD feeding despite the dramatic reduction in circulating inflammatory cells, we sought to further characterize the macrophages in AT by flow cytometry. To this end, we performed careful evaluation of the F4/80^{+} cells within AT. Based on our gating strategy the BM-CCR2$^{+/+}$ mice contained the expected F4/80^{-} and F4/80^{hi} populations (Figure 4.10A). Interestingly**,** the BM-CCR2$^{-/-}$ mice accumulated two discrete myeloid populations in their AT, F4/80^{lo} and F4/80^{hi} (Figures 4.10B). The discrete F4/80^{lo} population was observed in the SVF of the BM-CCR2$^{-/-}$ at the 6 (Figures 4.10B-C) and 12 week (Figure 4.11B & Figure 4.10C) time points, but was no longer detected after 20 weeks of HFD feeding (Figure 4.11D & Figures 4.10C).

Real-time RT-PCR analysis of RNA isolated from whole AT of BM-CCR2$^{-/-}$ mice showed that the presence of the F4/80^{lo} population at 6 and 12 weeks was associated with increases in gene expression of myeloperoxidase (*Mpo*; P<0.05), CXCR2 (*IL8rb*; P<0.01) *Cxcl1* (P<0.001) and *Cxcl2* (P<0.05) (Figure 4.10D & E). No differences in the expression of these genes were observed after 20 weeks of HFD, when the F4/80^{lo} cells were no longer detected (Figure 4.10F).

Similar to the BM-CCR2$^{-/-}$ model, analysis of the SVCs of the global CCR2$^{-/-}$ mice showed that CD11b^{lo}F4/80^{lo} cells aberrantly accumulate in the AT of global CCR2$^{-/-}$ mice with similar kinetics. The cells accumulate in the AT of CCR2$^{-/-}$ after 6 or 12 weeks of HFD feeding (Figure 4.12D-E), while no discrete population was found in the CCR2$^{+/+}$ controls (Figure 4.12A-B). Additionally, after

20 weeks of HFD feeding the CD11b^{lo}F4/80^{lo} were no longer found in either the AT of CCR2$^{-/-}$ or CCR2$^{+/+}$ mice (Figure 4.12F). Global CCR2$^{-/-}$ mice were utilized for subsequent characterization of the CD11b^{lo}F4/80^{lo} cells.

CD11b^{lo}F4/80^{lo} Cell Characterization: CD11b^{hi}F4/80^{hi} and CD11b^{lo}F4/80^{lo} cells were isolated from the AT of CCR2$^{-/-}$ mice 10 weeks post-HFD feeding by flow cytometry activated cell sorting (Figure 4.13A). Gene expression analysis was performed for both populations, and is presented as expression relative to the CD11b^{hi}F4/80^{hi} cells (Figure 4.13B). Expression of *Emr1* was significantly lower for CD11b^{lo}F4/80^{lo} cells as expected based on our gating strategy (P<0.001). The expression of *Arg1* (P<0.05), *Cd163* (P<0.001), *Il10* (P<0.01), *Il6* (P<0.01), *Ccr5* (P<0.05), *Ccl2* (P<0.01) and *Csfr1* (P<0.001) was significantly lower in the CD11b^{lo}F4/80^{lo} cells in comparison to the CD11b^{hi}F4/80^{hi} macrophages. Expression of *Itgax* (P<0.01), *Nos2* (P<0.05), *Ccl5* (P<0.01), *Mpo* (P<0.01), *Il8rb* (P<0.05) and *Csf1* (P<0.05) was significantly higher for the CD11b^{lo}F4/80^{lo} cells. H&E staining of the sorted CD11b^{lo}F4/80^{lo} cells showed that these cells have a granulocytic/monocytic morphology and are smaller in size than the CD11b^{hi}F4/80^{hi} macrophages (Figure 4.13C). Despite several reports of neutrophilia at sites of inflammation in CCR2$^{-/-}$ mice (129, 130), flow cytometry analysis of the CD11b^{lo}F4/80^{lo} population in the global CCR2$^{-/-}$ mice showed that these cells are Ly6G-negative and therefore unlikely to be neutrophils (Figure 4.14).

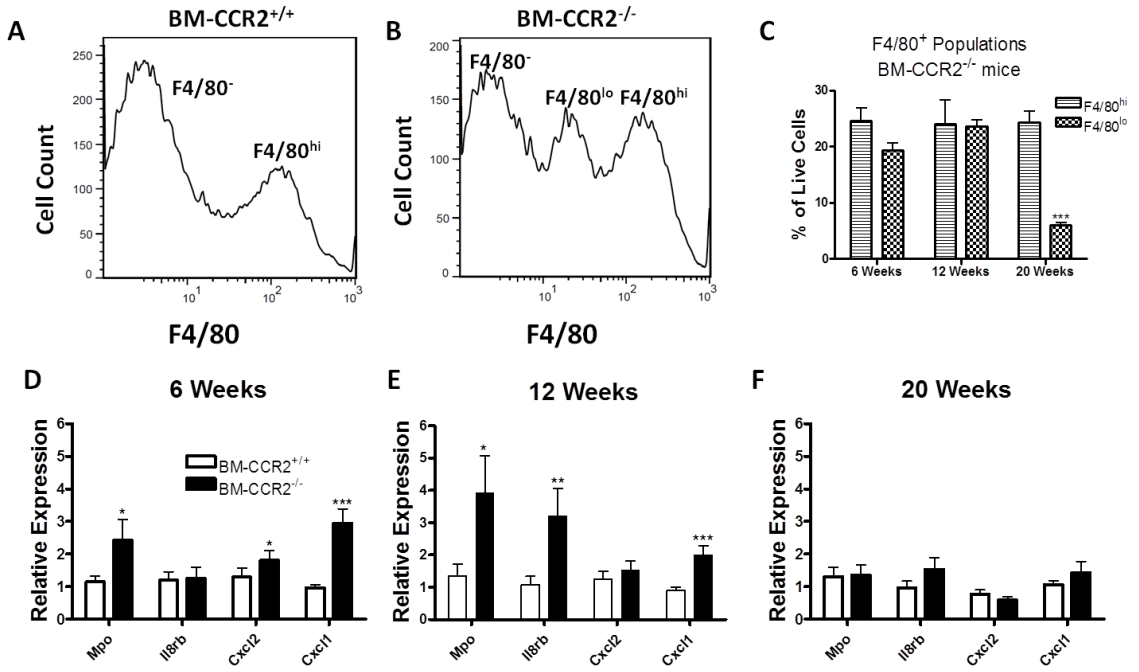

Figure 4.10 A unique F4/80^{lo} myeloid population accumulates in the SVF of the AT of BM-CCR2$^{-/-}$ mice.

SVCs isolated from BM-CCR2$^{+/+}$ and BM-CCR2$^{-/-}$ mice were analyzed by flow cytometry. Representative flow cytometry histogram of F4/80-expressing populations in a A) BM-CCR2$^{+/+}$ mouse and in a B) BM-CCR2$^{-/-}$ mouse gated on all live cells. C) Quantification of F4/80^{lo} vs. F4/80^{hi} cell percentages after 6, 12 and 20 weeks of HFD in the BM-CCR2$^{-/-}$ (mean ± SEM; n = 3-5). D- F) RNA was isolated from AT and used for gene expression analysis by real-time RT-PCR. The mRNA expression of *Mpo*, *Il8rb*, *Cxcl2* and *Cxcl1* was assessed after 6, 12 and 20 weeks of HFD feeding and plotted as expression relative to the BM-CCR2$^{+/+}$ group of each time point (mean ± SEM; n = 7-10 mice per group).

*P<0.05 compared to the BM-CCR2$^{+/+}$ group

**P<0.01 compared to the BM-CCR2$^{+/+}$ group

***P<0.001 compared to the BM-CCR2$^{+/+}$ group

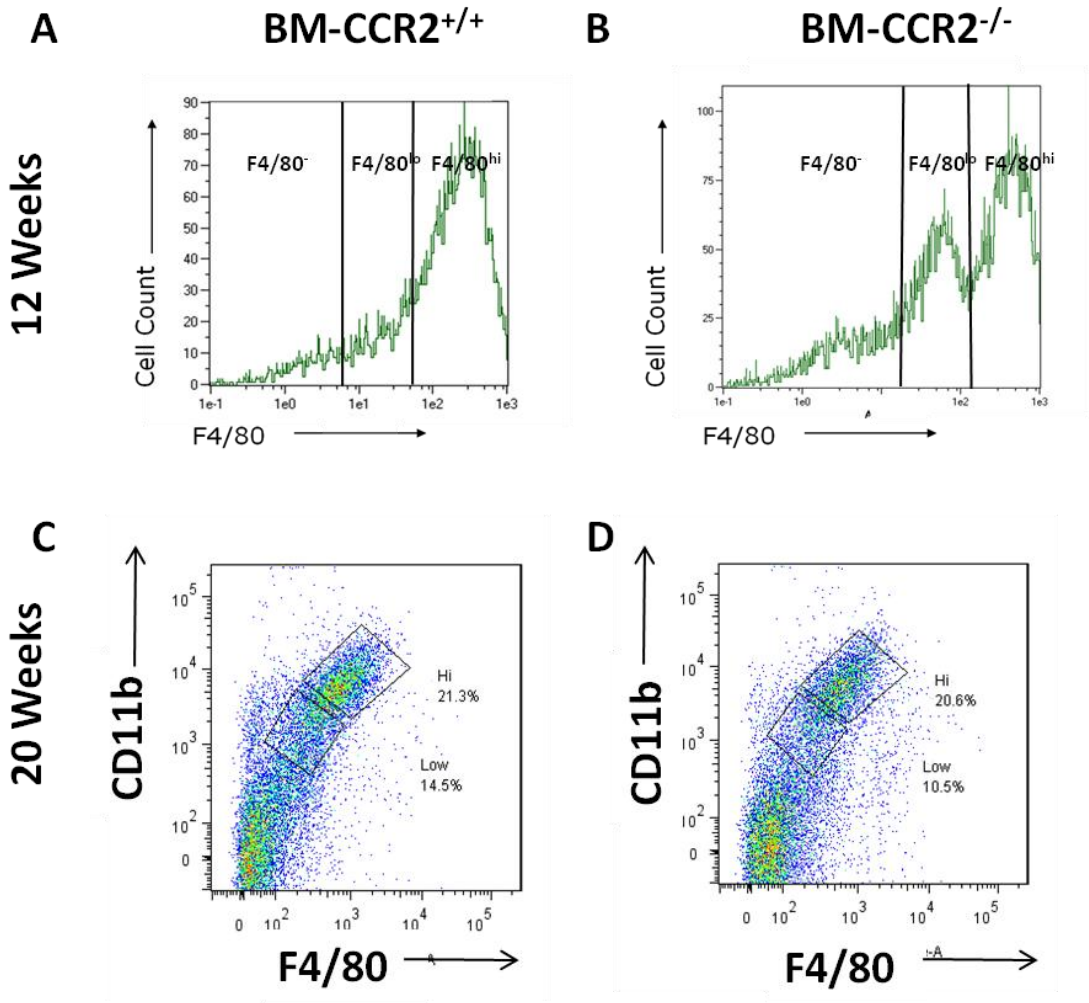

Figure 4.11 BM-CCR2$^{-/-}$ mice have a unique CD11bF4/80^{lo} population after 12 weeks of HFD feeding.
Representative histograms of F4/80^{+} cells for A) BM-CCR2$^{+/+}$ and B) BM-CCR2$^{-/-}$ mice after 12 weeks of HFD feeding. Representative plots of CD11b^{+}F4/80^{+} cells for C) BM-CCR2$^{+/+}$ and D) BM-CCR2$^{-/-}$ mice after 20 weeks of HFD feeding.

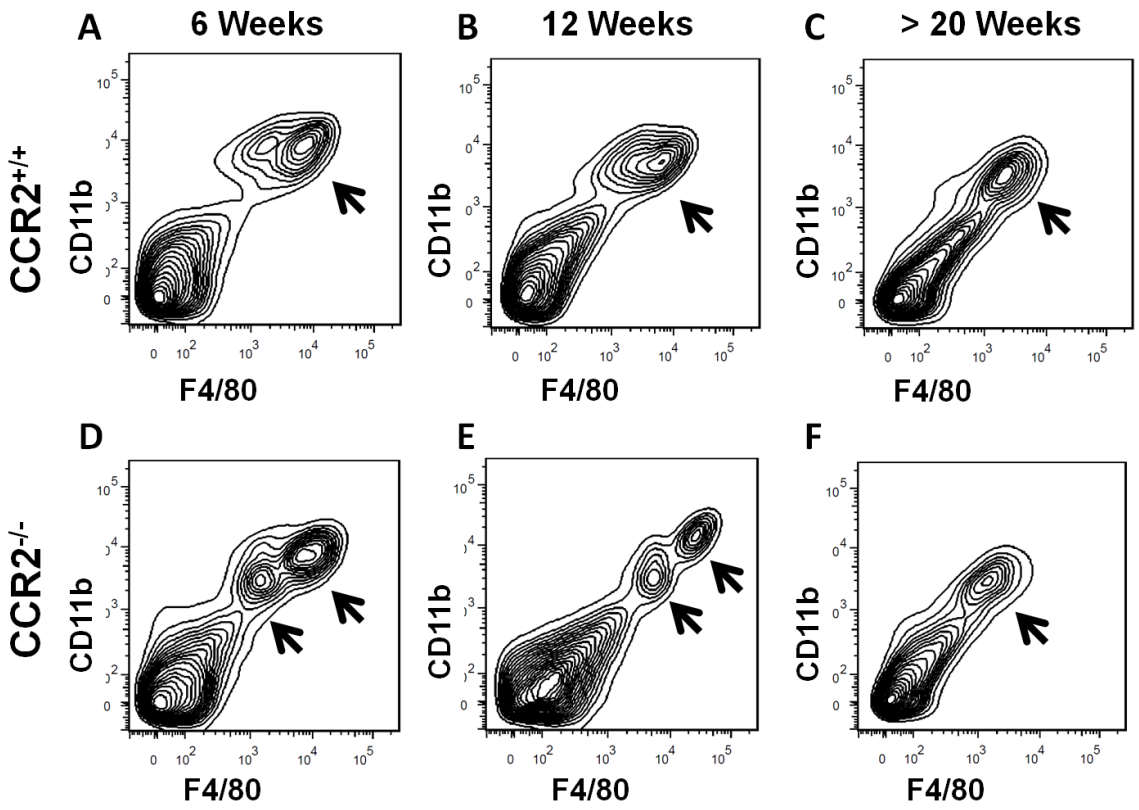

Figure 4.12 CD11b^{lo}F4/80^{lo} cells accumulate in global CCR2$^{-/-}$ mice.
Representative contour plots of F4/80 versus CD11b expression in SVCs from CCR2$^{+/+}$ mice after A) 6 Weeks B) 12 weeks and C) 20 weeks on a HFD. Representative contour plots of F4/80 versus CD11b expression in SVCs from CCR2$^{-/-}$ mice after A) 6 Weeks B) 12 weeks and C) 20 weeks on a HFD. (n = 4 biological replicates)

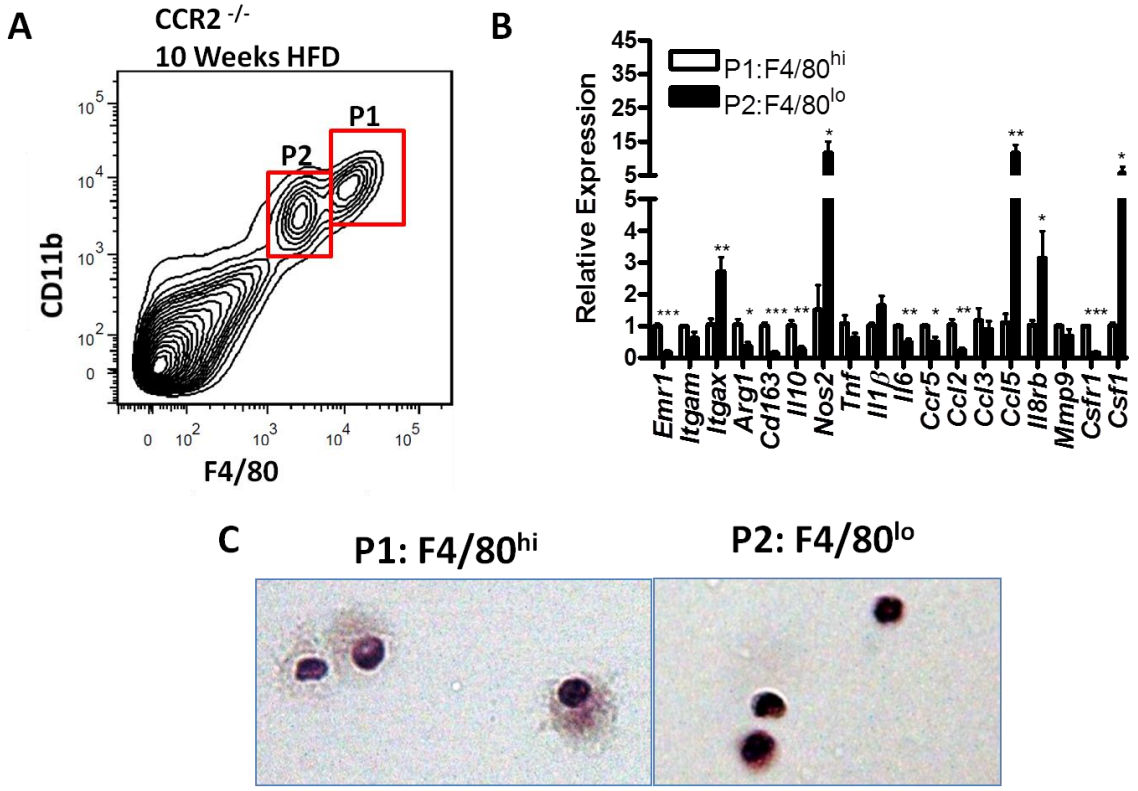

Figure 4.13 CD11b^{lo}F4/80^{lo} cells have an inflammatory expression profile and a granulocytic morphology.

CD11b^{lo}F4/80^{lo} and CD11b^{hi}F4/80^{hi} cells were isolated by fluorescence activated cell sorting from CCR2$^{-/-}$ mice fed a HFD for 10 weeks. A) Gating strategy used for cell sorting; CD11b^{hi}F4/80^{hi} (P1) and CD11b^{lo}F4/80^{lo} (P2). RNA was isolated from the sorted cells and used for gene expression analysis by real-time RT-PCR. B) Gene expression profiles in CD11b^{lo}F4/80^{lo} (P2) cells relative to CD11b^{hi}F4/80^{hi} (P1) cells in CCR2$^{-/-}$ mice was assessed (mean ± SEM; n = 4 biological replicates) C) Representative images of H&E stained CD11b^{hi}F4/80^{hi} (P1) and CD11b^{lo}F4/80^{lo} (P2) cells.

*P<0.05 compared to the CD11b^{hi}F4/80^{hi}

**P<0.01 compared to the CD11b^{hi}F4/80^{hi}

***P<0.001 compared to the CD11b^{hi}F4/80^{hi}

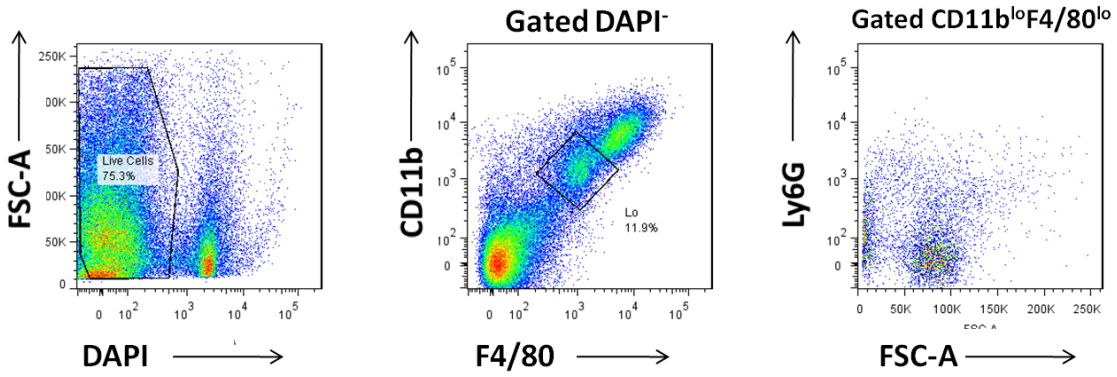

Figure 4.14 CD11b^{lo}F4/80^{lo} cells have a Ly6G (negative) immunophenotype
SVCs were isolated from the AT of CCR2$^{-/-}$ mice fed a HFD for 10 weeks. Representative image of gating strategy used to assess the expression of Ly6G in the CD11b^{lo}F4/80^{lo} cells.

CD11b^{lo}F4/80^{lo} Cells are Transiently Found in CCR2$^{+/+}$ mice

To determine the physiological relevance of the CD11b^{lo}F4/80^{lo} cells in wild type conditions, we isolated CD11b^{lo}F4/80^{lo} and CD11b^{hi}F4/80^{hi} macrophages from CCR2$^{+/+}$ mice fed a HFD for 7 weeks by fluorescence activated cell sorting using the gating strategy shown in Figure 4.13A. Despite the absence of two discrete populations in the CCR2$^{+/+}$ mice we were able to isolate cells using the same gating strategy as in Figure 4.13A and found cells that have identical gene expression (Figure 4.15B) and morphology (Figure 4.15C) as the CD11b^{lo}F4/80^{lo} cells isolated from the AT of CCR2$^{-/-}$ mice. In addition, we assessed if HFD feeding was necessary for the accumulation of CD11b^{lo}F4/80^{lo} cells. The expression of several key genes in the CD11b^{lo}F4/80^{lo} cells isolated from CD-fed CCR2$^{-/-}$ and CCR2$^{+/+}$ mice (Figure 4.16) was similar to that of CD11b^{lo}F4/80^{lo} cells isolated from the HFD mice (Figures 4.13B & 4.15B).

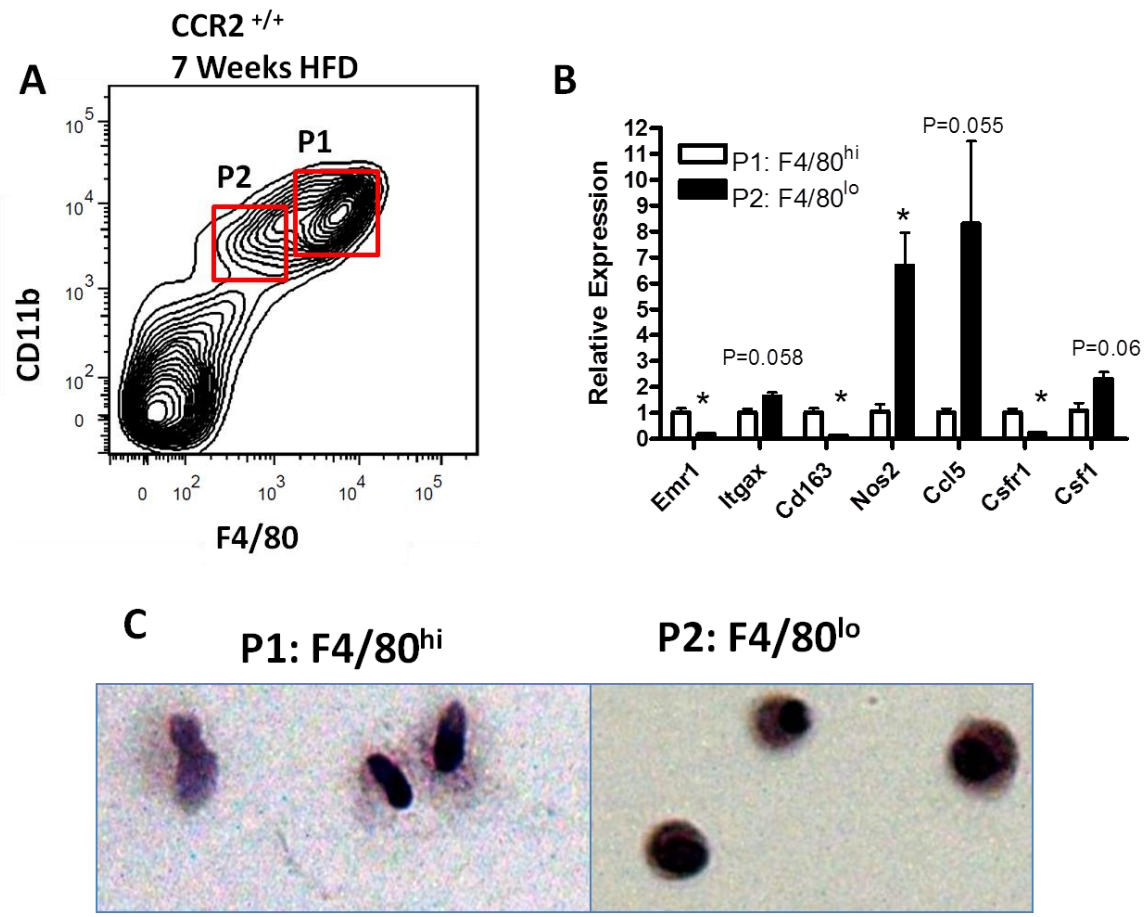

Figure 4.15 CD11b^{lo}F4/80^{lo} cells are transiently found in the AT of HFD-fed CCR2$^{+/+}$ mice

CD11b^{lo}F4/80^{lo} and CD11b^{hi}F4/80^{hi} cells were isolated by fluorescence activated cell sorting from CCR2$^{+/+}$ mice fed a HFD for 7 weeks. A) Gating strategy used for cell sorting; CD11b^{hi}F4/80^{hi} (P1) and CD11b^{lo}F4/80^{lo} (P2). RNA was isolated from the sorted cells and used for expression analysis of key CD11b^{lo}F4/80^{lo} genes by real-time RT-PCR. B) Gene expression profiles in CD11b^{lo}F4/80^{lo} (P2) cells relative to CD11b^{hi}F4/80^{hi} (P1) cells in CCR2$^{+/+}$ mice was assessed (mean ± SEM; n = 4 biological replicates) C) Representative images of H&E stained CD11b^{hi}F4/80^{hi} (P1) and CD11b^{lo}F4/80^{lo} (P2) cells.

*P<0.05 compared to the CD11b^{hi}F4/80^{hi}

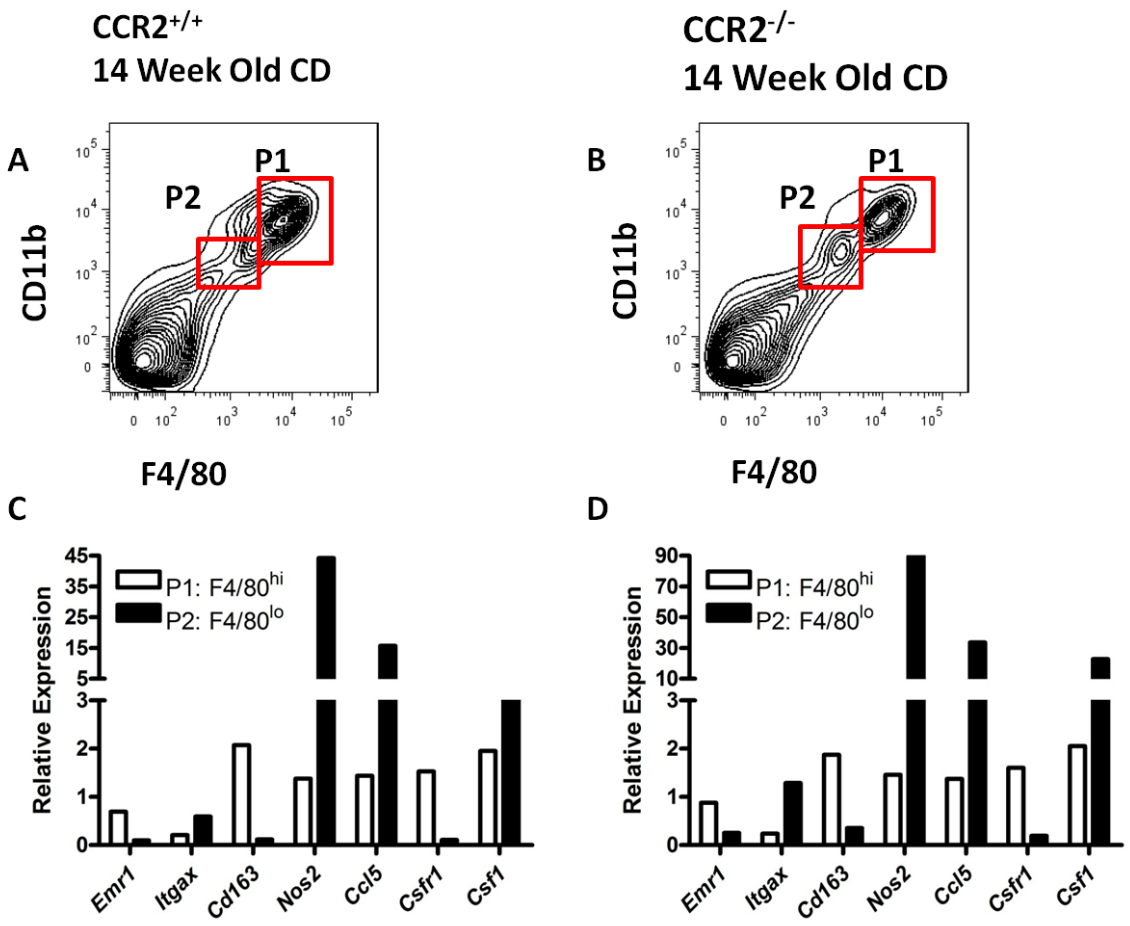

Figure 4.16 CD11b^{lo}F4/80^{lo} cells are found in the AT of CD fed CCR2$^{+/+}$ and CCR2$^{-/-}$ mice.

SVCs were isolated from 14 weeks old CD fed CCR2$^{+/+}$ and CCR2$^{-/-}$ mice. Gating strategy used for FACS sorting of CD11b^{lo}F4/80^{lo} and CD11b^{hi}F4/80^{hi} cells in A) CCR2$^{+/+}$ mice and B) CCR2$^{-/-}$ mice. B) Gene expression of key CD11b^{lo}F4/80^{lo} genes relative to CD11b^{hi}F4/80^{hi} cells in C) CCR2$^{+/+}$ mice and D) CCR2$^{-/-}$ mice (n = 3 pooled biological samples).

Part II: (Gutierrez *et al*. Manuscript in Preparation, 2012)

CD11b^{lo}F4/80^{lo} Myeloid Cells in the AT and Peritoneum are Eosinophils

We reported in Part I of this chapter the discovery of a novel myeloid cell population in the peritoneal cavity and AT of CCR2$^{-/-}$ mice. Further analysis of their expression of extracellular markers indicated that the CD11b^{lo}F4/80^{lo} cells in the peritoneum are Siglec-F^{+} and therefore eosinophils (Figure 4.17).

AT CD11b^{lo}F4/80^{lo} cells were Siglec-F positive, suggesting that the CD11b^{lo}F4/80^{lo} cells in AT are also a population of eosinophils. Isolation of these cells by flow activated cell sorting showed a combination of cells with eosinophil and monocyte morphology; however isolating the CD11b^{lo}F4/80^{lo} Siglec-F^{+} population gives a homogenous cell population with eosinophil-like morphology (Figure 4.18).

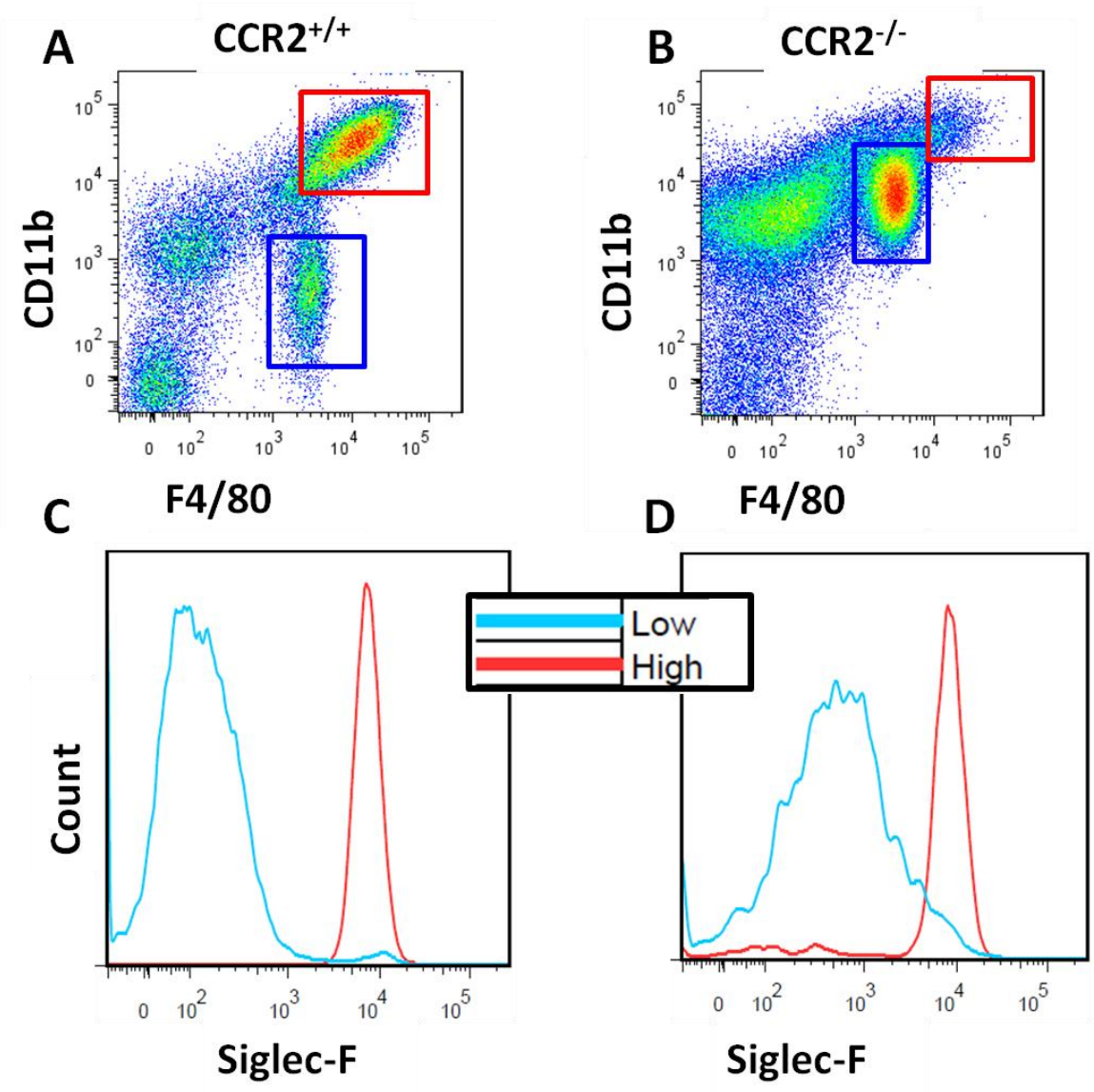

Figure 4.17 Expression of Siglec-F in peritoneal CD11b^{lo}F4/80^{lo} cells. Expression of Siglec-F in peritoneal CD11b^{lo}F4/80^{lo} cells was assessed by flow cytometry analysis. Representative images of flow cytometry plots of peritoneal cells indicating the gates used on the CD11b^{lo}F4/80^{lo} (blue) and CD11b^{hi}F4/80^{hi} (red) populations in A) CCR2$^{+/+}$ and B) CCR2$^{-/-}$ mice. Representative histograms of Siglec-F expression in the CD11b^{lo}F4/80^{lo} (blue) and CD11b^{hi}F4/80^{hi} (red) populations in C) CCR2$^{+/+}$ and D) CCR2$^{-/-}$ mice.

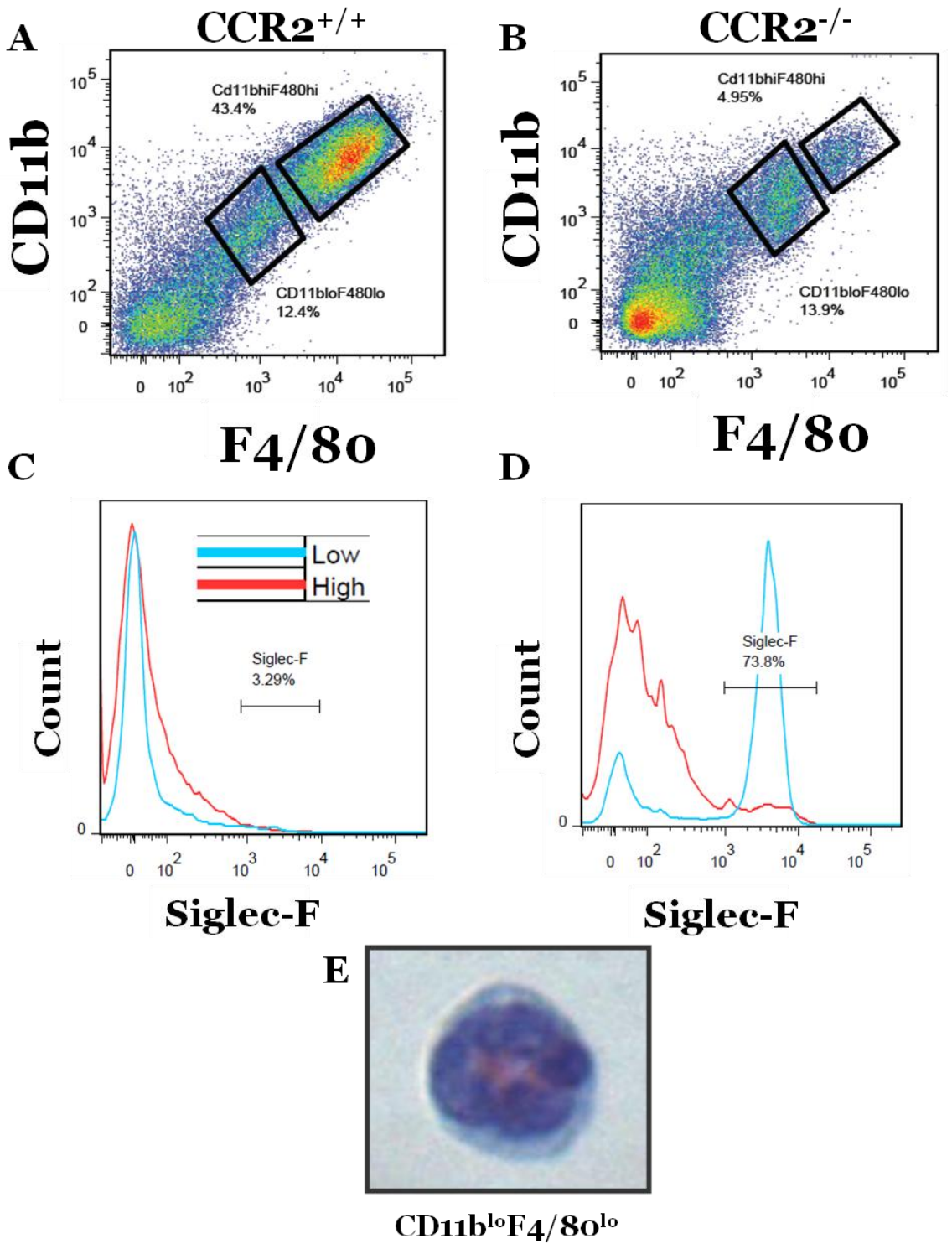

Figure 4.18 AT CD11b^{lo}F4/80^{lo} cells express siglec-F. Representative images of flow cytometry plots of SVF cells indicating the gates used on the CD11b^{lo}F4/80^{lo} and CD11b^{hi}F4/80^{hi} populations in A) CCR2$^{+/+}$ and B) CCR2$^{-/-}$

mice. Representative histograms of Siglec-F expression in the $CD11b^{lo}F4/80^{lo}$ and $CD11b^{hi}F4/80^{hi}$ populations in C) $CCR2^{+/+}$ and D) $CCR2^{-/-}$ mice. E) Flow activated sorted $CD11b^{lo}F4/80^{lo}$ eosinophil stained with Diff-Quick.

Eosinophils are Found in All AT Depots

Once we established that the $CD11b^{lo}F4/80^{lo}$ cell population are eosinophils, we used expression of CD11b versus Siglec-F to accurately quantify the percentage of these cells in the AT of $CCR2^{+/+}$ and $CCR2^{-/-}$ mice (Figure 4.19). The percentage of eosinophils in the epididymal, peri-renal, mesenteric and subcutaneous AT depots of $CCR2^{+/+}$ and $CCR2^{-/-}$ mice fed a chow or high fat diet for 6 weeks was quntified. In general, in the $CCR2^{+/+}$ mice, HFD feeding decreased the percentage of eosinophils in all AT depots. In contrast, in the $CCR2^{-/-}$ mice HFD feeding for this short period of time increased the number of eosinophils as we previously reported (Figure 4.10C). The epididymal AT depot had the highest percentage and absolute number of eosinophils in both the $CCR2^{+/+}$ and $CCR2^{-/-}$ mice, followed by the mesenteric and peri-renal depots, and lastly the subcutaneous AT depot (Epidydimal > Mesenteric = Peri-Renal > Subcutaneous) (Figure 4.20 A-D). This hierarchy is congruent with that of the most metabolically active AT depots, where the subcutaneous is the least metabolically active.

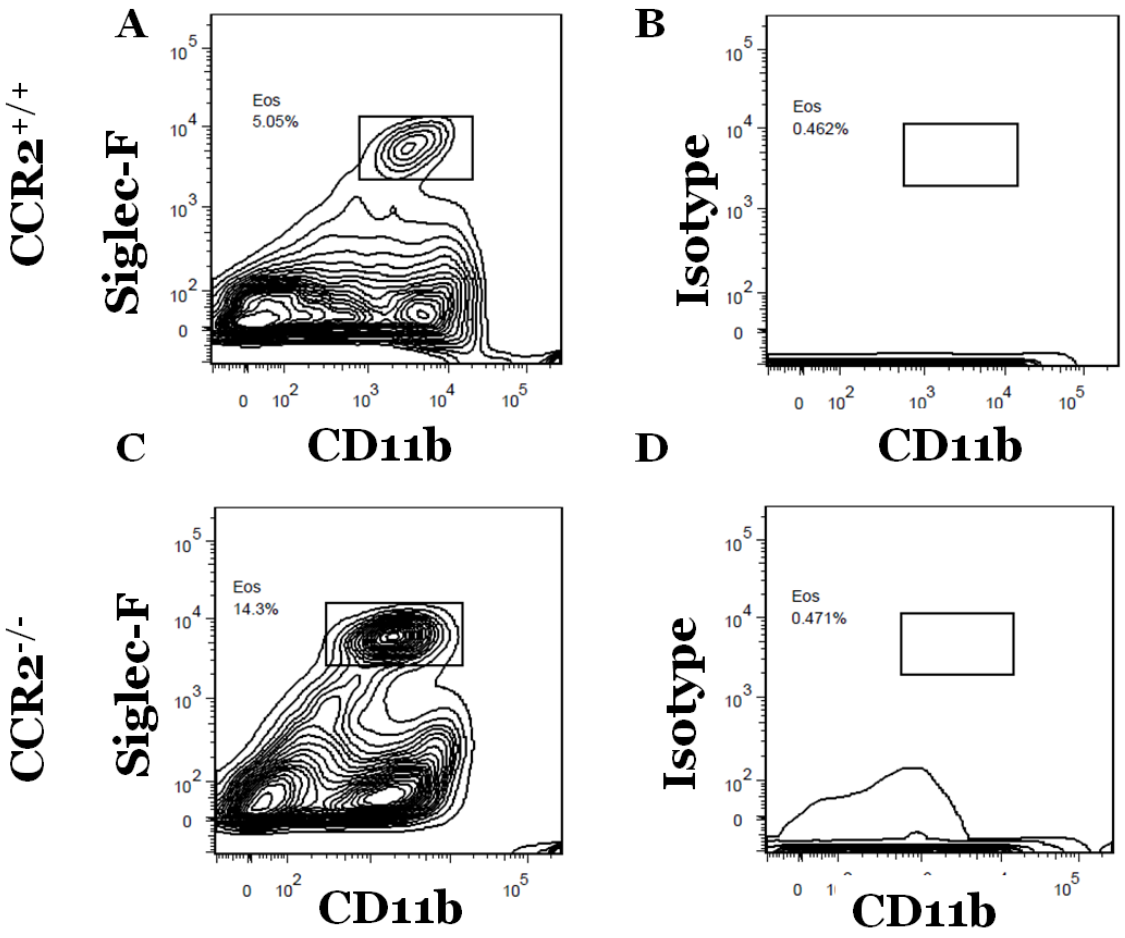

Figure 4.19 Flow cytometry analysis of AT eosinophils. Representative images of eosinophil quantification in A) CCR2$^{+/+}$ and C) CCR2$^{-/-}$ mice gated on all live single cells. Represenstative images of Siglec-F isotype control for B) CCR2$^{+/+}$ and C) CCR2$^{-/-}$ mice gated on all live single cells.

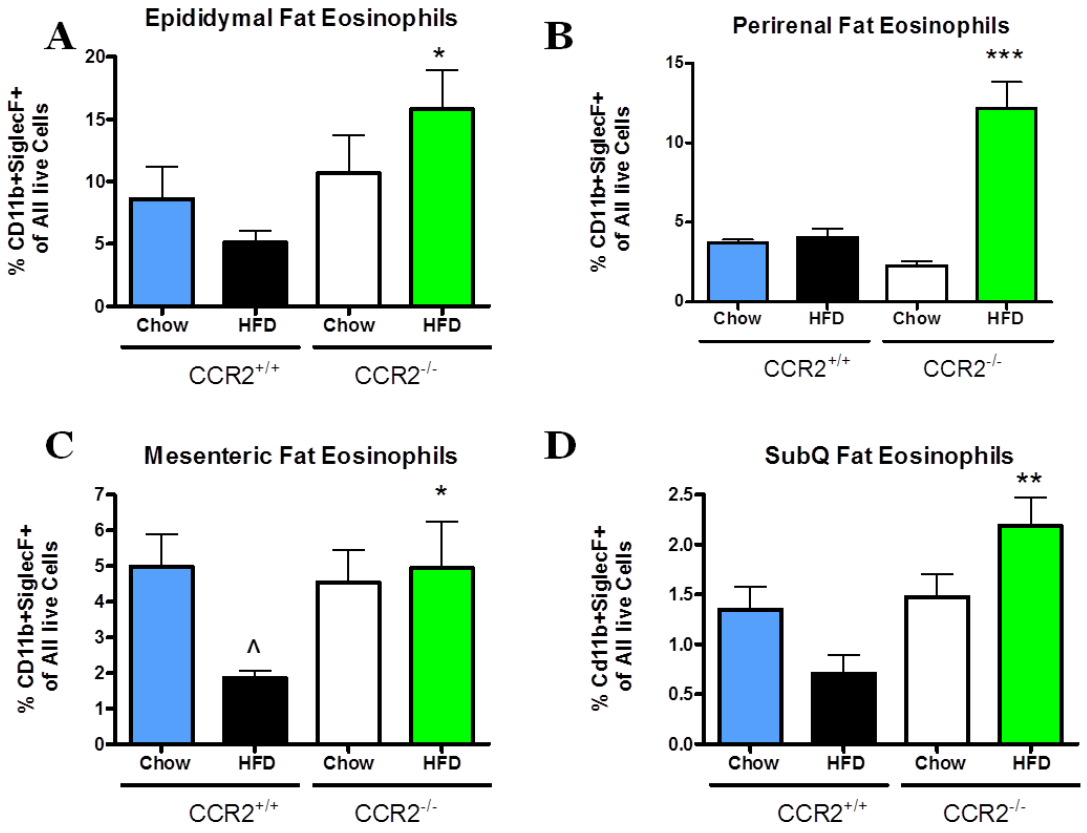

Figure 4.20. **Quantification of eosinophils in AT depots.** $CCR2^{+/+}$ and $CCR2^{-/-}$ mice were fed a chow or high fat diet for 6 weeks. Quantification of the percentage of eosinophils in the A) epididymal depot, B) peri-renal depot, C) mesenteric depot and D) subcutaneous depot. Data are presented as mean ± SEM, n=5-6 per group.

*P<0.05 Between genotypes, same diet.

**P<0.01 Between genotypes, same diet.

***P<0.001 Between genotypes, same diet.

^P<0.05 Between diets, same genotype.

Eosinophils are Localized in the Interstitial Space of AT

Epididymal AT sections were fixed and stained by immunofluorescence with an antibody against Siglec-F (Green), using DAPI (Blue) as a nuclei marker. Immunoflurorescence imaging of AT from $CCR2^{+/+}$ and $CCR2^{-/-}$ mice showed that Siglec-F^{+} eosinophils are localized in the interstitial space between adipocytes and not in crown-like structures. Additionally, in support of the flow cytometry data we observe a larger number of eosinophils in AT from $CCR2^{-/-}$ mice in contrast to that of $CCR2^{+/+}$ mice (Figure 4.21).

Eosinophilia is Restricted to AT and Peritoneum

To determine if the observed eosinophilia in $CCR2^{-/-}$ mice was specific to AT and the peritoneum or if it was due global eosinophilia, we measured the eosinophil levels in circulation and bone marrow by flow cytometry. There were no differences in the bone marrow or blood levels of eosinophils between $CCR2^{+/+}$ and $CCR2^{-/-}$ mice in either diet (Figure 4.22). Additionally, there were no differences in eosinophil levels in the liver or spleen of $CCR2^{-/-}$ mice when compared to the $CCR2^{+/+}$ controls (data not shown).

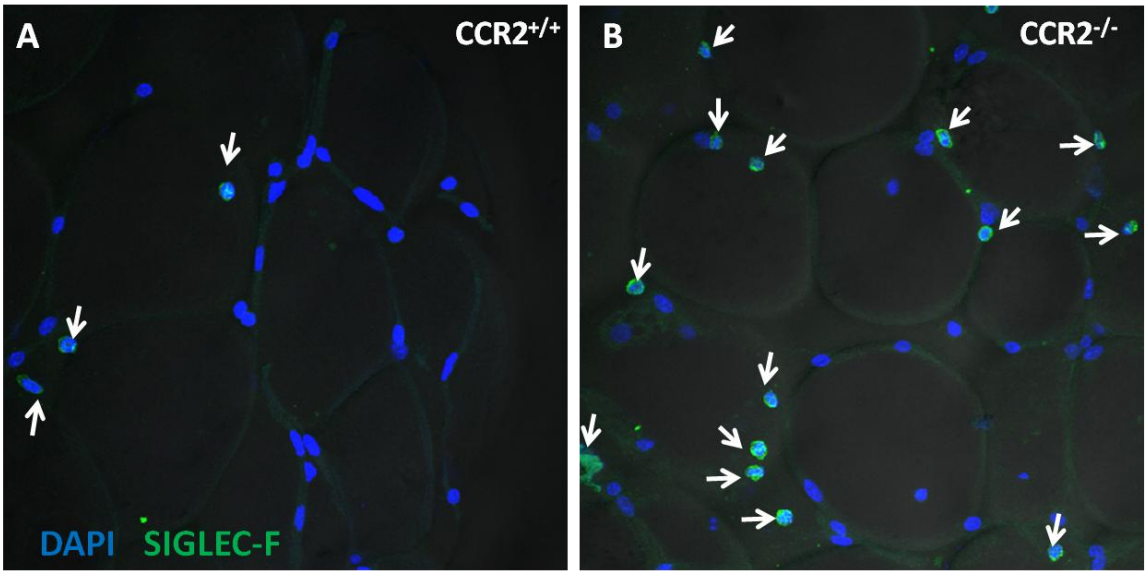

Figure 4.21 AT Siglec-F Immunofluorescence.

Representative immunofluorescence images of epididymal AT sections from A) $CCR2^{+/+}$ and B) $CCR2^{-/-}$ mice fed an HFD for 6 weeks; DAPI (Blue) and Siglec-F (Green). White arrows represent eosinophils.

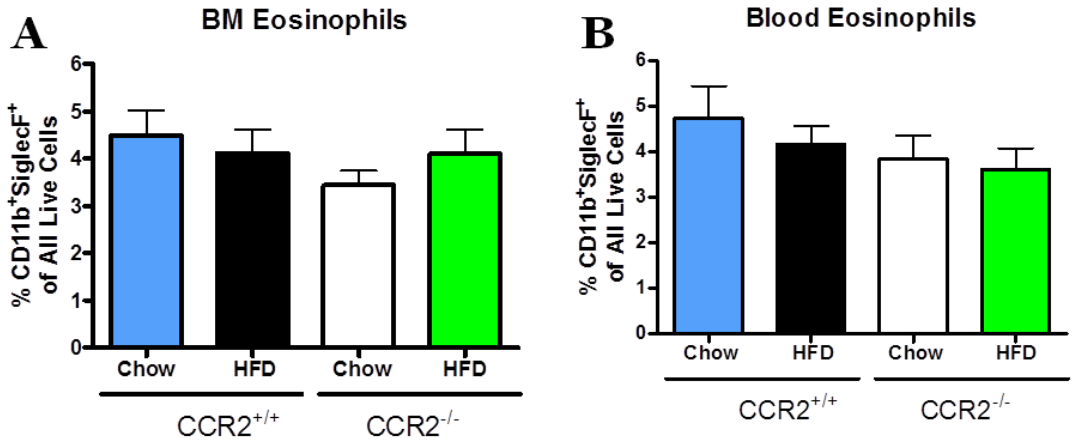

Figure 4.22. Quantification of eosinophils in bone marrow and blood. $CCR2^{+/+}$ and $CCR2^{-/-}$ mice were fed a chow or high fat diet for 6 weeks. Quantification of the percentage of eosinophils in the A) bone marrow and B) blood. Data are presented as mean ± SEM, n=4-6 per group.

Eosinophil Levels are Correlated with IL5 and Arg1 Expression in AT

Total RNA was purified from epididymal AT of $CCR2^{+/+}$ and $CCR2^{-/-}$ mice and analyzed by real-time RT-PCR. Analysis of the expression of *Il5*, a cytokine known to increase eosinophil recruitment and local proliferation, showed a close correlation with the levels of eosinophils in this tissue (Figure 4.23A). Furthermore, assessment of mRNA expression of *Arg1* showed an increase in the expression of this gene in the $CCR2^{-/-}$ mice when compared to their diet matched $CCR2^{+/+}$ counterparts (Figure 4.23B). The increased expression of this M2 marker supports a regulation of alternative activation by the newly identified eosinophil population it AT.

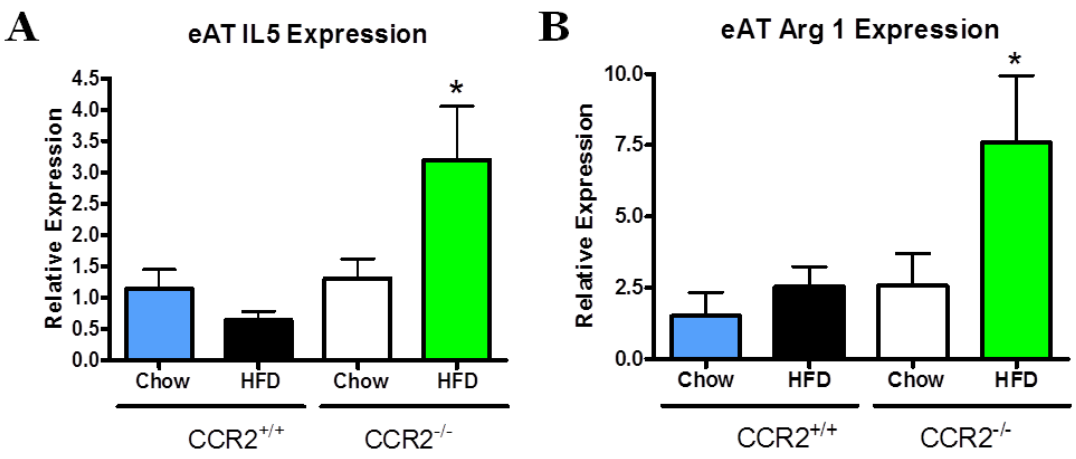

Figure 4.23 Expression of *Il5* and *Arg1* in epididymal AT. Total RNA was isolated from epididymal AT of CCR2$^{+/+}$ and CCR2$^{-/-}$ mice fed either a chow or high fat diet. Real-time RT-PCR expression of A) *Il5* and B) *Arg1*. Data are presented as mean ± SEM, n=5-6 per group.

*P<0.05 Between genotypes, same diet.

DISCUSSION

$CCR2^{-/-}$ mice have been shown to have a modest reduction in macrophage recruitment to AT after extended periods of HFD feeding (35, 120). Given that the pool of circulating inflammatory monocytes is strikingly reduced in these mice (111) (Figure 4.2), inflammatory macrophage recruitment to AT should be correspondingly decreased. Thus, inflammation and IR in $CCR2^{-/-}$ mice is expected to be markedly decreased in comparison to $CCR2^{+/+}$ controls upon placement on a HFD. However, inflammation and inflammatory macrophage recruitment in $CCR2^{-/-}$ mice are only partially decreased and only after substantial obesity is attained (35, 120). Our current studies explored mice with global and hematopoietic CCR2 deficiency at different periods of HFD feeding to investigate the mechanism involved in the delayed improvement in inflammation and insulin sensitivity.

To understand processes that take place at earlier stages of obesity that could prevent improvements in inflammation and IR, we analyzed myeloid populations in AT of BM-$CCR2^{-/-}$ and $CCR2^{-/-}$ mice and the control mice after 6, 12 and 20 weeks of HFD by flow cytometry. Our data provide evidence for the accumulation of a unique $CD11b^{lo}F4/80^{lo}$ myeloid population in the AT of BM-$CCR2^{-/-}$ (Figure 4.10 & 4.11) and $CCR2^{-/-}$ (Figure 4.12) mice after 6 and 12 weeks of HFD feeding. These $CD11b^{lo}F4/80^{lo}$ cells are no longer detected in the AT of the BM-$CCR2^{-/-}$ and $CCR2^{-/-}$ mice after extended periods (> 20 weeks) of HFD feeding (Figure 4.10C, 4.12C & F). Our data suggest that the presence of the $CD11b^{lo}F4/80^{lo}$ cells is associated with the mechanism(s) for the delay in

improvements in inflammation and IR observed in these mice, and that substantial obesity and disappearance of the CD11b^{lo}F4/80^{lo} cells are temporally correlated with these metabolic improvements.

To determine the identity and phenotype of the novel CD11b^{lo}F4/80^{lo} cells, we isolated RNA from these cells for gene expression characterization relative to that of the CD11b^{hi}F4/80^{hi} cells in Part I of this chapter. Altogether the expression data suggested that the CD11b^{lo}F4/80^{lo} cells do not exhibit classical M1 or M2 expression profiles, but instead have a unique inflammatory expression in contrast to that of CD11b^{hi}F4/80^{hi} macrophages. However, we later showed in Part II, that this was a mixed population of monocytic/granulocytic cells.

Chomarat *et al.* showed that during monocyte to macrophage differentiation there is an upregulation of CD115 (*Csf1r*) coupled by a downregulation of its ligand M-CSF (*Csf1*) (131). We measured the expression of both *Csfr1* and *Csf1*, and found that in fact *Csfr1* was downregulated while *Csf1* was upregulated in the CD11b^{lo}F4/80^{lo} cells, suggesting that these cells might be in a monocytic transition stage. To test this, we performed H&E staining of isolated cells and found that CD11b^{lo}F4/80^{lo} cells have a monocytic/granulocytic morphology in contrast to the CD11b^{hi}F4/80^{hi} cells, which have a morphology characteristic of macrophages (Figure 4.13). The expression profile and morphological analysis of the mixed CD11b^{lo}F4/80^{lo} indicated that these are monocytic/granulocytic cells that accumulated in AT in the absence of CCR2.

We also sought to investigate the presence of the CD11b^{lo}F4/80^{lo} cells in wild type mice, independent of CCR2 deficiency. We isolated CD11b^{lo}F4/80^{lo} and

$CD11b^{hi}F4/80^{hi}$ macrophages from $CCR2^{+/+}$ mice using identical gates as previously used for the $CCR2^{-/-}$ mice (Figure 4.13). Despite the absence of a discrete population under the $CD11b^{lo}F4/80^{lo}$ (P2) gate, we were able to isolate a relatively high number of cells. Gene expression analysis of key markers of $CD11b^{lo}F4/80^{lo}$ cells described previously, showed that $CD11b^{lo}F4/80^{lo}$ cells isolated from $CCR2^{+/+}$ mice have identical gene expression patterns as those of the $CCR2^{-/-}$ mice (Figure 4.14). Additionally, H&E staining of isolated cells showed a similar monocytic/granulocytic morphology between the $CCR2^{-/-}$ and $CCR2^{+/+}$ $CD11b^{lo}F4/80^{lo}$ cells. Moreover, we found that HFD feeding was not necessary for the accumulation of these cells in AT, as $CD11b^{lo}F4/80^{lo}$ cells were found in CD-fed $CCR2^{+/+}$ and $CCR2^{-/-}$ mice (Figure 4.16). Next, we assessed whether these cells were found in other metabolically relevant tissues such as the liver. We did not observe their accumulation in this tissue; on the other hand, we did observe a decrease in recruited macrophages and no effects on resident Kupffer cells as recently described by Obstfeld *et al.* (132) (data not shown). These findings indicate that although CCR2 deficiency is not necessary for the recruitment of $CD11b^{lo}F4/80^{lo}$ cells to AT, it leads to the aberrant accumulation of these cells, which would otherwise only transiently be found in this AT depot.

The identity of these cells was further studied in Part II of this chapter. After careful flow cytometric analysis, the peritoneal $CD11b^{lo}F4/80^{lo}$ cells were found to be $CCR3^{+}$Siglec-F^{+}, indicating unquestionably that they were eosinophils. When the immunophenotype of the AT $CD11b^{lo}F4/80^{lo}$ cells was assessed, these cells were CCR3-negative; however, they were Siglec-F positive

and had an eosinophil morphology. Altogether these data suggested that the $CD11b^{lo}F4/80^{lo}$ cells previously isolated in Part I are a combination of eosinophils and undifferentiated monocytes. Thus, the gene expression assessed previously is a reflection of the mixed population and not that of the homogeneous eosinophil population.

Our study also tested whether the origin of the epididymal AT and peritoneal eosinophilia in $CCR2^{-/-}$ mice was caused by global eosinophilia, increased recruitment due to increased eotaxin expression, or local proliferation. Our data showed that eosinophilia was found in all white AT depots including: epididymal, peri-renal, mesenteric and subcutaneous. However, no eosinophilia was observed in the liver or spleens of $CCR2^{-/-}$ mice. The levels of eosinophils in the bone marrow and blood were also not different between $CCR2^{+/+}$ and $CCR2^{-/-}$ mice. Furthermore, AT expression of the eosinophil chemoattractants: CCL11, CCL24 and CCL26, was not different between genotypes (data not shown). These data suggest that AT and peritoneal eosinophilia was not caused by global eosinophilia or increased recruitment, but likely by local proliferation of these cells. IL-5 is cytokine well known to induce local eosinophil proliferation (67, 133, 134). In fact, mRNA expression of *Il5* in epididymal AT closely correlated with the levels of eosinophils in this tissue. Furthermore, preliminary evidence indicates that the "M2" macrophages in this tissue are the main producers of this cytokine in AT. Eosinophils have been shown to sustain the "M2" activation of macrophages in the AT (49); thus, now we present evidence that "M2" cells are in turn probably inducing eosinophil local proliferation.

In conclusion, our data are the first to provide evidence for the aberrant accumulation of eosinophils in the AT of $CCR2^{-/-}$ mice, which is indirectly associated with improvements in inflammation and glucose tolerance. We found that eosinophils are also found in the AT of $CCR2^{+/+}$ mice (albeit in lower numbers) and that HFD diet reduces the numbers of eosionophils in these mice. Our study has provided *in vivo* evidence for the role of CCR2 in macrophage polarization in AT, as well as the sustainment of the levels of eosinophils in this tissue. Furthermore, we have highlighted the metabolic consequences of the aberrant accumulation of eosinophils in this tissue. The discovery of eosinophilia in the AT of $CCR2^{-/-}$ mice has large implications on the use of CCR2 antagonism as a therapy for chronic inflammatory diseases, as it could lead to undesired side effects associated with eosinophilia (135, 136). Future and ongoing studies will investigate the specific roles of these cells in AT function as well as confirm the mechanism for their accumulation.

CHAPTER V

COMPLEMENT FACTOR 5 DEFICIENCY LEADS TO SEVERE SYSTEMIC INSULIN RESISTSNCE, INDEPENDENT OF INFLAMMATION

(Adapted from Gutierrez *et al.* Manuscript in Preparation, 2012)

INTRODUCTION

The prevalence of adult and childhood obesity and associated co-morbidities has significantly increased in the past three decades in the United States and other industrialized nations (137, 138). Obesity is associated with a state of chronic inflammation that leads to IR in AT, muscle and the liver (139-141). IR is characterized by elevated circulating levels of pro-inflammatory cytokines, including tumor necrosis factor α (TNF-α), interleukin-6 (IL-6), monocyte chemoattractant protein 1 (MCP-1), IL-1β and C-reactive protein (142). Systemic inflammation, IR and subsequent β cell failure are the primary causes of T2DM (9).

The complement system is a vital component of the innate immune response (143). There are three known different complement activation pathways the classical, alternative, and lectin binding pathways. The classical pathway is activated by antigen-antibody complexes. The alternative pathway is initiated by surface molecules containing carbohydrates or lipids. The lectin-binding pathway is activated by the binding of mannose-binding lectin protein (58) to bacterial carbohydrate structures. High expression of complement components has been

shown in the omental AT of obese humans in comparison to lean individuals (81).

In this study, we examined the effects of deficiency in circulating C5 on systemic glucose tolerance and IR. Because C5a is a strong chemoattractant, we hypothesized that C5 deficiency would lead to decreased inflammation in AT and subsequent improved insulin sensitivity in a diet-induced obese mouse model. However, our studies show that C5 deficiency has no significant effects on AT and liver inflammation, but leads to severe glucose intolerance and systemic IR through the downregulation of the insulin receptor in liver, muscle and AT. These findings represent a novel role for a complement component in metabolism and introduce a novel mouse model for the study of IR and T2DM.

RESULTS

Complement Expression in AT and Liver of High Fat Fed Mice

C57BL/6 mice were fed either a: 10%, 45 % or 60% fat diet for 16 weeks. At the end of the study total mRNA was collected from AT and liver. Expression of complement factor 5 (*Hc*) was gradually increased in total AT as the percentage of fat in the diet increased; mice fed a 60% fat diet had a >10-fold increase in *Hc* expression when compared to mice fed a 10% diet (Figure 5.1A). *Hc* was unchanged in the liver with increasing diet fat percentage (Figure 1B). The expression of complement factor 3 (C3) and complement factor B, which are required for C5 cleavage, was unchanged in the AT and liver with HFD feeding (Figure 5.1 C-E). The expression of complement factor 6 (C6), which is required for the formation of the membrane attack complex with C5b and C7-9, was significantly reduced in both the AT ($P<0.01$) and liver ($P<0.05$) in the group fed a 60% fat diet (Figure 5.1 F-G).

Basal Parameters of C5D Mice

C5D and WT mice were weighed at 8 weeks of age before placement on a diet. C5D mice had a significantly lower body weight ($P<0.0001$) (Figure 5.2A). Body composition analysis showed that C5D mice had similar adiposity (Figure 5.2B) to that of WT controls but lower lean mass ($P<0.0001$) (Figure 5.2C). Baseline fasting glucose measurement showed that C5D mice were mildly

hypoglycemic (P<0.001; Figure 5.2D); however, this was accompanied by a 40% increase in fasting insulin levels (P<0.001; Figure 5.2E).

Weight Gain, Body Composition and Food Consumption

C5D and WT mice were placed on a LFD (10% fat) or HFD (60% fat) for 12 weeks. WT mice were significantly heavier than C5D mice after 5 weeks of HFD feeding (P<0.05). Mice on a LFD had similar end weight and weight gain rates (Figure 5.3A). Food consumption was not statistically different between groups; however, there was a trend towards higher Kcal/day consumption in both C5D LFD and HFD groups when compared to the WT mice in their respective diets (Figure 5.4). Body composition analysis showed the expected increase in adiposity in both the WT and C5D groups with HFD feeding after 6 (P<0.01; diet effect) and 12 weeks (P<0.001; diet effect) when compared to the LFD controls (Figure 5.3B & D). The WT HFD fed mice had significantly higher lean mass (P<0.05, 6 weeks; P<0.001, 12 weeks; diet effect) than their LFD controls, while lean mass remained unchanged between HFD and LFD groups in the C5D mice (Figure 5.3C & E). C5D mice had significantly lower adiposity after 6 (P<0.05; genotype effect) and 12 weeks (P<0.001; genotype effect) of HFD feeding when compared to HFD fed WT mice (Figure 5.3B& D). Total lean mass was not significantly different between HFD fed groups after either diet period (Figure 5.3C & E). Both HFD groups had significantly heavier (P<0.001; diet effect) epididymal AT pads than their LFD counterparts (Figure 5.3F). Epididymal AT pad weight at the end of the study was 33% lower (P<0.001; genotype effect) for

the C5D HFD mice when compared to the WT HFD controls (Figure 5.3F). HFD fed WT mice had significantly higher liver mass ($P<0.01$; diet effect) than their LFD counterparts; conversely, the liver weight between LFD and HFD fed C5D mice was not different (Figure 5.3G). HFD fed C5D mice had lower liver weights ($P<0.01$; genotype effect) than HFD WT mice (Figure 5.3G).

Bone Marrow and Blood Leukocytes

Bone marrow and blood leukocyte levels were measured by flow cytometry after 12 weeks on either a LFD or HFD. Cells were first gated on all DAPI-negative live cells. The cells were identified by their expression of the following extracellular markers: B cells ($CD19^+$), neutrophils ($CD11b^+Ly6G^{hi}$), $Ly6C^{hi}$ monocytes ($CD11b^+Ly6C^{hi}$), $Ly6C^{lo}$ monocytes ($CD11b^+Ly6C^{lo}$) and total T cells ($CD3^+$). There were no significant differences in any of the tested leukocytes in the bone marrow or blood between C5D and WT mice fed either a LFD or HFD (Figure 5.5A-B). The proportion of $CD4^+$ and $CD8^+$ T cells in either the blood or bone marrow were also not different between genotype and/or diets (data not shown).

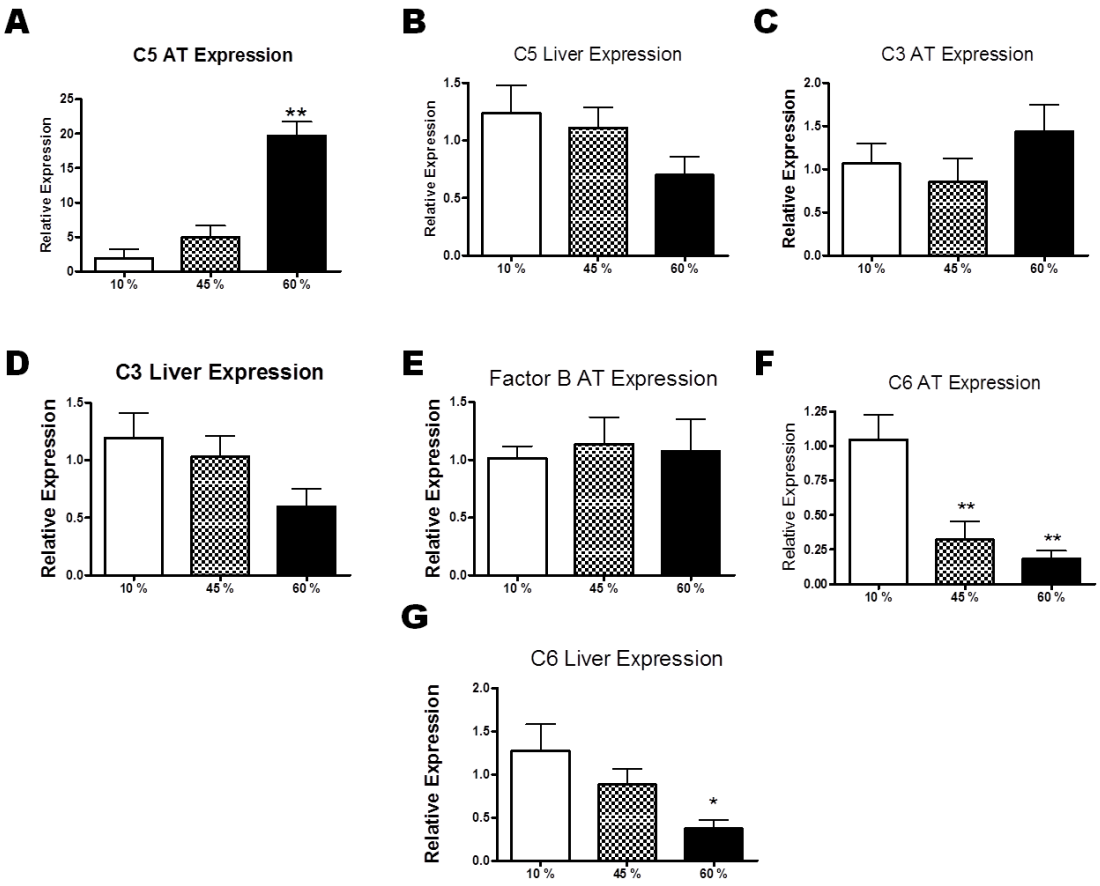

Figure 5.1 Complement expression in AT and liver during HFD feeding

C57BL/6 mice were placed on either a 10%, 45% or 60% fat diet for 16 weeks; total mRNA expression was assessed by real-time RT-PCR. *Hc* (C5) mRNA expression in the A) AT and B) liver. Expression of *C3* in: C) AT and D) liver. AT expression of: E) *Fb* and F) *C6*. G) Liver expression of *C6*. Data are presented as mean ± SEM (n=4-7).

*P<0.05; between 10% and 60%.

**P<0.01; between 60% group and 45% and 10% group.

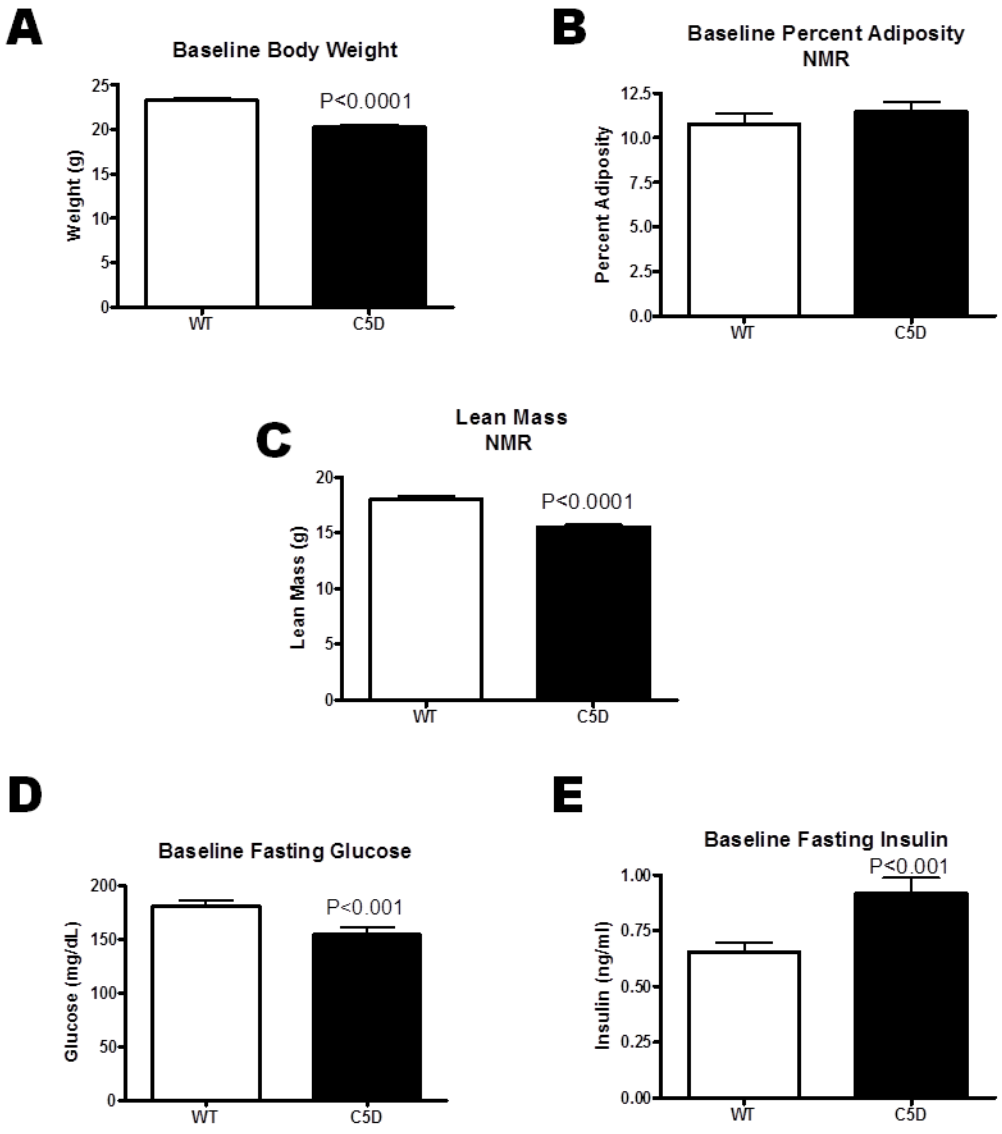

Figure 5.2 Basal parameters of WT and C5D mice

Eight week old B10.D2-*Hc*^{0} *H2*^{d} *H2-T18*^{c}/oSnJ (C5D) and C57BL/10SnJ (WT controls) were used in this study. Baseline: C) body weight; D) percent adiposity (total AT mass divided body weight); E) total lean mass; F) fasting glucose (5h morning fast) and G) Fasting Insulin (5h morning fast). Data are presented as mean ± SEM (n=26-27).

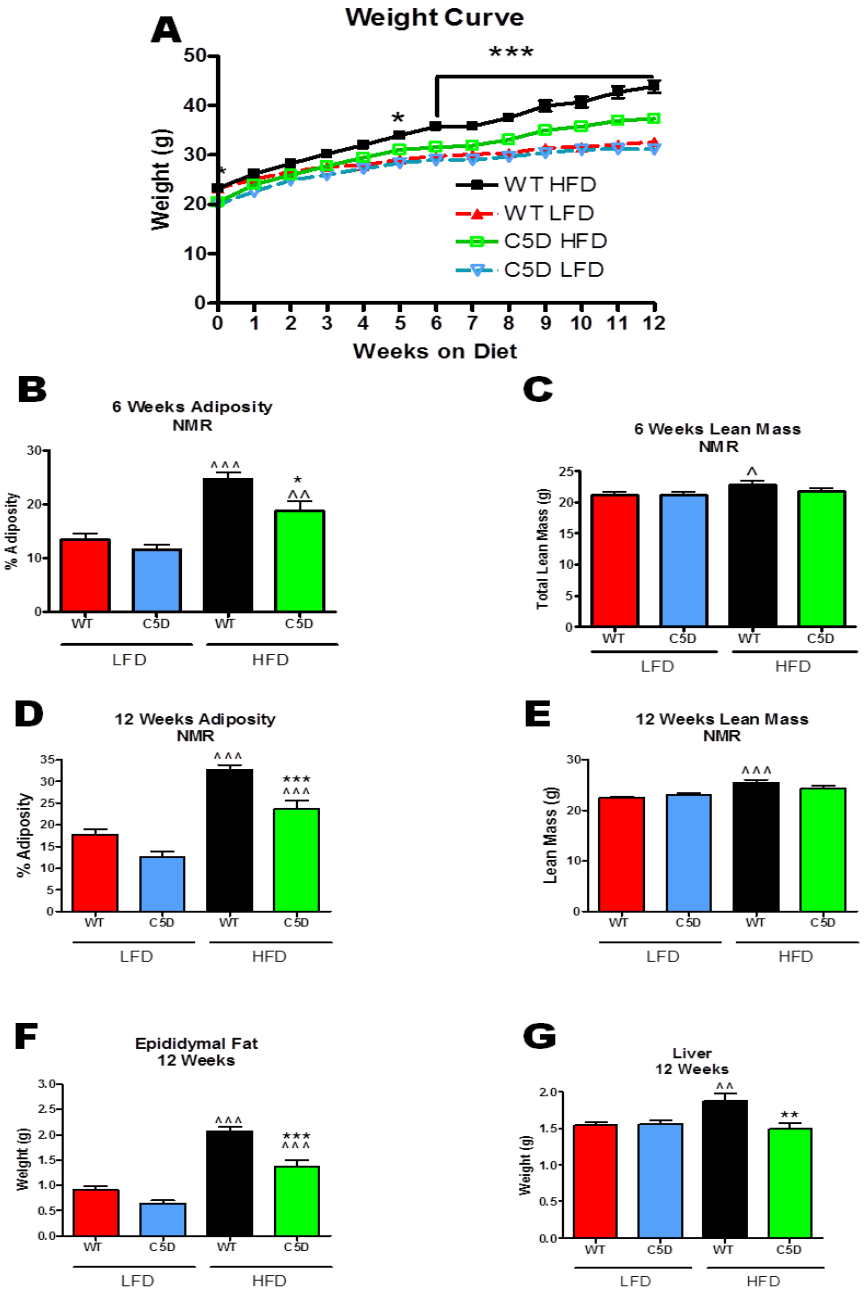

Figure 5.3 Metabolic Parameters of C5D mice.

WT and C5D mice were placed on either a 10% or 60% fat diet for 12 weeks. A) Weight curve of WT and C5D mice in both HFD and LFD diet (n=12-14). NMR-measured B) Percent adiposity and C) Total lean mass after 6 weeks of feeding (n=12-14). NMR-measured D) Percent adiposity and E) Total lean mass after 12

weeks of feeding (n=11-14). F) Epididymal fat pad weight and G) Liver weight at the end of the study (n=11-14). Data are presented as mean ± SEM.

*P<0.05; between WT and C5D HFD groups (genotype effect).

**P<0.01; between WT and C5D HFD groups (genotype effect).

***P<0.001; between WT and C5D HFD groups (genotype effect).

^P<0.05; diet effect

^^P<0.01; diet effect

^^^P<0.001; diet effect

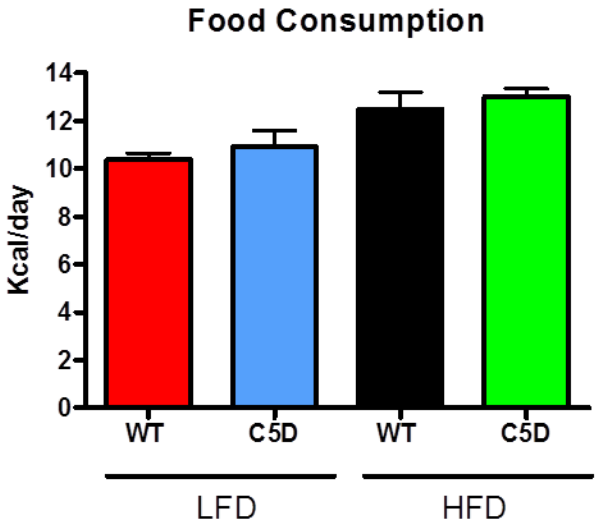

Figure 5.4 Food consumption.

Food intake was measured by calculating the daily difference between weight of initial food given and weight of food at the end of the week per mouse. Data are presented as Kcal/day per mouse. Data are presented as mean ± SEM (n=4-7).

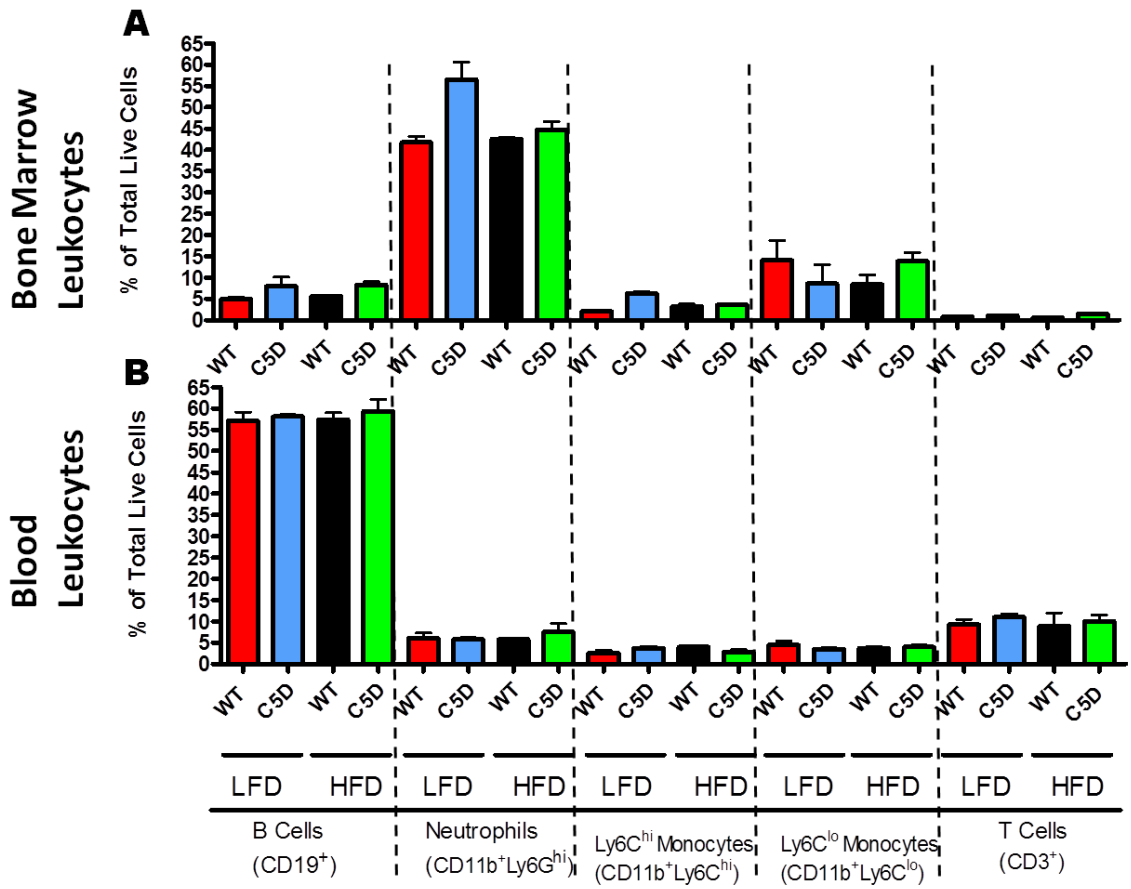

Figure 5.5 Bone marrow and blood leukocytes.

The levels of B cells, neutrophils, Ly6C^{hi} monocytes, Ly6C^{lo} monocytes and T cells from WT and C5D mice after 12 weeks on either a LFD or HFD diet were assessed by flow cytometry. Cells were first gated on the DAPI-negative live population. B cells were classified as all CD19(+) cells; Neutrophils CD11b(+)Ly6G(High); Ly6C^{hi} monocytes CD11b(+)Ly6C(High); Ly6C^{lo} monocytes CD11b(+)Ly6C(Low); T cells CD3ε(+). A) Quantification of flow cytometry data in bone marrow of LFD and HFD fed WT and C5D mice. B) Quantification of leukocytes in the blood of LFD and HFD fed WT and C5D mice. Data are presented as mean ± SEM (n=2-5).

AT Inflammation and Histology

AT inflammation was assessed by measuring the mRNA expression of several inflammatory and immune cell markers in all groups after 12 weeks of HFD feeding.(19, 24, 139) Expression of the cytokines *Il1β*, *Tnf*, *Ccl2* and *Il10* showed the expected increase with HFD feeding in both C5D and WT mice when compared to LFD controls; however statistical significance was only reached for *Tnf* ($P<0.001$) and *Ccl2* ($P<0.01$) in both genotypes, and *Il10* in the WT group ($P<0.00$; Figure 5.6A-D). Comparison of both HFD groups showed that C5D mice had similar *Il1β* and *Tnf* expression, a trend towards a reduction in *Ccl2* expression, and a significant reduction in *Il10* expression ($P<0.05$) (Figure 5.6A-D). Analysis of *Emr1* (F4/80) expression, a well established AT macrophage marker (24), showed a significant increase in macrophage content in the WT HFD mice when compared to the LFD counterparts ($P<0.001$; diet effect); this increase in *Emr1* expression was attenuated in the C5D mice (Figure 5.6E). Expression of the T cell marker *Cd3ε* was not different between groups (Figure 5.6F). Thus, contrary to our hypothesis, AT inflammation was not significantly affected by C5 deficiency.

The C57BL/6, B10.D2-*Hc*^{0} *H2*^{d} *H2-T18*^{c}/oSnJ (C5D) mice are able to transcribe *Hc* mRNA and synthesize the C5 protein; however, due to a 2-base pair deletion at the 5'-exon, they are not able to secrete this protein (144-146). We analyzed the effects of HFD feeding on *Hc* gene expression. Similar to what was observed in C57BL/6 mice, HFD feeding increased *Hc* expression in the WT

(C57BL/10) mice ($P<0.001$); this increase was completely attenuated in the C5D mice (Figure 5.6G). There was a small increase in the expression of C3 in HFD fed WT mice compared to WT LFD fed mice ($P<0.05$) and a trend towards an increase in C3 expression in C5D HFD fed mice when compared to their LFD counterparts (Figure 5.6H).

AT sections were stained with H&E and analyzed by light microscopy. Representative 100X and 400X images are shown (Figures 5.6I-N). The adipocyte diameter was increased in both HFD groups in comparison to their LFD counterparts ($P<0.001$). In addition, there was a significant decrease in adipocyte size in the C5D HFD group when compared to the WT HFD group ($P<0.05$) (Figure 5.6O). There was a trend towards a decrease in the number of crown-like structures in the HFD fed C5D mice when compared to the HFD WT mice (Figure 5.6P).

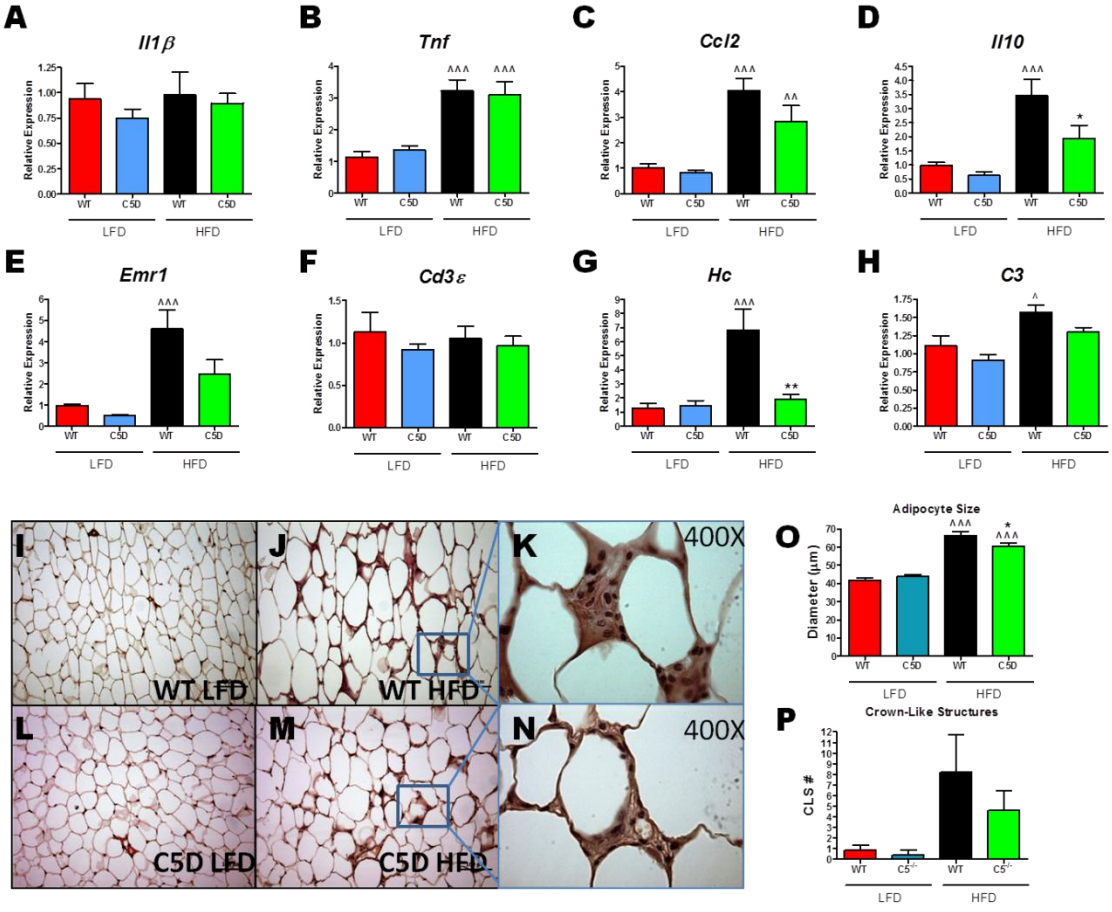

Figure 5.6 Adipose tissue inflammation and histology.

AT was collected at the end of the study for mRNA expression and histology analyses. Relative mRNA expression of: A) *Il1β*, B) *Tnf*, C) *Ccl2*, D) *Il10*, E) *Emr1*, F) *Cd3ε*, G) *Hc* and H) *C3*. Data are presented as mean ± SEM (n=11-13). Fixed AT sections were stained using H&E. Representative images of I) WT LFD mice (100X), J) WT HFD mice (100X) and K) WT HFD mice (400X). Representative images of: L) C5D LFD mice (100X), M) C5D HFD mice (100X) and N) C5D HFD mice (400X). O) Adipocyte diameter in micrometers (All adipocytes in 100X field counted; n=4) P) Number of crown-like structures per field. Data are presented as Mean ± SEM (n=3-4).

*P<0.05; between WT and C5D HFD groups (genotype effect).

**P<0.01; between WT and C5D HFD groups (genotype effect).

^P<0.05; diet effect

^^P<0.01; diet effect

^^^P<0.001; diet effect

Hepatic Inflammation and Function

The majority of complement proteins are synthesized in the liver, including most of the circulating C5 (61). Thus it is important to evaluate the effects of C5 deficiency on liver inflammation and function. Total liver RNA was isolated and mRNA expression levels were analyzed by real-time RT-PCR. Expression of the inflammatory cytokines *Il1β* and *Tnf* was not affected by the genotype or diet of the mice (Figure 5.7A-B). *Ccl2* expression was significantly increased ($P<0.05$; genotype effect) in C5D HFD mice when compared to WT HFD mice; there was a trend toward an increase in the expression of this gene in the C5D LFD group in comparison to the WT LFD group (Figure 5.7C). Expression of *Il10* was increased ($P<0.05$; diet effect) in the WT HFD group when compared to the WT LFD group and this increase was attenuated in the C5D HFD group (Figure 5.7D). The expression of the macrophage marker *Emr1* and the T cell marker *Cd3ε* was unchanged between genotypes and diets (Figure 5.7E-F).

Hepatocytes are the main producers of C5 in the body. In fact, the levels of *Hc* transcript in the livers of WT LFD mice are 4700-fold higher than the levels of this transcript in total AT of the same mice. The expression of the *Hc* gene was significantly decreased ($P<0.001$; genotype effect) in both LFD and HFD C5D mice in comparison to their WT counterparts, indicating a downregulation of this transcript upon the lack of C5 protein secretion (Figure 5.7G). Conversely, the transcription of C3 was unaffected by C5 deficiency, and similar to the expression in the C57BL/6 mice, it was unchanged by HFD feeding (Figure 5.7H).

Frozen liver sections were stained with H&E and images captured by light microscopy. Representative 100X images are shown (Figure 5.7I-L). These images showed no gross morphological differences between genotypes and diets. Additionally, no overt differences in immune cell infiltration were observed.

In view of the fact that C5 is synthesized at high levels in the hepatocytes of C5D mice, but not secreted (144-146), this condition could lead to endoplasmic reticulum stress (ER stress) and/or oxidative stress and ER stress-induced inflammation. We tested several markers of ER stress, oxidative stress and inflammation by Western blot analysis. Contrary to what was expected, the protein levels of the ER stress marker IRE-1α were decreased ($P=0.0553$; genotype effect) in C5D LFD mice when compared to WT LFD mice. The protein levels of the ER stress marker BiP, the phosphorylation levels of the inflammatory mediator JNK1/2 and the protein levels of the oxidative stress marker SOD-2 were unchanged between both LFD groups (Figure 5.8A & C). Similarly to the LFD groups, total IRE-1α expression was significantly ($P<0.05$) decreased in the C5D HFD group when compared to the WT HFD group. Additionally, levels of BiP, phospho-JNK1/2 and SOD-2 were unchanged in the C5D HFD group when compared to the WT HFD mice (Figure 5.8B & D).

Liver triglyceride content was measured by gas chromatography mass spectrometry. Hepatic triglyceride content increased in WT mice with HFD diet feeding ($P<0.001$; diet effect). However, this increase in triglycerides with HFD feeding was attenuated in C5D mice (Figure 5.9A). In fact, total triglyceride

content in the C5D HFD group was 70% lower in comparison to the WT HFD group ($P<0.001$; genotype effect). In support of the mass spectrometry data, Oil Red O staining of liver sections showed a marked increase in neutral lipid staining in WT HFD mice in comparison to LFD fed WT mice (Figure 5.9C). In contrast, the liver images from C5D HFD fed mice (Figure 5.9E) show an attenuation in the accumulation of neutral lipid when compared to C5D LFD fed mice and WT HFD fed mice (Figure 5.9E). Hepatic lipid content is regulated by lipid and glucose metabolism in the liver. We assessed the gene expression of genes associated with gluconeogenesis, glycolysis, fatty acid synthesis and fatty acid oxidation. The expression of the gluconeogenic protein glucose-6-phosphatase was paradoxically decreased with HFD feeding on the WT mice ($P<0.01$; diet effect); however, there was no diet effect found in the C5D mice (Figure 5.9F). Conversely, the expression of phosphoeno pyruvate carboxykinase another gluconeogenic enzyme was increased with HFD feeding in C5D mice ($P<0.05$; diet effect) and there was a trend towards an increase in HFD fed WT mice in comparison to LFD fed WT mice (Figure 5.9G). Expression of the hepatic glycolytic enzyme glucokinase was not affected by the genotype or diet of the mice (Figure 5.9H). Acetyl CoA carboxylase, an enzyme important in fatty acid synthesis, was decreased with HFD feeding in both WT ($P<0.001$; diet effect) and C5D ($P<0.001$; diet effect) mice (Figure 5.9I). In contrast there was an increase in the expression of the β oxidation enzyme, peroxisomal acyl-coenzyme A oxidase, with HFD feeding ($P<0.001$; diet effect); this increase was attenuated in HFD fed C5D mice (Figure 5.9J).

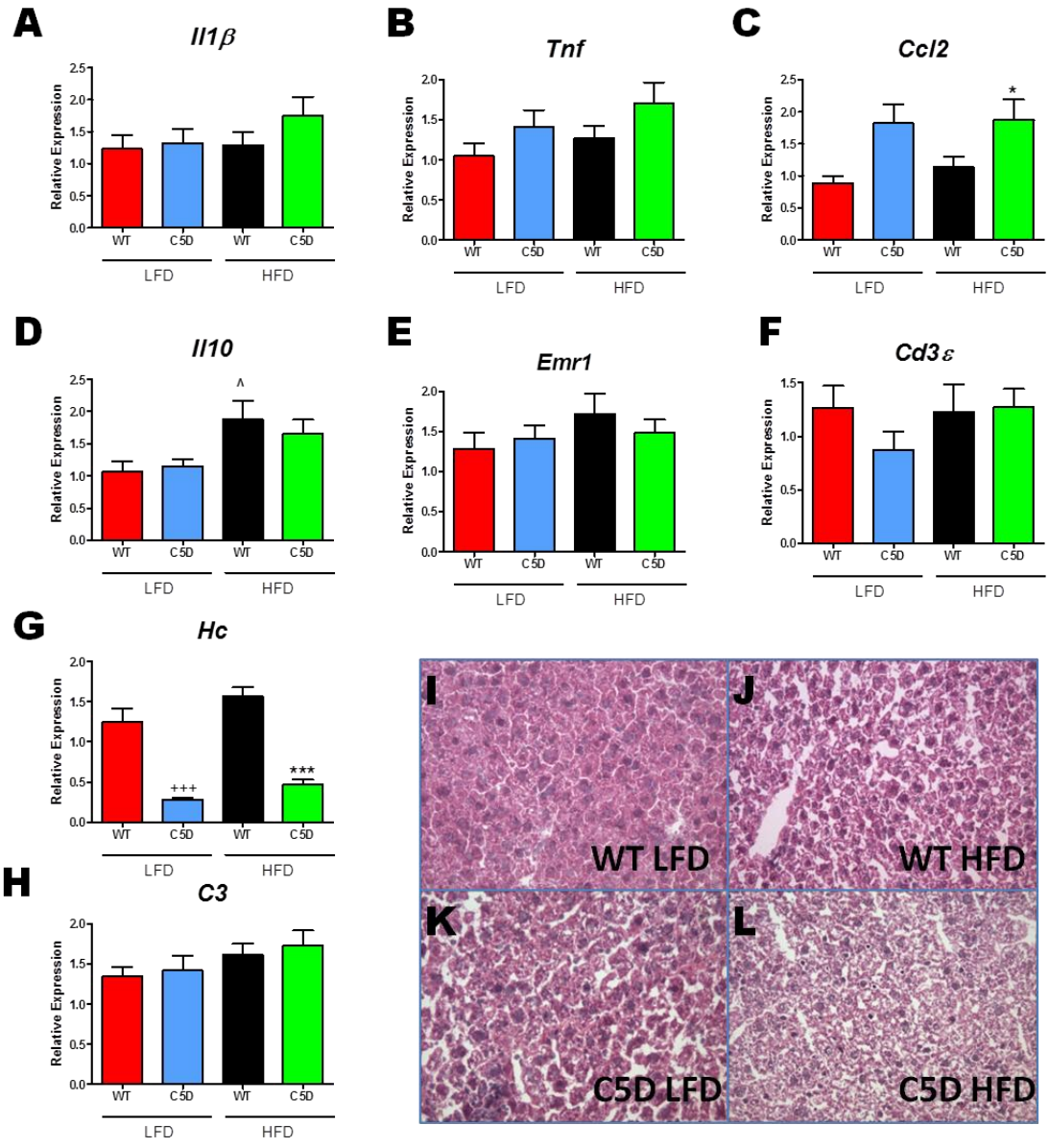

Figure 5.7 Hepatic inflammation and histology.

Liver sections were collected at the end of the study and used for mRNA expression and histology analyses. Relative mRNA expression of: A) *Il1β*, B) *Tnf*, C) *Ccl2*, D) *Il10*, E) *Emr1*, F) *Cd3ε*, G) *Hc* and H) *C3*. Data are presented as mean ± SEM (n=11-13). Frozen liver sections were stained by H & E. Representative (100X) images of: I) WT LFD mice, and J) WT HFD mice. Representative images of: K) C5D LFD mice and L) C5D HFD mice.

*P<0.05; between WT and C5D HFD groups (genotype effect).

***P<0.001; between WT and C5D HFD groups (genotype effect).

+++P<0.001; between WT and C5D LFD groups (genotype effect).

^P<0.05; diet effect

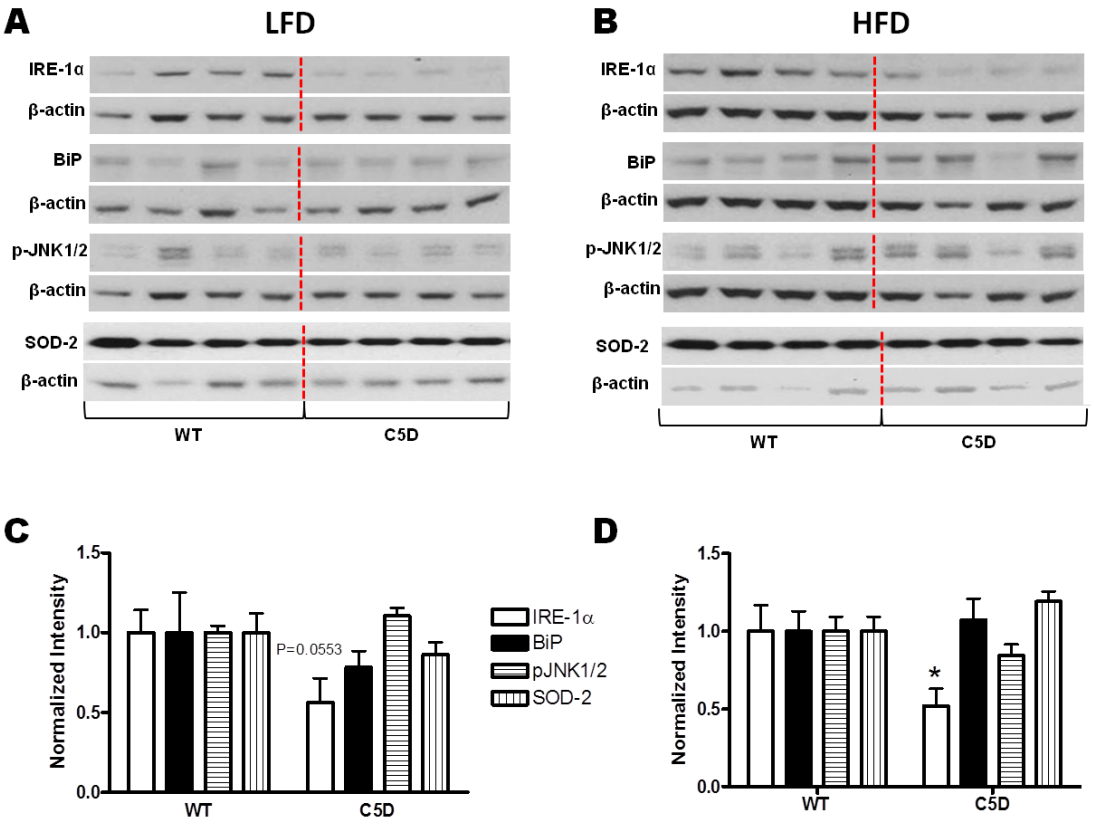

Figure 5.8 Hepatic ER- and oxidative-stress markers.

Protein lysates were prepared from the livers of the mice. Western blot analysis was conducted to measure the protein expression of IRE-1α, BiP, phospho-JNK, and SOD2 in A) LFD and B) HFD WT and C5D mice. β-actin was used as a protein loading control. Quantification of IRE-1α, BiP, phospho-JNK, and SOD2 protein expression in C) LFD and D) HFD WT and C5D mice. Data are presented as mean ± SEM (n=8).

*P<0.05; between WT and C5D HFD groups (genotype effect).

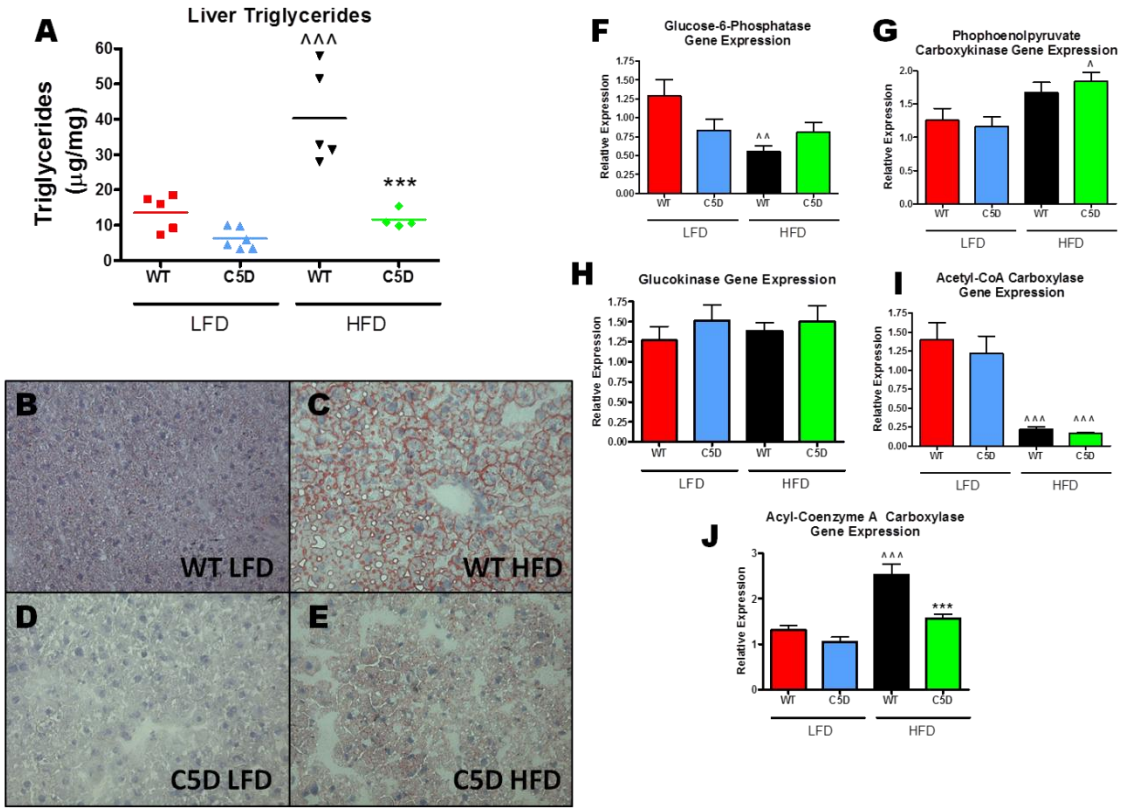

Figure 5.9 Hepatic lipid and glucose metabolism.

Total liver triglyceride content in LFD and HFD fed WT and C5D mice was assessed by mass spectrometry. A) Levels of triglyceride in WT and C5D mice presented as micrograms of triglyceride per milligram of liver (n=4-6). Frozen liver sections were stained with Oil-Red-O, which stains all neutral lipids. B-E) Representative 100X images of Oil-Red-O stained liver sections of LFD and HFD fed WT and C5D mice. Liver sections were collected at the end of the study and used for mRNA expression analysis. Relative mRNA expression of: F) *G6pc*, G) *Pck1*, H) *Gck*, I) *Acacb*, J) *Acox1*. Data are presented as mean ± SEM (n=11-13).

***P<0.001; between WT and C5D HFD groups (genotype effect).

^P<0.05; diet effect

^^P<0.01; diet effect

^^^P<0.001; diet effect

C5D Mice Have Severe Glucose Intolerance and Insulin Resistance

It is well established that HFD feeding leads to glucose intolerance and IR (36). A glucose tolerance test (GTT) was performed on the mice 6 weeks after LFD or HFD feeding. The WT HFD mice (black solid line & square) were significantly more glucose intolerant than the WT LFD group ($P<0.05$; diet effect) (red dashed line & solid triangle) at 30 minutes post-glucose injection and there was a trend towards more glucose intolerance in the WT HFD group at every other time point. The C5D HFD group (green line & open square) had significantly more glucose intolerance than the C5D LFD group (blue dashed line & open triangle) after 60 ($P<0.05$; diet effect), 90 ($P<0.001$; diet effect) and 120 ($P<0.001$; diet effect) minutes post injection; thus demonstrating a diet effect on glucose intolerance in C5D mice. Furthermore, when comparing the WT and C5D mice, C5 deficiency led to severe glucose intolerance in both the HFD ($P<0.05$, 45 min; $P<0.001$ 60-120 min; genotype effect) and LFD mice ($P<0.01$, 45, 90 min; $P<0.05$, 45 min; genotype effect) (Figure 5.10A). A second GTT was performed after 12 weeks of LFD or HFD feeding. As expected due to longer time on HFD, a more severe diet effect was observed between the HFD and LFD fed WT ($P<0.05$; diet effect) and C5D mice ($P<0.05$; diet effect). Additionally, there was a strong genotype effect; C5D HFD fed mice were significantly more glucose intolerant than WT HFD mice ($P<0.01$ 30 min; $P<0.001$ 45-150 min). The genotype effect was also present on the LFD fed mice, where the C5D mice were significantly ($P<0.01$; 45-90 min) more glucose intolerant than their WT counterparts (Figure 5.10B).

To investigate if the observed glucose intolerance was due to an insulin secretion defect by the β cells or due to systemic IR, fasting insulin levels were measured by ELISA. After 6 weeks on the diet, HFD fed C5D mice had 83% more circulating insulin than LFD C5D mice ($P<0.01$; diet effect) (Figure 5.10C). High fat fed C5D mice had 1.6-fold ($P<0.001$; genotype effect) more circulating insulin than the HFD fed WT mice (Figure 5.10C). At the 12 week time point there was a 1.25-fold ($P<0.01$; genotype effect) increase in fasting insulin in the C5D LFD group when compared to the WT LFD group ($P<0.01$; genotype effect). Both the C5D and WT HFD groups had significantly higher fasting insulin than the corresponding LFD groups ($P<0.05$; diet effect; Figure 5.10D).

To further analyze islet physiology and function in these mice we performed H&E and insulin immunohistochemistry on frozen pancreata sections. H&E staining images showed no overt defects on the islets of either genotype and/or diet, there were also no signs of insulitis or pancreatitis (data not shown). Insulin immunohistochemistry images showed no obvious differences in islet morphology; additionally, we observed an overall increase in islet size with HFD feeding, consistent with the fasting insulin levels observed after 12 weeks of HFD feeding. Representative insulin immunohistochemistry images are shown in Figure 5.10E-H.

The WT controls utilized throughout most of this study are on a C57BL/10 background with a $MHCII^{b}$ haplotype. The C5D mice are also on C57BL/10 background, but have a $MHCII^{d}$ haplotype. To test whether the phenotype

observed in these mice was due to the deficiency in C5 and not the different haplotypes, we performed a separate study to measure the glucose tolerance of C5D MHCII^{d}, WT MHCII^{b} and WT MHCII^{d} mice. Similarly to the previous study, after 6 and 12 weeks of HFD feeding, C5D mice were more glucose intolerant than WT MHCII^{b} mice, which were more glucose intolerant than WT MHCII^{d} mice (C5D > MHCII^{b} > MHCI (Figure 5.11A-B). Thus, we can rule out the haplotype difference as being responsible for the insulin resistant phenotype noted in the C5D mice.

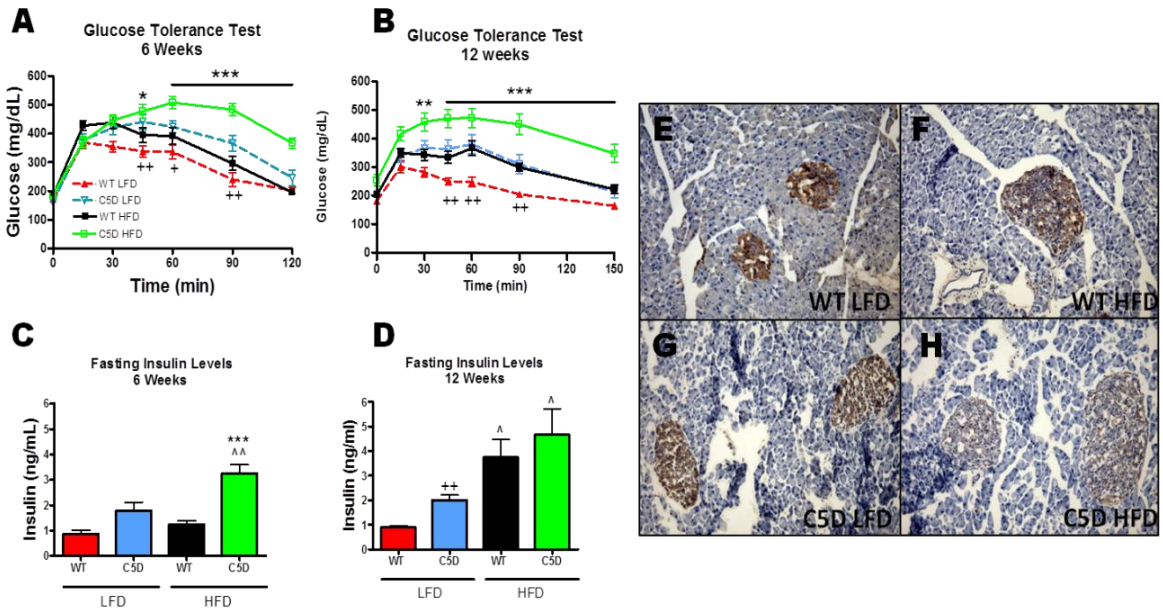

Figure 5.10 Glucose tolerance, insulin resistance and islet histology.

After a 5h fast mice were injected with 1 g of dextrose per kg of lean mass, and glucose clearance was tracked for 120 or 150 min. A) Glucose tolerance test curve after 6 weeks of diet feeding for LFD and HFD fed WT and C5D mice (n=9-13). B) Glucose tolerance test curve after 12 weeks of diet feeding for LFD and HFD fed WT and C5D mice (n=11-14). Fasting insulin levels after a 5h fast following C) 6 weeks (n=10-14) and D) 12 weeks of HFD feeding (n=10-13). E-H) Representative 100X images of pancreas sections stained by immunohistochemistry using an antibody against insulin. Staining performed in the Vanderbilt IHC core.

*P<0.05; between WT and C5D HFD groups (genotype effect).

**P<0.01; between WT and C5D HFD groups (genotype effect).

***P<0.001; between WT and C5D HFD groups (genotype effect).

+P<0.05; between WT and C5D LFD groups (genotype effect).

++P<0.01; between WT and C5D LFD groups (genotype effect).

+++P<0.001; between WT and C5D LFD groups (genotype effect).

^P<0.05; diet effect

^^P<0.01; diet effect

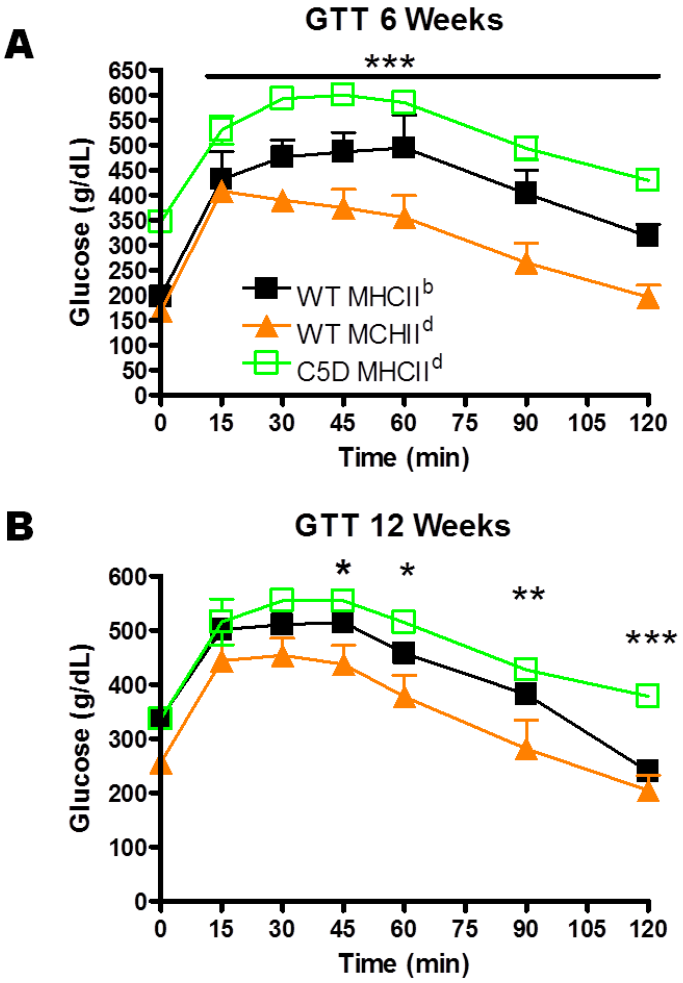

Figure 5.11 Glucose tolerance tests for the WT MHCII^b, WT MHCII^d and C5D MHCII^d study.

After a 5h fast mice were injected with 1 g of dextrose per kg of lean mass, and glucose clearance was tracked for 120 min. A) Glucose tolerance test curve after 6 weeks of HFD feeding for WT MHCII^b, WT MHCII^d and C5D MHCII^d mice. B) Glucose tolerance test curve after 12 weeks of HFD feeding for WT MHCII^b, WT MHCII^d and C5D MHCII^d mice. Data are presented as mean ± SEM (n=3-4).

*P<0.05; between WT MHCII^d and C5D MHCII^d HFD groups.

**P<0.01; between WT MHCII^d and C5D MHCII^d HFD groups.

***P<0.001; between WT MHCII^d and C5D MHCII^d HFD groups.

Mechanism(s) for Insulin Resistance

Given the absence of a genotype effect on AT and hepatic inflammation, we sought to find inflammation-independent mechanisms for the observed IR in the C5D mice. Analysis of the mRNA expression of the insulin receptor (*Insr*) showed a ~ 50% decrease ($P<0.001$; genotype effect) in *Insr* expression in both the liver and AT of C5D mice fed a low or high fat diet (Figure 5.12A-B). The expression of other molecular components that modulate insulin signaling was also assessed. There were no genotype or diet effects on the hepatic mRNA expression of insulin-like growth factor 1 receptor (*Igf1r*), the insulin-like growth factor 1 (*Igf1*), *Irs1*, *Irs2* or the insulin-like growth factor binding protein 3 (*Igfbp3*) (Figure 5.13). Western blot analysis using an antibody against the β subunit of the INSR showed a >60% decrease ($P<0.01$; genotype effect) in the mature active form of this subunit in LFD fed C5D mice, in the liver (Figure 5.14A), AT (Figure 5.14C) and skeletal muscle when compared to the WT LFD group (Figure 5.14). Similar results were obtained for the HFD fed groups (Figure 5.15).

Analysis of AKT phosphorylation at serine 473, which is a mediator downstream of INSR signaling, showed increased phosphorylation in the livers of WT LFD mice 15 min after a bolus injection of 1.0 U of insulin per kilogram of lean mass, when compared to mice injected with saline ($P<0.001$). Interestingly, this increase in AKT phosphorylation was blunted in C5D LFD mice (Figure 5.14B). Similar to the liver, AKT phophorylation in AT was increased in WT LFD mice after insulin injection, and this increase in phosphorylation was blunted in

the C5D LFD mice ($P<0.01$) (Figure 5.14D). AKT phosphorylation in the liver and AT after insulin injection was blunted in both HFD groups; however, the WT HFD mice had a trend towards increased phosphorylation when injected with insulin, while AKT phosphorylation remained virtually unchanged in the C5D group after the injection (Figure 5.15B & D). Unlike the liver and AT, AKT phosphorylation in the skeletal muscle was not disrupted by C5 deficiency (Figure 5.14F & Figure 5.15F), despite the observed decrease in INSR β expression.

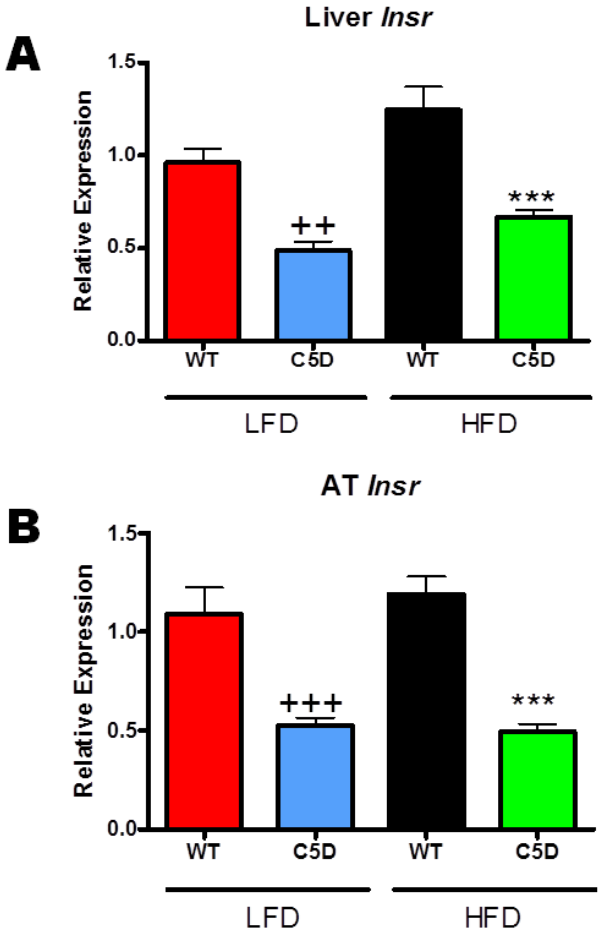

Figure 5.12 Insulin receptor mRNA expression in the liver and AT.

Total RNA was collected from liver and AT at the end of the study and used for real-time RT-PCR analysis. Expression of *Insr* in the: A) Liver and B) AT after 12 weeks of LFD or HFD feeding in WT and C5D mice. Data are presented as mean ± SEM (n=11-13).

***P<0.001; between WT and C5D HFD groups (genotype effect).

++P<0.01; between WT and C5D LFD groups (genotype effect).

+++P<0.001; between WT and C5D LFD groups (genotype effect).

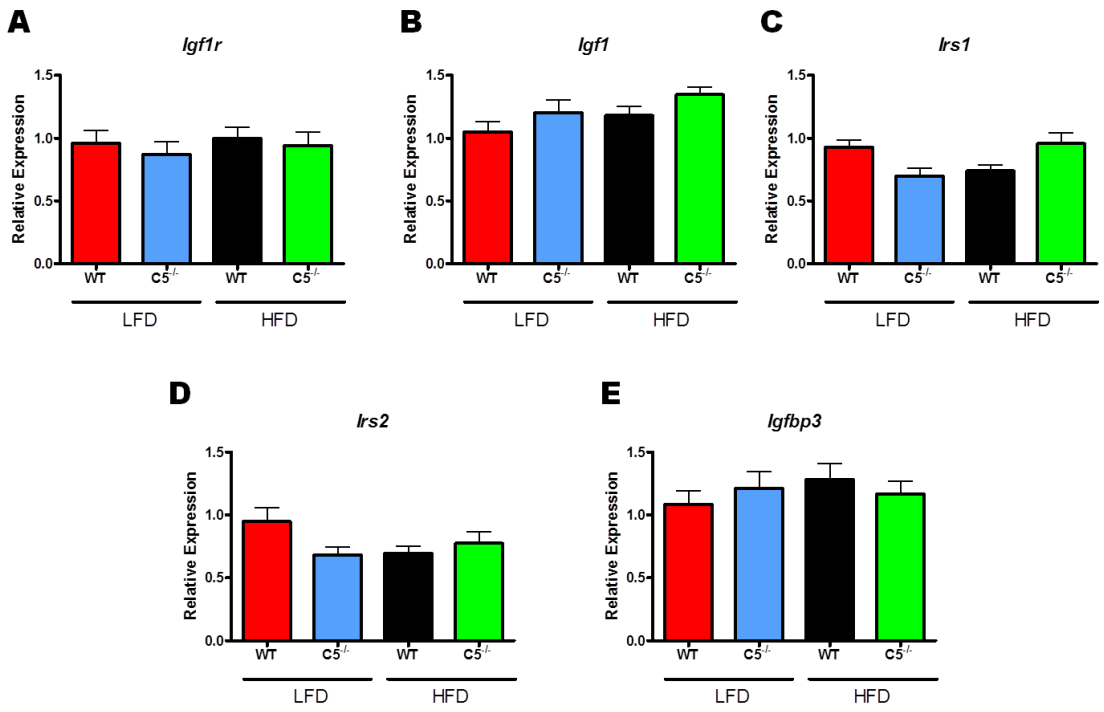

Figure 5.13 Gene expression of modulators of insulin signaling in the liver.

Liver sections were collected at the end of the study and used for mRNA expression analysis. Relative mRNA expression of: A) *Igf1r*, B) *Igf1*, C) *Irs1*, D) *Irs2*, E) *Igfbp3*. Data are presented as mean ± SEM (n=11-13).

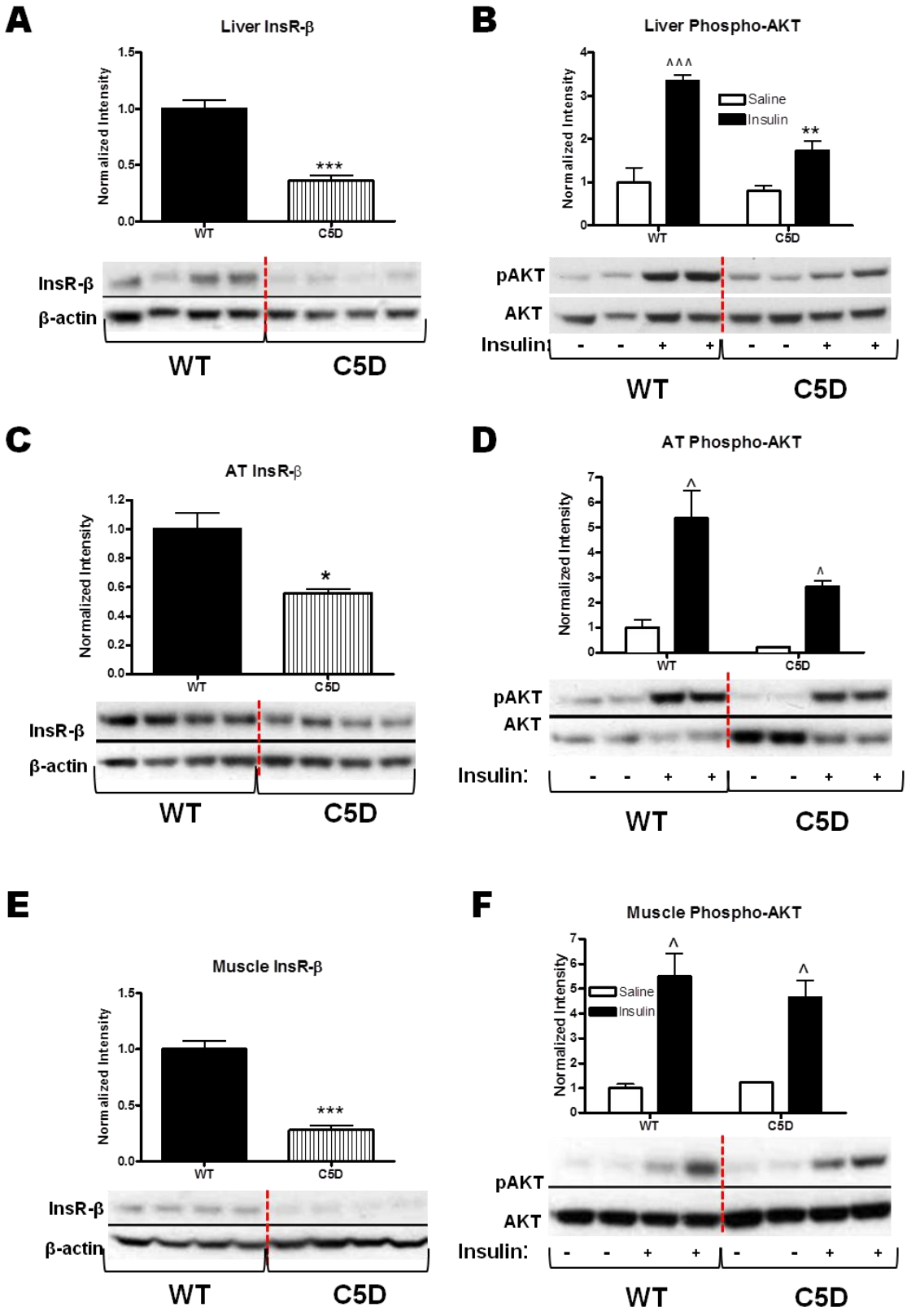
A
Liver InsR-β
Normalized Intensity
1.5
1.0
0.5
0.0
***
WT
C5D
InsR-β
β-actin
WT
C5D
B
Liver Phospho-AKT
Normalized Intensity
4
3
2
1
0
^^^
**
Saline
Insulin
WT
C5D
pAKT
AKT
Insulin:
- - + + - - + +
WT
C5D
C
AT InsR-β
Normalized Intensity
1.2
1.0
0.8
0.6
0.4
0.2
0.0
*
WT
C5D
InsR-β
β-actin
WT
C5D
D
AT Phospho-AKT
Normalized Intensity
7
6
5
4
3
2
1
0
^
^
WT
C5D
pAKT
AKT
Insulin:
- - + + - - + +
WT
C5D
E
Muscle InsR-β
Normalized Intensity
1.5
1.0
0.5
0.0
***
WT
C5D
InsR-β
β-actin
WT
C5D
F
Muscle Phospho-AKT
Normalized Intensity
7
6
5
4
3
2
1
0
^
^
Saline
Insulin
WT
C5D
pAKT
AKT
Insulin:
- - + + - - + +
WT
C5D

Figure 5.14 Levels of insulin receptor protein and insulin signaling in liver, AT and muscle of LFD fed WT and C5D mice.

Protein lysates were collected from liver, AT, and muscle of LFD fed WT and C5D mice at the end of the study, and protein expression and phosphorylation levels assessed by Western blot analysis. A) INSR-β expression (n=8) and B) Phopho-AKT levels in the liver (n=2-6). C) INSR-β expression (n=8) and D) Phopho-AKT levels in the AT (n=2-6). E) INSR-β expression (n=8) and F) Phopho-AKT levels in the muscle (n=2-6). Data are presented as mean ± SEM.

*P<0.05; between WT and C5D LFD groups (genotype effect).

**P<0.01; between WT and C5D LFD groups (genotype effect).

***P<0.001; between WT and C5D LFD groups (genotype effect).

^P<0.05 between saline injected and insulin injected LFD WT and C5D mice.

^P<0.05 between saline injected and insulin injected LFD WT and C5D mice.

^^^P<0.05 between saline injected and insulin injected LFD WT and C5D mice.

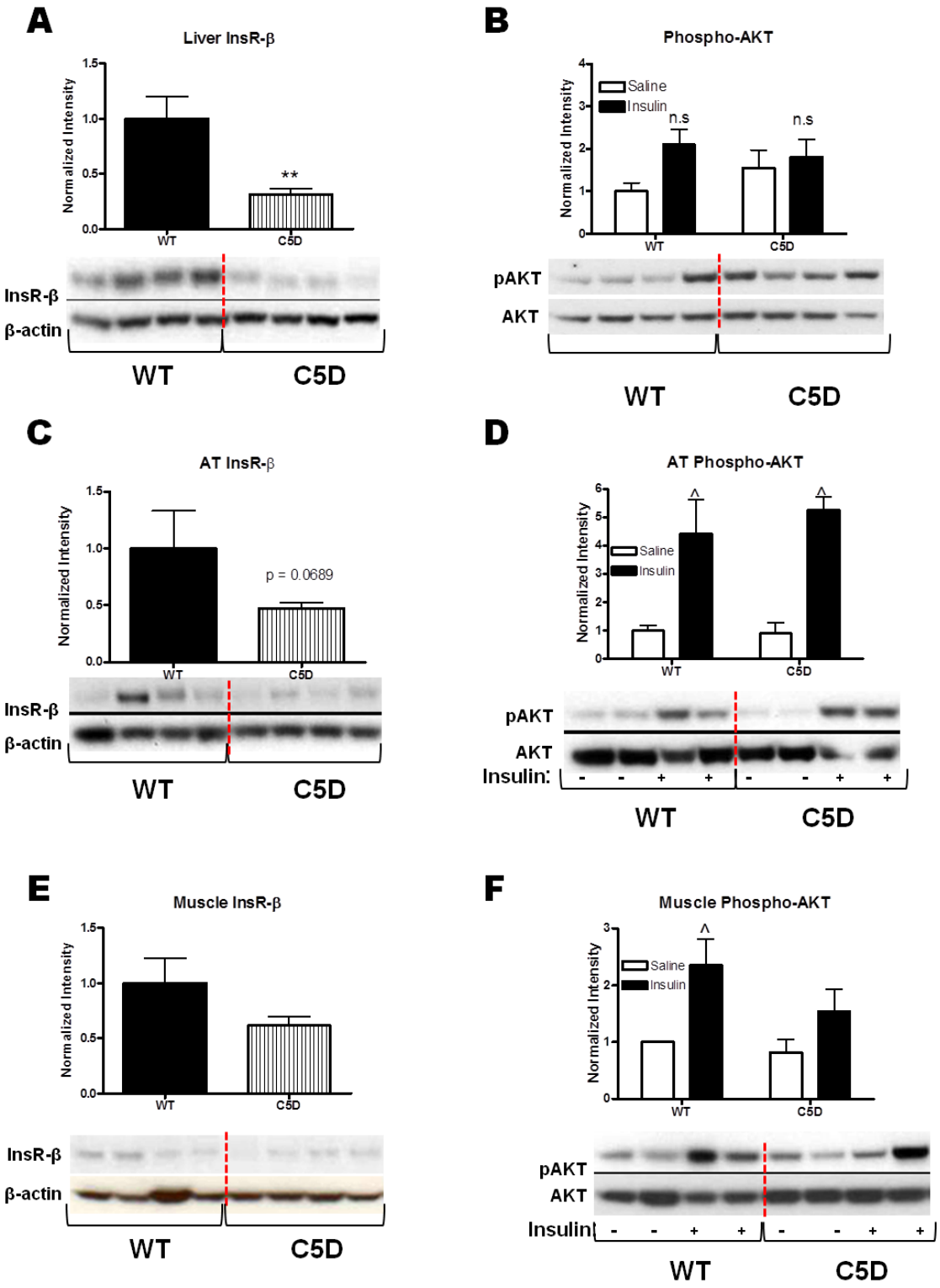
A
Liver InsR-β
Normalized Intensity
1.5
1.0
0.5
0.0
**
WT
C5D
InsR-β
β-actin
WT
C5D
B
Phospho-AKT
Saline
Insulin
n.s
n.s
Normalized Intensity
4
3
2
1
0
WT
C5D
pAKT
AKT
WT
C5D
C
AT InsR-β
Normalized Intensity
1.5
1.0
0.5
0.0
p = 0.0689
WT
C5D
InsR-β
β-actin
WT
C5D
D
AT Phospho-AKT
Saline
Insulin
Normalized Intensity
6
5
4
3
2
1
0
^
^
WT
C5D
pAKT
AKT
Insulin:
- - + + - - + +
WT
C5D
E
Muscle InsR-β
Normalized Intensity
1.5
1.0
0.5
0.0
WT
C5D
InsR-β
β-actin
WT
C5D
F
Muscle Phospho-AKT
Saline
Insulin
Normalized Intensity
3
2
1
0
^
WT
C5D
pAKT
AKT
Insulin
- - + + - - + +
WT
C5D

Figure 5.15 Levels of insulin receptor protein and insulin signaling in liver, AT and muscle of HFD fed WT and C5D mice.

Protein lysates were collected from liver, AT and muscle of HFD fed WT and C5D mice at the end of the study; protein expression and phosphorylation levels were assessed by Western blot analysis. A) INSR-β expression (n=8) and B) Phopho-AKT levels in the liver (n=2-6). C) INSR-β expression (n=8) and D) Phopho-AKT levels in the AT (n=2-6). E) INSR-β expression (n=8) and F) Phopho-AKT levels in the muscle (n=2-6). Data are presented as mean ± SEM.

**P<0.01; between WT and C5D HFD groups (genotype effect).

^P<0.05 between saline injected and insulin injected HFD WT and C5D mice.

The Pro-INSR in C5D Mice Has a Differential Glycosylation State

In view of the fact that the decrease in mature INSR levels was greater than that observed in the *Insr* message, we assessed whether there was a defect in post-transcriptional processing of the INSR. We used an antibody against the β subunit of the INSR, which recognizes both the mature β subunit and the precursor for the insulin receptor (pro-INSR). Two different lanes of the pro-INSR were detected for the liver (Figure 5.16A) and AT (Figure 5.16B) of C5D mice at ~ 190 and 180 KDa, while only the 190 KDa lane was detected in the WT mice. In contrast, the skeletal muscle of the C5D mice have, only one pro-INSR lane (Figure 5.16C), similarly to the WT mice.

Incubation of liver protein lysates from C5D and WT mice with N-glycosidase F (PNGase F), leads to the formation of a single 170 KDa sized protein, which corresponds to the non-glycosylated pro-INRS molecular weight, and the disappearance of the 190 and 180 KDa lanes in the C5D mice (Figure 5.16D). This indicated that C5D mice have differential glycosylation of the pro-INSR protein in comparison to the WT mice.

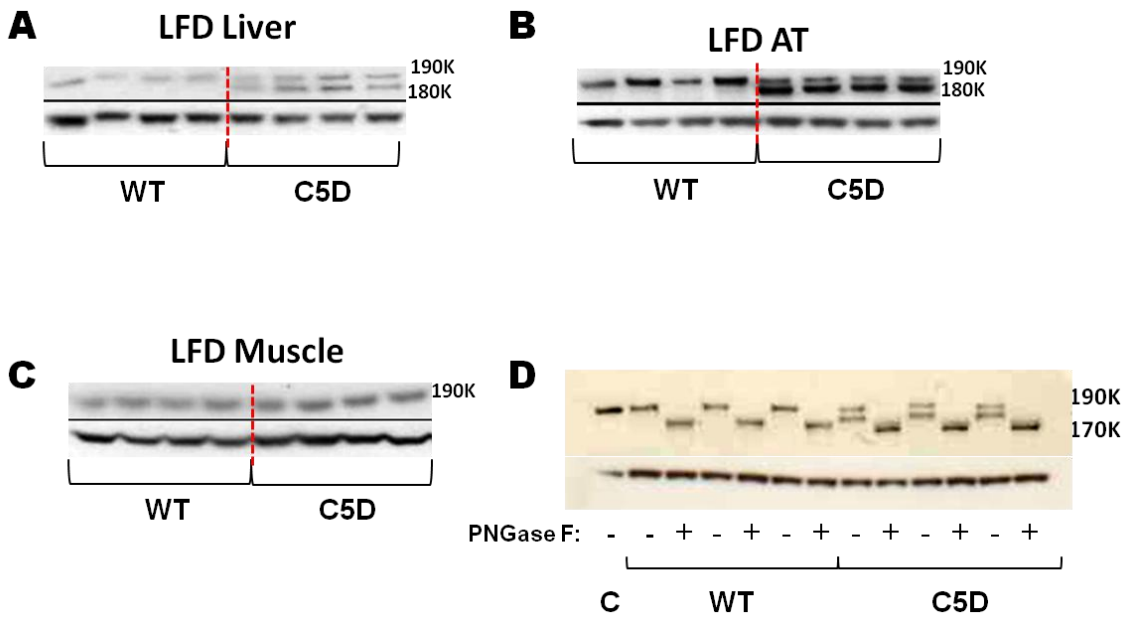

Figure 5.16 Differential glycosylation of the INSR of C5D mice.

Western blot analysis of the precursor of INSR (pro-INSR) in the: A) liver, B) AT, and C) muscle (190 KDa lane is fully glycosylated pro-INSR; 180 KDa lane is partially glycosylated pro-INSR). An F-glycosidase reaction of liver protein samples from LFD WT and C5D mice was performed. D) Western blot analysis of pro-INSR in protein samples of LFD WT and C5D mice incubated with (+) or without (-) PNGase F (190 KDa: fully glycosidated; 170 KDa: no glycosylation). (n=4).

DISCUSSION

The complement system, an important component of the innate immune system, is activated in response to pathogen invasion and in several diseases. Several roles for the cleavage products of C5 during infection have been identified, including: recruitment and activation of inflammatory cells, induction of phagocytosis, oxidative burst, release of granule enzymes, cell lysis, and hematopoiesis (61). Furthermore, C5 has been shown to play important non-inflammatory homeostatic functions such as promotion of tissue regeneration and angiogenesis (147), stem cell mobilization (148), development of the central nervous system and embryogenesis (149). However, to this date, no studies have evaluated the effects of C5 deficiency on either normal metabolism or obesity. Our studies showed that C5 plays a vital inflammation-independent role in metabolism, and its deficiency leads to the dysregulation of glucose metabolism by disrupting insulin signaling in both the lean and obese states.

The complement system, specifically the cleavage products of C5, has been shown to play a role in stem cell mobilization from the bone marrow into the circulation (148, 150). Leukocyte mobilization from the bone marrow into the circulation and into tissues is an important factor in tissue inflammation and its disruption leads to changes in the inflammatory sate of the target tissue. Such is the case of CCR2 deficiency, where blunted egress of $Ly6C^{hi}$ monocytes leads to changes in the inflammatory state of AT (35,37,111). Therefore, it was important to examine if C5 deficiency affected the levels of leukocytes that could impact

inflammation and thus metabolism. We analyzed the levels of bone marrow and blood leukocytes by flow cytometric analysis and found no overt differences in the levels of B cells, neutrophils, monocytes or T cells in either the bone marrow or blood of C5D mice when compared to WT mice, regardless of the diet (Figure 5.5). Thus any changes observed in the metabolic state of these mice were unlikely to be due to differences in leukocyte populations.

Recently the immune system has been shown to play a pivotal role in metabolism, especially in the obese state (141). However, the role of the immune system in immunometabolism has always been associated with regulating/causing a heightened state of inflammation observed during obesity (139). Of vast importance is the presence of macrophages and other immune cells in AT and their role in their regulation of AT function and insulin sensitivity (25, 54). The current study was designed with the hypothesis that C5 deficiency would lead to decreased AT inflammation and thus improved insulin sensitivity in the obese state. However, our study fortuitously led to finding a seminal inflammation-independent role of a component of the complement system on glucose metabolism.

When placed on an HFD, C5D mice showed resistance towards weight gain and after 12 weeks of HFD feeding were on average 5 grams smaller than HFD fed WT mice (Figure 5.3A). This difference in total mass was accounted for by a significant decrease in AT mass (Figure 5.3D & F). Lower fat mass by itself, in most cases, (except for cases of lipodystrophy) leads to decreased leukocyte

infiltration of AT and decreased inflammation, leading to improvements in insulin sensitivity. In fact, C5D mice had a mild decrease in AT expression of inflammatory and macrophage markers and a trend towards a reduction of crown like structures in comparison to their diet-matched WT counterparts (Figure 5.6). Thus, C5D directly through modulating the immune system or indirectly by affecting weight gain led to decreased AT inflammation. However, in this case, reduced AT inflammation did not lead to systemic improvements in IR as will be discussed below.

Total liver RNA extracts in this study had $4.7X10^3$ more copies of *Hc* (C5) transcript than the same quantity of total RNA in AT. In view of the fact that C5 in the B10.D2-*Hc*^{0} *H2*^{d} *H2-T18*^{c}/oSnJ mice is transcribed but not secreted because of a two-base pair deletion in exon 1 of this gene, generating an early stop codon at the 5' end of the transcript (146), accumulation of C5 in the hepatic ER could lead to ER-stress-induced inflammation and deleterious effects on metabolism. To assess this, we first contrasted C5 expression in C5D mice to that of diet-matched WT mice; C5D mice had a 70% reduction in the expression of C5 in both diets (Figure 5.7G). Assessment of ER and oxidative stress showed either no effect or a reduction in markers of both processes (Figure 5.8). Additionally, evaluation of the inflammatory state of the liver by mRNA expression of inflammatory cytokines, leukocyte markers or levels of phosphorylation of JNK showed no significant differences in inflammation between C5D and WT mice in either diet (Figures 5.7-5.8). Evaluation of H & E stained liver sections showed no overt differences or abnormal immune infiltration. Furthermore, the gene

expression of macrophage (*Emr1*) and T cell *(Cd3ε*) markers showed no differences in the levels of these cells between WT and C5D mice. Altogether these data indicates that any differences in hepatic insulin sensitivity are likely independent of inflammation and/or ER stress.

C5D mice showed marked glucose intolerance and IR when fed a LFD and this was worsened when mice were fed an HFD. C5a has been shown to have an anti-inflammatory effect in the pancreas and its deficiency led to worsened acute pancreatitis (151). To rule out pancreatitis and/or insulitis as the cause for glucose intolerance, pancreata sections were analyzed by H&E staining and insulin immunohistochemistry; there was no insulitis or pancreatitis observed in the pancreata of C5D mice, additionally the islet size and architecture appeared normal. In support of the histology data, the levels of fasting plasma insulin suggested that the observed glucose intolerance was caused by systemic IR.

A more in depth analysis of insulin signaling showed decreased AKT phosphorylation after a bolus injection of insulin in the livers and AT of C5D mice when compared to WT mice (Figure 5.14). However, AKT signaling was not affected in the muscle of the C5D mice. This result is similar to that obtained for the muscle-specific *Insr* knockout (MIRKO), mouse where signaling downstream of IGF-1R was shown to play an important compensatory role in the muscle (152). Additionally, the metabolic phenotype observed in the C5D mice was congruent with that found in other tissue-specific *Insr* knockout models. For

example, the AT-specific *Insr* knockout (FIRKO) (153) mice have lower fat mass and decreased total body triglyceride content, both of which were observed in the C5D mice (Figure 5.3D & Supp. Figure 5.9A). The liver-specific knock out model (LIRKO) (154) develops severe insulin resistance and hyperinsulinemia, both of these phenotypes were observed in the C5D mice (Figure 5.14B & Figure 5.10C-D). Altogether, these data indicate that C5D mice have resistance to insulin signaling in all metabolic tissues except the muscle, similar to the insulin receptor tissue specific knockout mouse models.

In support of the systemic insulin sensitivity data and tissue specific IR, defective expression levels and processing of the INSR were found in C5D mice. First, expression of *Insr* mRNA was found to be decreased by >50% in both the liver and AT of C5D mice in comparison to WT mice (Figure 5.12A-B). Second, analysis of the mature protein INSR-β by Western Blot showed a 70% decrease in the liver and a >50% decrease in AT and muscle (Figure 5.14 & 5.15). Additionally, differential glycosylation was observed in the pro-INSR molecule in the AT and livers of C5D mice. C5D mice, rather than having 100% of the pro-INSR molecules fully glycosylated at a molecular weight of 190 KDa, had two different bands at 190 and 180 KDa, indicating differential or incomplete glycosylation (Figure 5.15A-B). A glycosidase assay using N-Glycosidase F showed that in fact the two different molecular weight bands were a result of differential glycosylation between the WT and C5D mice. The mechanism by which C5 deficiency led to differential glycosylation and decreased INSR expression remains unknown. However, we are actively investigating a direct

effect of C5a on *Insr* expression and INSR glycosylation, as well as the effects of C5a antagonism on the same processes.

A second hypothesis for the observed phenotype is that C5a can act as a hypoglycemic hormone that supplements the activity of insulin in metabolism. There is strong evidence for a function of C5a as potent hypoglycemic molecule in neutrophils and eosinophils (155, 156); this increase in glucose uptake has been shown to be glucose transporter mediated. Furthermore, mice deficient in C5L2, one of the receptors for C5a, have an almost identical phenotype to that observed for C5D mice in the current study (157, 158). Therefore, we are investigating a potential role of C5a as a hypoglycemic hormone in metabolic tissues, which if found, would explain the metabolic phenotype of the C5D mice.

In conclusion our studies for the first time have shown a role of the complement system in non-inflammatory modulation of metabolism. C5D mice have severe glucose intolerance and systemic IR that is independent of inflammation and/or obesity. Systemic IR is caused by defective INSR processing that leads to decreased *Insr* mRNA expression and decreased mature INSR levels in all metabolic tissues. Additionally, we are currently testing whether C5a acts as a hypoglycemic hormone in metabolic tissues. Whether or not a direct effect of C5a and C5 deficiency on glucose uptake or INSR expression/processing is found in future studies, we have now established a novel model of T2DM, that can become a useful tool for the study of drugs and therapies, as well as the study of cardiovascular complications associated with

this disease. Unlike global INSR knockout mouse models, these mice are viable, yet they have significant decreases in the expression of this receptor and insulin signaling at metabolic tissues.

CHAPTER VI

SUMMARY, CONCLUSIONS AND FUTURE DIRECTIONS

The incidence of obesity and T2DM is on the rise in the United Sates and other industrialized nations. The World Health Organization estimated that more than 1.5 billion adults worldwide were overweight and 500 million were clinically obese in the year 2008 (159). Obesity has been shown to be associated with many diseases including several cancers and sleep apnea; however, the impact of obesity in most tissues involved in nutrient metabolism is due to its association with IR and T2DM. IR, defined as the decrease sensitivity in the liver, AT and muscle to increasing levels of insulin, has been shown to be the link between obesity and T2DM. Over the past decade a search towards a unifying mechanism that explains the association between obesity, IR and T2DM has revealed a close association between caloric excess and chronic inflammation. This has led to the redefinition of obesity as an inflammatory disease, termed "metainflammation" (50), and has created the new field of Immunometabolism that aims to study the effects of the immune system on metabolism (141).

"Metainflammation", or the chronic inflammation associated with obesity, is distinct from the "classical" inflammation which is a coordinated function of the immune system in response to a harmful stimulus or injury. This classical inflammation leads to the elimination of invading pathogens and the repair and

restoration of tissue homeostasis. The chronic inflammation associated with obesity involves many of the same mediators as “classical” acute inflammation, but rather than leading to tissue repair, it leads to tissue deterioration (50). Chronic inflammation associated with obesity involves all three organs associated with glucose metabolism and IR, liver, muscle and AT. All of these were studied in this dissertation; however, the focus was AT inflammation. AT inflammation has been shown to be one of the hallmarks of obesity and is likely the seminal process of metabolic tissue dysfunction systemically.

Assessment of gene expression associated with obesity in AT led to the identification of inflammatory genes normally associated with macrophages (18, 19, 22, 24). Increases in AT macrophage number and a pro-inflammatory gene expression profile are temporally associated with the development of IR (19, 29). Thus, investigating the mediators that initiate and promote macrophage recruitment to AT became vital towards understanding a unifying mechanism/solution for the metabolic dysregulation in obesity. When the work on this dissertation project began, much emphasis in this field was placed on identifying factors that could lead to the recruitment of macrophages to AT. With the goal of delineating the function of **leptin** as a chemokine in macrophage accumulation into AT, we designed the experiments in **Chapter III** to test its function *in vivo.* During the second through fourth years of my dissertation, several papers were published evaluating the importance of the macrophage phenotype as well as other immune cells in AT inflammation (52-54). Using **CCR2** deficient mice as a positive control for **Chapter III**, I made the discovery of

eosinophils in the AT of mice as well as the role of **CCR2/eosinophils** in regulating the polarization of macrophages and AT inflammatory state (**Chapter IV**). Lastly, with the goal of establishing the role of **C5a** in macrophage accumulation and inflammation in AT, I discovered a novel inflammation-independent regulation of glucose metabolism by a component of the immune system (**Chapter V**).

Macrophage Chemotaxis into AT

Several inflammatory chemokines and chemokine-receptors that could play a role in macrophage recruitment have been investigated including: CCR2, CCL2, CCL3 and CX3CR1 (30, 35, 38, 41). The initial project of this dissertation focused on testing a potential role for the adipokine leptin in this process. Leptin was shown by our laboratory to be a potent monocyte chemoattractant *in vitro*. Furthermore, our studies showed that the long form of the LepR was required for monocyte chemotaxis towards leptin (43). Additionally, a study by Curat *et al*. showed that leptin was important in upregulating adhesion molecules in the blood vessels to promote monocyte diapedesis in AT (103). These findings led many investigators to speculate that leptin could play a role in macrophage recruitment to AT *in vivo* (44, 45). In **Chapter III** of this dissertation, I showed that leptin receptor deficiency in hematopoietic cells does not affect macrophage recruitment to AT (36). This is the first published report that actually tested the commonly held belief that leptin is involved in macrophage infiltration into AT *in vivo* (21, 44, 45). Furthermore, this study also showed that leptin receptor

deficiency does not affect macrophage inflammatory gene expression *in vivo* or *in vitro*.

This was a surprising outcome for these studies at that time. However, they do not completely rule out that leptin is important in AT inflammation, due to the extensive compensation observed in other chemokine disruption experiments. However, from the time when these experiments were initiated up to now, several papers have been published suggesting that removal of a single chemokine receptor has little or no effect on macrophage accumulation in AT (32, 38-40). **Chapter III** not only adds a new chemokine whose disruption does not affect macrophage accumulation in AT to this field, but because I used mice that lacked both the LepR and CCR2 in their hematopoietic cells, my experiments showed that even in the absence of the function of four potent monocyte chemokines (leptin, CCL2, CCL7, and CCL8), there is little to no effect in the amount of macrophages that accumulate in AT. Collectively the results from **Chapter III** suggest that recruitment of macrophages to AT might not be an important factor in controlling the number of these cells found in AT during obesity. Furthermore, the turnover of these cells rather than their recruitment in AT maybe a more important determinant of the prevalence of macrophages in this tissue.

Macrophage Polarization and Other Immune Cells

Macrophages are merely one of the many immune cells that coordinate inflammation in AT. Several other cells have been shown to regulate AT inflammation, including **eosinophils,** which have been implicated in directly modulating the phenotype of AT macrophages. Eosinophils in AT were first described by Wu *et al*. who showed that eosinophils are the main producers of interleukin 4 (IL-4) in the AT (49). IL4 is a T_H2 cytokine that promotes macrophage alternative activation; thus, ablation of eosinophils leads to decreased M2 macrophages, increased IR and dysregulated AT function (49). In **Chapter IV** of this dissertation, I also describe the discovery of these cells in the AT of mice. More importantly, we were the first to report that eosinophils aberrantly accumulate in the AT of **CCR2$^{-/-}$** mice, which gave us insight into their regulation during obesity as well as their origin. Eosinophils constitute about 10% of the total stromal vascular cells in lean wild-type mice; this percentage is progressively decreased with increasing obesity, and they are no longer detected after 20 weeks of HFD feeding. In CCR2$^{-/-}$ mice they are initially increased with obesity; however, similar to the wild type mice, after extended periods of HFD feeding they eventually disappear. Eosinophils are localized in the interstitial space between adipocytes and not in crown-like structures, as is the case for most inflammatory immune cells. Eosinophilia is only detected in the AT and peritoneal cavity of CCR2$^{-/-}$ mice, which indicates that their increased numbers is likely due to local proliferation and not increased recruitment. In support of this, the levels of IL-5, an eosinopoeitic molecule, are closely correlated to the levels

of esosinophils in AT. Furthermore, the IL5 expression appears to be restricted to the M2 macrophages in AT. These data suggest that although eosinophils promote M2 activation in AT, their proliferation is also dependent on M2 macrophages themselves, in a self-renewing loop. Thus, targeting either cell type will lead to the ablation of other cell population.

Inflammation-Independent Modulation of Glucose Metabolism by the Immune System

Our laboratory is interested in AT-specific mechanisms of immune involvement in the pathogenesis of obesity. Along this common interest, I designed the AT-centered hypothesis that deficiency of **complement factor 5** would lead to decreased macrophage recruitment and AT inflammation. C5a, one of the cleavage products of C5, is known to be a potent chemoattractant for macrophages and other immune cells. Additionally, this anaphylatoxin has been shown to be one of the most potent inducers of inflammation in all leukeocytes, especially macrophages and neutrophils (61). To support my hypothesis, I showed that C5 expression was increased in visceral AT with increasing levels of obesity. As presented in **Chapter V** of this dissertation, using mice with a deficiency in C5, we discovered a unique case of inflammation-independent regulation of glucose metabolism by a component of the immune system.

In **Chapter V,** I showed the fortuitous finding that C5 deficiency directly affects glucose metabolism by modulating the expression and processing of the insulin receptor. Mice deficient in C5 (C5D) were highly glucose intolerant and

insulin resistant on a LFD diet, and HFD exacerbated this phenotype. I showed that C5 deficiency led to a small decrease in inflammation in both the liver and AT, in part supporting our initial hypothesis. However, despite decreased inflammation, C5D mice had dysregulated glucose tolerance and IR. In depth studies into the mechanism for glucose intolerance and IR showed a decrease in the mRNA expression and protein levels of the insulin receptor in all insulin sensitive tissues (liver, AT and muscle). Furthermore, we found a defect in the glycosylation of the insulin receptor precursor (Pro-INSR), which is necessary for the proper maturation of this receptor, in the liver and AT of the C5D mice. This coincided with a severe decrease in insulin signaling in these tissues, as shown by decrease AKT phosphorylation post-insulin injection.

Future Directions

Chapter III: the results of this study, as well as that of others that investigated the effects of chemokine disruption on AT macrophage accumulation (38-41), suggest that active macrophage recruitment to AT is likely not an important determinant of the number of macrophages in AT. However, recent data from our lab suggest that macrophage turnover is a more important factor in controlling macrophage numbers in AT. Future studies from our laboratory will investigate how important macrophage apoptosis in AT versus their recruitment is in maintaining the levels and activation of macrophages in this tissue. We are currently working under the hypothesis that obesity decreases

macrophage apoptosis and turnover, while lean AT conserves these processes, thus sustaining a lower number of macrophages in their AT.

Chapter IV: After the culmination of this work, the mechanism for the predominant M2 polarization of macrophages and the increased number of eosinophils in CCR2$^{-/-}$ mice remains to be tested. What comes first, M2 polarization, or increased numbers of eosinophils? Future directions for this project include: 1) to test the local proliferation of eosinophils by co-culturing eosinophils and M2 macrophages isolated from the peritoneal cavity and AT of CCR2$^{-/-}$ mice *ex vivo*, as well as *in vivo.* 2) To investigate if the predominant M2 polarization of macrophages in CCR2$^{-/-}$ mice is due to the presence of higher levels of eosinophils or if it is due to different mechanisms. Thus, the higher levels of eosinophils are a secondary effect of predominant M2 polarization. I hypothesize, that CCR2 deficiency leads to a preferential recruitment of Ly6C^{lo} monocytes to AT as opposed to the inflammatory Ly6C^{hi} monocytes, which are non-existent in this model. The Ly6C^{lo} monocytes predominantly differentiate into M2 macrophages (100), thus leading to increased local proliferation of eosinophils due to increased IL-5 production by the M2 macrophages. This hypothesis will be tested *in vivo* by performing adoptive transfer experiments of Ly6C^{lo} and Ly6C^{hi} monocyte from transgenic mice with GFP expression under a β-actin promoter. 3) To examine the metabolic effects of the systemic ablation of eosinophils during HFD feeding. 4) To test whether pharmacological inhibition of CCR2 replicates the observed eosinophilia phenotype in the genetic CCR2$^{-/-}$ mice by using a CCR2 antagonist in wild type mice. This will potentially extend

the application of our findings into humans and aid in understanding the results of clinical trials using these inhibitors.

Chapter V: The first unanswered question in this study is to investigate whether the observed phenotype is specific to the B10.D2-*Hc*^{0} *H2*^{d} *H2-T18*^{c}/oSnJ mice or if this is found in some of the other 16 mouse lines that can be purchased from the Jackson Laboratory that are also complement 5 deficient. Furthermore, a gene targeted knockout mouse of *Hc* could be used to test this phenotype. All the mouse models currently available to study C5 deficiency, are not gene targeted knockout models, but mice that fail to secrete C5; thus, the lack of secretion could be affecting insulin receptor expression indirectly and the lack of C5 becomes irrelevant in this context.

Second, I will test whether C5 deficiency is directly affecting the expression and processing of the insulin receptor by performing *in vitro* experiments in hepatocytes and adipocytes. In these experiments, we will treat adipocytes and hepatocytes with C5a and also use an antibody to antagonize this molecule.

Third, I could test the hypothesis that C5 deficiency is indirectly affecting the expression of the INSR by directly promoting glucose intolerance. C5a has been shown to potently induce glucose uptake by immune cells, specifically neutrophils and eosinophils (155, 156). This glucose uptake is insulin-independent; however, similar to insulin, it is transporter-mediated. Interestingly, mice with a gene deletion in C5L2 have an identical phenotype to what we

observed for the C5D mice in **Chapter V** (158, 160). C5L2 is one of the receptors for C5a that preferentially binds to C5a-desArg, which has been shown to have no role in promoting inflammation. The potent inflammatory molecule, C5a, has a very short half life and the arginase at its N-terminus is promptly cleaved leading to the generation of C5a-desArg, which has no inflammatory effects (61). Thus, we are now investigating a potential hypoglycemic function for C5a through signaling downstream of the C5L2 receptor in metabolic cell lines. Preliminary results show that C5a does in fact promote glucose uptake by a hepatocyte cell line *in vitro*. The data presented in **Chapter V** together with extensive literature research suggest that if found, this role for C5a might in fact be important in glucose metabolism.

Summary

In summary this dissertation has made important contributions to the field of Immunometabolism. As a whole this dissertation has contributed to four main areas in this field: chemokine-mediated macrophage recruitment to AT, macrophage polarization in AT, analysis/discovery of other immune cells in AT, and inflammation-independent modulation of metabolism by the immune system. **Chapter III** tested the intriguing hypothesis of a potential role of leptin signaling in hematopoietic cells in moncoyte/macrophage recruitment into AT. **Chapter IV** led to the discovery of eosinophils in AT of WT and $CCR2^{-/-}$ mice. This provided a mechanism for the delayed protection of $CCR2^{-/-}$ mice against glucose intolerance and IR. Additionally, this chapter elucidated a possible mechanism for

the sustainment of an M2-like activation of macrophages in AT during a lean state, and the promotion of an M1-like phenotype during obesity. **Chapter V** of this dissertation provided one of the first examples of inflammation-independent regulation of glucose metabolism and IR by the immune system. The combined findings of these Chapters are shown in Figure 6.1. This dissertation led to the identification of specific roles for all of these molecules in either macrophage recruitment to AT, macrophage polarization, regulation of other immune cells in AT, and inflammation-independent regulation of glucose metabolism.

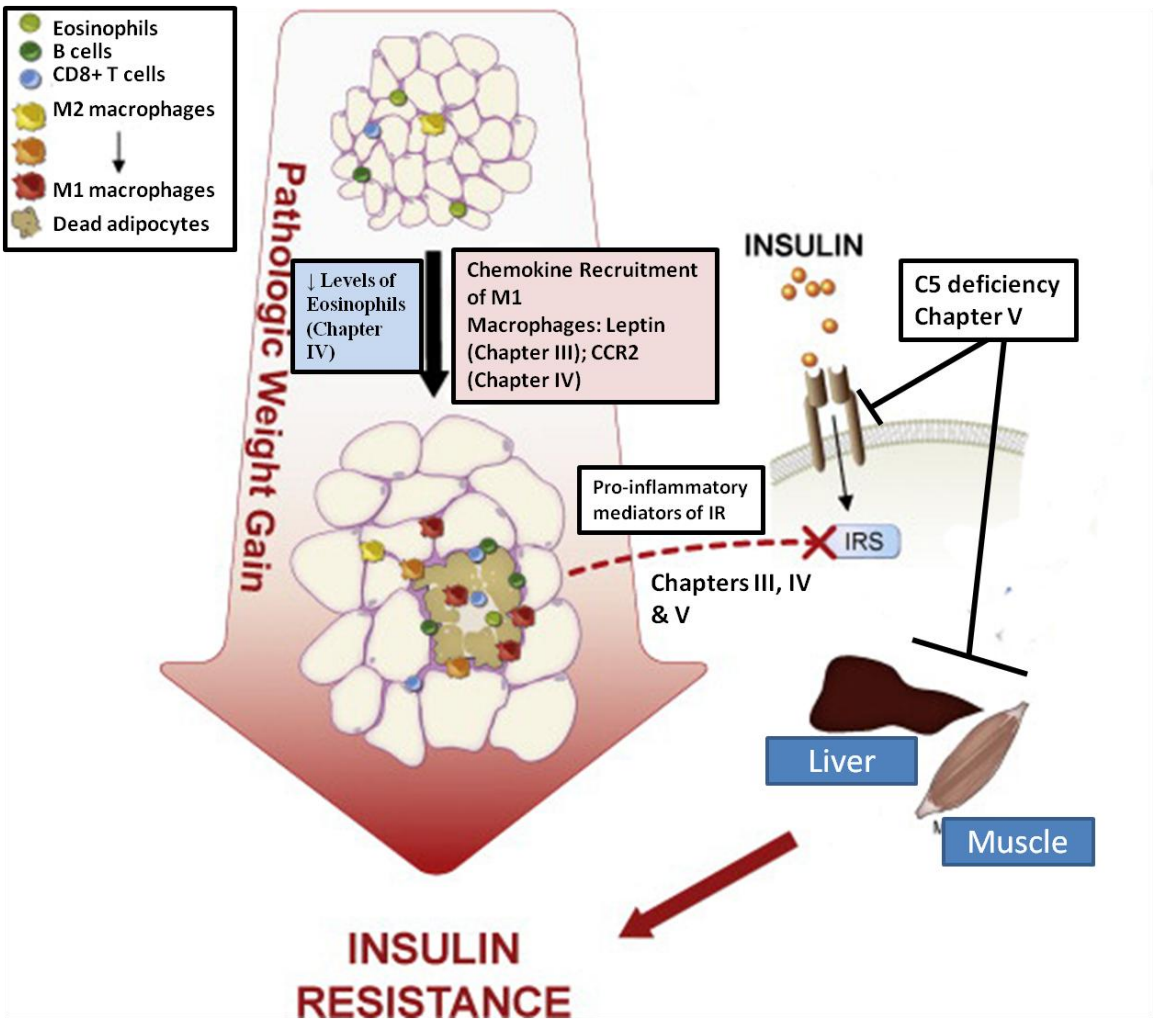

Figure 6.1 Model of contributions of this dissertation to the field of obesity, insulin resistance and type 2 diabetes. Adapted from Cipolletta *et al*. (55).

REFERENCES

1. Roth, J., Qiang, X., Marban, S.L., Redelt, H., and Lowell, B.C. 2004. The obesity pandemic: where have we been and where are we going? *Obes Res* 12 Suppl 2:88S-101S.

2. CDC. 2009. State-Specific Obesity Prevalence Among Adults. *CDC Vital Signs*.

3. Ogden, C.L., Carroll, M.D., Curtin, L.R., Lamb, M.M., and Flegal, K.M. 2010. Prevalence of high body mass index in US children and adolescents, 2007-2008. *JAMA* 303:242-249.

4. Guo, S.S., and Chumlea, W.C. 1999. Tracking of body mass index in children in relation to overweight in adulthood. *Am J Clin Nutr* 70:145S-148S.

5. Farooqi, I.S., and O'Rahilly, S. 2004. Monogenic human obesity syndromes. *Recent Prog Horm Res* 59:409-424.

6. O'Rahilly, S., Farooqi, I.S., Yeo, G.S., and Challis, B.G. 2003. Minireview: human obesity-lessons from monogenic disorders. *Endocrinology* 144:3757-3764.

7. Bray, G.A., and Gray, D.S. 1988. Obesity. Part I--Pathogenesis. *West J Med* 149:429-441.

8. Bacha, F., Lee, S., Gungor, N., and Arslanian, S.A. 2010. From pre-diabetes to type 2 diabetes in obese youth: pathophysiological characteristics along the spectrum of glucose dysregulation. *Diabetes Care* 33:2225-2231.

9. Donath, M.Y., and Shoelson, S.E. 2011. Type 2 diabetes as an inflammatory disease. *Nat Rev Immunol* 11:98-107.

10. Hotamisligil, G.S., and Erbay, E. 2008. Nutrient sensing and inflammation in metabolic diseases. *Nat Rev Immunol* 8:923-934.

11. Ehses, J.A., Ellingsgaard, H., Boni-Schnetzler, M., and Donath, M.Y. 2009. Pancreatic islet inflammation in type 2 diabetes: from alpha and beta cell compensation to dysfunction. *Arch Physiol Biochem* 115:240-247.

12. Cheng, Z., Tseng, Y., and White, M.F. 2010. Insulin signaling meets mitochondria in metabolism. *Trends Endocrinol Metab* 21:589-598.

13. Zick, Y. 2005. Ser/Thr phosphorylation of IRS proteins: a molecular basis for insulin resistance. *Sci STKE* 2005:pe4.

14. Emanuelli, B., Peraldi, P., Filloux, C., Chavey, C., Freidinger, K., Hilton, D.J., Hotamisligil, G.S., and Van Obberghen, E. 2001. SOCS-3 inhibits insulin signaling and is up-regulated in response to tumor necrosis factor-alpha in the adipose tissue of obese mice. *J Biol Chem* 276:47944-47949.

15. Kalupahana, N.S., Moustaid-Moussa, N., and Claycombe, K.J. 2012. Immunity as a link between obesity and insulin resistance. *Mol Aspects Med* 33:26-34.

16. Halaas, J.L., Gajiwala, K.S., Maffei, M., Cohen, S.L., Chait, B.T., Rabinowitz, D., Lallone, R.L., Burley, S.K., and Friedman, J.M. 1995. Weight-reducing effects of the plasma protein encoded by the obese gene. *Science* 269:543-546.

17. Maffei, M., Halaas, J., Ravussin, E., Pratley, R.E., Lee, G.H., Zhang, Y., Fei, H., Kim, S., Lallone, R., Ranganathan, S., et al. 1995. Leptin levels in human and rodent: measurement of plasma leptin and ob RNA in obese and weight-reduced subjects. *Nat Med* 1:1155-1161.

18. Hotamisligil, G.S., Arner, P., Caro, J.F., Atkinson, R.L., and Spiegelman, B.M. 1995. Increased adipose tissue expression of tumor necrosis factor-alpha in human obesity and insulin resistance. *J Clin Invest* 95:2409-2415.

19. Xu, H., Barnes, G.T., Yang, Q., Tan, G., Yang, D., Chou, C.J., Sole, J., Nichols, A., Ross, J.S., Tartaglia, L.A., et al. 2003. Chronic inflammation in fat plays a crucial role in the development of obesity-related insulin resistance. *J Clin Invest* 112:1821-1830.

20. Trayhurn, P., Bing, C., and Wood, I.S. 2006. Adipose tissue and adipokines--energy regulation from the human perspective. *J Nutr* 136:1935S-1939S.

21. Gutierrez, D.A., Puglisi, M.J., and Hasty, A.H. 2009. Impact of increased adipose tissue mass on inflammation, insulin resistance, and dyslipidemia. *Curr Diab Rep* 9:26-32.

22. Hotamisligil, G.S., Shargill, N.S., and Spiegelman, B.M. 1993. Adipose expression of tumor necrosis factor-alpha: direct role in obesity-linked insulin resistance. *Science* 259:87-91.

23. Spiegelman, B.M., Choy, L., Hotamisligil, G.S., Graves, R.A., and Tontonoz, P. 1993. Regulation of adipocyte gene expression in differentiation and syndromes of obesity/diabetes. *J Biol Chem* 268:6823-6826.

24. Weisberg, S.P., McCann, D., Desai, M., Rosenbaum, M., Leibel, R.L., and Ferrante, A.W., Jr. 2003. Obesity is associated with macrophage accumulation in adipose tissue. *J Clin Invest* 112:1796-1808.

25. Anderson, E.K., Gutierrez, D.A., and Hasty, A.H. 2010. Adipose tissue recruitment of leukocytes. *Curr Opin Lipidol* 21:172-177.

26. Hosogai, N., Fukuhara, A., Oshima, K., Miyata, Y., Tanaka, S., Segawa, K., Furukawa, S., Tochino, Y., Komuro, R., Matsuda, M., et al. 2007. Adipose tissue hypoxia in obesity and its impact on adipocytokine dysregulation. *Diabetes* 56:901-911.

27. Ye, J., Gao, Z., Yin, J., and He, Q. 2007. Hypoxia is a potential risk factor for chronic inflammation and adiponectin reduction in adipose tissue of ob/ob and dietary obese mice. *Am J Physiol Endocrinol Metab* 293:E1118-1128.

28. Cinti, S., Mitchell, G., Barbatelli, G., Murano, I., Ceresi, E., Faloia, E., Wang, S., Fortier, M., Greenberg, A.S., and Obin, M.S. 2005. Adipocyte death defines macrophage localization and function in adipose tissue of obese mice and humans. *J Lipid Res* 46:2347-2355.

29. Strissel, K.J., Stancheva, Z., Miyoshi, H., Perfield, J.W., 2nd, DeFuria, J., Jick, Z., Greenberg, A.S., and Obin, M.S. 2007. Adipocyte death, adipose tissue remodeling, and obesity complications. *Diabetes* 56:2910-2918.

30. Kanda, H., Tateya, S., Tamori, Y., Kotani, K., Hiasa, K., Kitazawa, R., Kitazawa, S., Miyachi, H., Maeda, S., Egashira, K., et al. 2006. MCP-1 contributes to macrophage infiltration into adipose tissue, insulin resistance, and hepatic steatosis in obesity. *J Clin Invest* 116:1494-1505.

31. Sartipy, P., and Loskutoff, D.J. 2003. Monocyte chemoattractant protein 1 in obesity and insulin resistance. *Proc Natl Acad Sci U S A* 100:7265-7270.

32. Chen, Y., Hallenbeck, J.M., Ruetzler, C., Bol, D., Thomas, K., Berman, N.E., and Vogel, S.N. 2003. Overexpression of monocyte chemoattractant protein 1 in the brain exacerbates ischemic brain injury and is associated with recruitment of inflammatory cells. *J Cereb Blood Flow Metab* 23:748-755.

33. Coenen, K.R., Gruen, M.L., Chait, A., and Hasty, A.H. 2007. Diet-induced increases in adiposity, but not plasma lipids, promote macrophage infiltration into white adipose tissue. *Diabetes* 56:564-573.

34. Huber, J., Kiefer, F.W., Zeyda, M., Ludvik, B., Silberhumer, G.R., Prager, G., Zlabinger, G.J., and Stulnig, T.M. 2008. CC chemokine and CC chemokine receptor profiles in visceral and subcutaneous adipose tissue are altered in human obesity. *J Clin Endocrinol Metab* 93:3215-3221.

35. Weisberg, S.P., Hunter, D., Huber, R., Lemieux, J., Slaymaker, S., Vaddi, K., Charo, I., Leibel, R.L., and Ferrante, A.W., Jr. 2006. CCR2 modulates inflammatory and metabolic effects of high-fat feeding. *J Clin Invest* 116:115-124.

36. Gutierrez, D.A., and Hasty, A. 2011. Hematopoietic Leptin Receptor Deficiency Does Not Affect Macrophage Accumulation in Adipose Tissue or Systemic Insulin Sensitivity. *J Endocrinol*.

37. Gutierrez, D.A., Kennedy, A., Orr, J.S., Anderson, E.K., Webb, C.D., Gerrald, W.K., and Hasty, A.H. 2011. Aberrant accumulation of undifferentiated myeloid cells in the adipose tissue of CCR2-deficient mice delays improvements in insulin sensitivity. *Diabetes* 60:2820-2829.

38. Surmi, B.K., Webb, C.D., Ristau, A.C., and Hasty, A.H. 2010. Absence of macrophage inflammatory protein-1{alpha} does not impact macrophage accumulation in adipose tissue of diet-induced obese mice. *Am J Physiol Endocrinol Metab* 299:E437-445.

39. Inouye, K.E., Shi, H., Howard, J.K., Daly, C.H., Lord, G.M., Rollins, B.J., and Flier, J.S. 2007. Absence of CC chemokine ligand 2 does not limit obesity-associated infiltration of macrophages into adipose tissue. *Diabetes* 56:2242-2250.

40. Kirk, E.A., Sagawa, Z.K., McDonald, T.O., O'Brien, K.D., and Heinecke, J.W. 2008. Monocyte chemoattractant protein deficiency fails to restrain macrophage infiltration into adipose tissue [corrected]. *Diabetes* 57:1254-1261.

41. Morris, D.L., Oatmen, K.E., Wang, T., Delproposto, J.L., and Lumeng, C.N. 2012. CX(3)CR1 Deficiency Does Not Influence Trafficking of Adipose Tissue Macrophages in Mice With Diet-Induced Obesity. *Obesity (Silver Spring)*.

42. Bourlier, V., and Bouloumie, A. 2009. Role of macrophage tissue infiltration in obesity and insulin resistance. *Diabetes Metab* 35:251-260.

43. Gruen, M.L., Hao, M., Piston, D.W., and Hasty, A.H. 2007. Leptin requires canonical migratory signaling pathways for induction of monocyte and macrophage chemotaxis. *Am J Physiol Cell Physiol* 293:C1481-1488.

44. Fernandez-Riejos, P., Najib, S., Santos-Alvarez, J., Martin-Romero, C., Perez-Perez, A., Gonzalez-Yanes, C., and Sanchez-Margalet, V. 2010. Role of leptin in the activation of immune cells. *Mediators Inflamm* 2010:568343.

45. Vona-Davis, L., and Rose, D.P. 2009. Angiogenesis, adipokines and breast cancer. *Cytokine Growth Factor Rev* 20:193-201.

46. Martinez, F.O., Sica, A., Mantovani, A., and Locati, M. 2008. Macrophage activation and polarization. *Front Biosci* 13:453-461.

47. Lumeng, C.N., Bodzin, J.L., and Saltiel, A.R. 2007. Obesity induces a phenotypic switch in adipose tissue macrophage polarization. *J Clin Invest* 117:175-184.

48. Lumeng, C.N., Deyoung, S.M., Bodzin, J.L., and Saltiel, A.R. 2007. Increased inflammatory properties of adipose tissue macrophages recruited during diet-induced obesity. *Diabetes* 56:16-23.

49. Wu, D., Molofsky, A.B., Liang, H.E., Ricardo-Gonzalez, R.R., Jouihan, H.A., Bando, J.K., Chawla, A., and Locksley, R.M. 2011. Eosinophils sustain adipose alternatively activated macrophages associated with glucose homeostasis. *Science* 332:243-247.

50. Hotamisligil, G.S. 2006. Inflammation and metabolic disorders. *Nature* 444:860-867.

51. Stienstra, R., Duval, C., Keshtkar, S., van der Laak, J., Kersten, S., and Muller, M. 2008. Peroxisome proliferator-activated receptor gamma activation promotes infiltration of alternatively activated macrophages into adipose tissue. *J Biol Chem* 283:22620-22627.

52. Odegaard, J.I., Ricardo-Gonzalez, R.R., Goforth, M.H., Morel, C.R., Subramanian, V., Mukundan, L., Red Eagle, A., Vats, D., Brombacher, F., Ferrante, A.W., et al. 2007. Macrophage-specific PPARgamma controls alternative activation and improves insulin resistance. *Nature* 447:1116-1120.

53. Odegaard, J.I., Ricardo-Gonzalez, R.R., Red Eagle, A., Vats, D., Morel, C.R., Goforth, M.H., Subramanian, V., Mukundan, L., Ferrante, A.W., and

Chawla, A. 2008. Alternative M2 activation of Kupffer cells by PPARdelta ameliorates obesity-induced insulin resistance. *Cell Metab* 7:496-507.

54. Winer, S., and Winer, D.A. 2012. The adaptive immune system as a fundamental regulator of adipose tissue inflammation and insulin resistance. *Immunol Cell Biol*.

55. Cipolletta, D., Kolodin, D., Benoist, C., and Mathis, D. 2011. Tissular T(regs): A unique population of adipose-tissue-resident Foxp3+CD4+ T cells that impacts organismal metabolism. *Semin Immunol* 23:431-437.

56. Nishimura, S., Manabe, I., Nagasaki, M., Eto, K., Yamashita, H., Ohsugi, M., Otsu, M., Hara, K., Ueki, K., Sugiura, S., et al. 2009. CD8+ effector T cells contribute to macrophage recruitment and adipose tissue inflammation in obesity. *Nat Med* 15:914-920.

57. Kintscher, U., Hartge, M., Hess, K., Foryst-Ludwig, A., Clemenz, M., Wabitsch, M., Fischer-Posovszky, P., Barth, T.F., Dragun, D., Skurk, T., et al. 2008. T-lymphocyte infiltration in visceral adipose tissue: a primary event in adipose tissue inflammation and the development of obesity-mediated insulin resistance. *Arterioscler Thromb Vasc Biol* 28:1304-1310.

58. Yang, H., Youm, Y.H., Vandanmagsar, B., Ravussin, A., Gimble, J.M., Greenway, F., Stephens, J.M., Mynatt, R.L., and Dixit, V.D. 2010. Obesity increases the production of proinflammatory mediators from adipose tissue T cells and compromises TCR repertoire diversity: implications for systemic inflammation and insulin resistance. *J Immunol* 185:1836-1845.

59. Winer, S., Chan, Y., Paltser, G., Truong, D., Tsui, H., Bahrami, J., Dorfman, R., Wang, Y., Zielenski, J., Mastronardi, F., et al. 2009. Normalization of obesity-associated insulin resistance through immunotherapy. *Nat Med* 15:921-929.

60. Winer, S., Paltser, G., Chan, Y., Tsui, H., Engleman, E., Winer, D., and Dosch, H.M. 2009. Obesity predisposes to Th17 bias. *Eur J Immunol* 39:2629-2635.

61. Guo, R.F., and Ward, P.A. 2005. Role of C5a in inflammatory responses. *Annu Rev Immunol* 23:821-852.

62. Sakaguchi, S., Yamaguchi, T., Nomura, T., and Ono, M. 2008. Regulatory T cells and immune tolerance. *Cell* 133:775-787.

63. Feuerer, M., Herrero, L., Cipolletta, D., Naaz, A., Wong, J., Nayer, A., Lee, J., Goldfine, A.B., Benoist, C., Shoelson, S., et al. 2009. Lean, but not

obese, fat is enriched for a unique population of regulatory T cells that affect metabolic parameters. *Nat Med* 15:930-939.

64. Winer, D.A., Winer, S., Shen, L., Wadia, P.P., Yantha, J., Paltser, G., Tsui, H., Wu, P., Davidson, M.G., Alonso, M.N., et al. 2011. B cells promote insulin resistance through modulation of T cells and production of pathogenic IgG antibodies. *Nat Med* 17:610-617.

65. Liu, J., Divoux, A., Sun, J., Zhang, J., Clement, K., Glickman, J.N., Sukhova, G.K., Wolters, P.J., Du, J., Gorgun, C.Z., et al. 2009. Genetic deficiency and pharmacological stabilization of mast cells reduce diet-induced obesity and diabetes in mice. *Nat Med* 15:940-945.

66. Ohmura, K., Ishimori, N., Ohmura, Y., Tokuhara, S., Nozawa, A., Horii, S., Andoh, Y., Fujii, S., Iwabuchi, K., Onoe, K., et al. 2010. Natural killer T cells are involved in adipose tissues inflammation and glucose intolerance in diet-induced obese mice. *Arterioscler Thromb Vasc Biol* 30:193-199.

67. Rothenberg, M.E., and Hogan, S.P. 2006. The eosinophil. *Annu Rev Immunol* 24:147-174.

68. Magni, P., Liuzzi, A., Ruscica, M., Dozio, E., Ferrario, S., Bussi, I., Minocci, A., Castagna, A., Motta, M., and Savia, G. 2005. Free and bound plasma leptin in normal weight and obese men and women: relationship with body composition, resting energy expenditure, insulin-sensitivity, lipid profile and macronutrient preference. *Clin Endocrinol (Oxf)* 62:189-196.

69. Reilly, M.P., Iqbal, N., Schutta, M., Wolfe, M.L., Scally, M., Localio, A.R., Rader, D.J., and Kimmel, S.E. 2004. Plasma leptin levels are associated with coronary atherosclerosis in type 2 diabetes. *J Clin Endocrinol Metab* 89:3872-3878.

70. Leshan, R.L., Bjornholm, M., Munzberg, H., and Myers, M.G., Jr. 2006. Leptin receptor signaling and action in the central nervous system. *Obesity (Silver Spring)* 14 Suppl 5:208S-212S.

71. Leinninger, G.M., and Myers, M.G., Jr. 2008. LRb signals act within a distributed network of leptin-responsive neurones to mediate leptin action. *Acta Physiol (Oxf)* 192:49-59.

72. Robertson, S.A., Leinninger, G.M., and Myers, M.G., Jr. 2008. Molecular and neural mediators of leptin action. *Physiol Behav* 94:637-642.

73. Horuk, R. 2001. Chemokine receptors. *Cytokine Growth Factor Rev* 12:313-335.

74. Boring, L., Gosling, J., Chensue, S.W., Kunkel, S.L., Farese, R.V., Jr., Broxmeyer, H.E., and Charo, I.F. 1997. Impaired monocyte migration and reduced type 1 (Th1) cytokine responses in C-C chemokine receptor 2 knockout mice. *J Clin Invest* 100:2552-2561.

75. Fife, B.T., Huffnagle, G.B., Kuziel, W.A., and Karpus, W.J. 2000. CC chemokine receptor 2 is critical for induction of experimental autoimmune encephalomyelitis. *J Exp Med* 192:899-905.

76. Boring, L., Gosling, J., Cleary, M., and Charo, I.F. 1998. Decreased lesion formation in CCR2-/- mice reveals a role for chemokines in the initiation of atherosclerosis. *Nature* 394:894-897.

77. Peters, W., Scott, H.M., Chambers, H.F., Flynn, J.L., Charo, I.F., and Ernst, J.D. 2001. Chemokine receptor 2 serves an early and essential role in resistance to Mycobacterium tuberculosis. *Proc Natl Acad Sci U S A* 98:7958-7963.

78. Baldo, A., Sniderman, A.D., St-Luce, S., Avramoglu, R.K., Maslowska, M., Hoang, B., Monge, J.C., Bell, A., Mulay, S., and Cianflone, K. 1993. The adipsin-acylation stimulating protein system and regulation of intracellular triglyceride synthesis. *J Clin Invest* 92:1543-1547.

79. Choy, L.N., Rosen, B.S., and Spiegelman, B.M. 1992. Adipsin and an endogenous pathway of complement from adipose cells. *J Biol Chem* 267:12736-12741.

80. Kalant, D., Cain, S.A., Maslowska, M., Sniderman, A.D., Cianflone, K., and Monk, P.N. 2003. The chemoattractant receptor-like protein C5L2 binds the C3a des-Arg77/acylation-stimulating protein. *J Biol Chem* 278:11123-11129.

81. Gabrielsson, B.G., Johansson, J.M., Lonn, M., Jernas, M., Olbers, T., Peltonen, M., Larsson, I., Lonn, L., Sjostrom, L., Carlsson, B., et al. 2003. High expression of complement components in omental adipose tissue in obese men. *Obes Res* 11:699-708.

82. Banda, N.K., Levitt, B., Wood, A.K., Takahashi, K., Stahl, G.L., Holers, V.M., and Arend, W.P. 2009. Complement activation pathways in murine immune complex-induced arthritis and in C3a and C5a generation in vitro. *Clin Exp Immunol* 159:100-108.

83. Zhou, W., Farrar, C.A., Abe, K., Pratt, J.R., Marsh, J.E., Wang, Y., Stahl, G.L., and Sacks, S.H. 2000. Predominant role for C5b-9 in renal ischemia/reperfusion injury. *J Clin Invest* 105:1363-1371.

84. Snyderman, R., Pike, M.C., McCarley, D., and Lang, L. 1975. Quantification of mouse macrophage chemotaxis in vitro: role of C5 for the production of chemotactic activity. *Infect Immun* 11:488-492.

85. Jauneau, A.C., Ischenko, A., Chan, P., and Fontaine, M. 2003. Complement component anaphylatoxins upregulate chemokine expression by human astrocytes. *FEBS Lett* 537:17-22.

86. Weinrauch, Y., Elsbach, P., Madsen, L.M., Foreman, A., and Weiss, J. 1996. The potent anti-Staphylococcus aureus activity of a sterile rabbit inflammatory fluid is due to a 14-kD phospholipase A2. *J Clin Invest* 97:250-257.

87. Biancone, L., David, S., Della Pietra, V., Montrucchio, G., Cambi, V., and Camussi, G. 1994. Alternative pathway activation of complement by cultured human proximal tubular epithelial cells. *Kidney Int* 45:451-460.

88. Kilgore, K.S., Schmid, E., Shanley, T.P., Flory, C.M., Maheswari, V., Tramontini, N.L., Cohen, H., Ward, P.A., Friedl, H.P., and Warren, J.S. 1997. Sublytic concentrations of the membrane attack complex of complement induce endothelial interleukin-8 and monocyte chemoattractant protein-1 through nuclear factor-kappa B activation. *Am J Pathol* 150:2019-2031.

89. Hansch, G.M., Seitz, M., and Betz, M. 1987. Effect of the late complement components C5b-9 on human monocytes: release of prostanoids, oxygen radicals and of a factor inducing cell proliferation. *Int Arch Allergy Appl Immunol* 82:317-320.

90. Mathieson, P.W., Wurzner, R., Oliveria, D.B., Lachmann, P.J., and Peters, D.K. 1993. Complement-mediated adipocyte lysis by nephritic factor sera. *J Exp Med* 177:1827-1831.

91. Chudek, J., and Wiecek, A. 2006. Adipose tissue, inflammation and endothelial dysfunction. *Pharmacol Rep* 58 Suppl:81-88.

92. Coenen, K.R., Gruen, M.L., Lee-Young, R.S., Puglisi, M.J., Wasserman, D.H., and Hasty, A.H. 2009. Impact of macrophage toll-like receptor 4 deficiency on macrophage infiltration into adipose tissue and the artery wall in mice. *Diabetologia* 52:318-328.

93. Pfaffl, M.W. 2001. A new mathematical model for relative quantification in real-time RT-PCR. *Nucleic Acids Res* 29:e45.

94. Lowry, O.H., Rosebrough, N.J., Farr, A.L., and Randall, R.J. 1951. Protein measurement with the Folin phenol reagent. *J Biol Chem* 193:265-275.

95. Saraswathi, V., Morrow, J.D., and Hasty, A.H. 2009. Dietary fish oil exerts hypolipidemic effects in lean and insulin sensitizing effects in obese LDLR-/- mice. *J Nutr* 139:2380-2386.

96. Lumeng, C.N., DelProposto, J.B., Westcott, D.J., and Saltiel, A.R. 2008. Phenotypic switching of adipose tissue macrophages with obesity is generated by spatiotemporal differences in macrophage subtypes. *Diabetes* 57:3239-3246.

97. La Cava, A., and Matarese, G. 2004. The weight of leptin in immunity. *Nat Rev Immunol* 4:371-379.

98. Zarkesh-Esfahani, H., Pockley, G., Metcalfe, R.A., Bidlingmaier, M., Wu, Z., Ajami, A., Weetman, A.P., Strasburger, C.J., and Ross, R.J. 2001. High-dose leptin activates human leukocytes via receptor expression on monocytes. *J Immunol* 167:4593-4599.

99. Dixit, V.D., Mielenz, M., Taub, D.D., and Parvizi, N. 2003. Leptin induces growth hormone secretion from peripheral blood mononuclear cells via a protein kinase C- and nitric oxide-dependent mechanism. *Endocrinology* 144:5595-5603.

100. Geissmann, F., Manz, M.G., Jung, S., Sieweke, M.H., Merad, M., and Ley, K. 2010. Development of monocytes, macrophages, and dendritic cells. *Science* 327:656-661.

101. Bouhlel, M.A., Derudas, B., Rigamonti, E., Dievart, R., Brozek, J., Haulon, S., Zawadzki, C., Jude, B., Torpier, G., Marx, N., et al. 2007. PPARgamma activation primes human monocytes into alternative M2 macrophages with anti-inflammatory properties. *Cell Metab* 6:137-143.

102. Westcott, D.J., Delproposto, J.B., Geletka, L.M., Wang, T., Singer, K., Saltiel, A.R., and Lumeng, C.N. 2009. MGL1 promotes adipose tissue inflammation and insulin resistance by regulating 7/4hi monocytes in obesity. *J Exp Med* 206:3143-3156.

103. Curat, C.A., Miranville, A., Sengenes, C., Diehl, M., Tonus, C., Busse, R., and Bouloumie, A. 2004. From blood monocytes to adipose tissue-resident macrophages: induction of diapedesis by human mature adipocytes. *Diabetes* 53:1285-1292.

104. Kato, H., Ueki, S., Kamada, R., Kihara, J., Yamauchi, Y., Suzuki, T., Takeda, M., Itoga, M., Chihara, M., Ito, W., et al. 2011. Leptin Has a Priming Effect on Eotaxin-Induced Human Eosinophil Chemotaxis. *Int Arch Allergy Immunol* 155:335-344.

105. Caldefie-Chezet, F., Poulin, A., Tridon, A., Sion, B., and Vasson, M.P. 2001. Leptin: a potential regulator of polymorphonuclear neutrophil bactericidal action? *J Leukoc Biol* 69:414-418.

106. Caldefie-Chezet, F., Poulin, A., and Vasson, M.P. 2003. Leptin regulates functional capacities of polymorphonuclear neutrophils. *Free Radic Res* 37:809-814.

107. Conde, J., Scotece, M., Gomez, R., Gomez-Reino, J.J., Lago, F., and Gualillo, O. 2010. At the crossroad between immunity and metabolism: focus on leptin. *Expert Rev Clin Immunol* 6:801-808.

108. Wood, I.S., de Heredia, F.P., Wang, B., and Trayhurn, P. 2009. Cellular hypoxia and adipose tissue dysfunction in obesity. *Proc Nutr Soc* 68:370-377.

109. Maeda, T., Kiguchi, N., Kobayashi, Y., Ikuta, T., Ozaki, M., and Kishioka, S. 2009. Leptin derived from adipocytes in injured peripheral nerves facilitates development of neuropathic pain via macrophage stimulation. *Proc Natl Acad Sci U S A* 106:13076-13081.

110. Surmi, B.K., and Hasty, A.H. 2008. Macrophage infiltration into adipose tissue: initiation, propagation and remodeling. *Future Lipidol* 3:545-556.

111. Tsou, C.L., Peters, W., Si, Y., Slaymaker, S., Aslanian, A.M., Weisberg, S.P., Mack, M., and Charo, I.F. 2007. Critical roles for CCR2 and MCP-3 in monocyte mobilization from bone marrow and recruitment to inflammatory sites. *J Clin Invest* 117:902-909.

112. Shaul, M.E., Bennett, G., Strissel, K.J., Greenberg, A.S., and Obin, M.S. 2010. Dynamic, M2-like remodeling phenotypes of CD11c+ adipose tissue macrophages during high-fat diet--induced obesity in mice. *Diabetes* 59:1171-1181.

113. Chen, A., Mumick, S., Zhang, C., Lamb, J., Dai, H., Weingarth, D., Mudgett, J., Chen, H., MacNeil, D.J., Reitman, M.L., et al. 2005. Diet induction of monocyte chemoattractant protein-1 and its impact on obesity. *Obes Res* 13:1311-1320.

114. Mantovani, A. 1999. The chemokine system: redundancy for robust outputs. *Immunol Today* 20:254-257.

115. Ouchi, N., Parker, J.L., Lugus, J.J., and Walsh, K. 2011. Adipokines in inflammation and metabolic disease. *Nat Rev Immunol* 11:85-97.

116. Monteiro, R., and Azevedo, I. 2010. Chronic inflammation in obesity and the metabolic syndrome. *Mediators Inflamm* 2010.

117. Ramos, E.J., Xu, Y., Romanova, I., Middleton, F., Chen, C., Quinn, R., Inui, A., Das, U., and Meguid, M.M. 2003. Is obesity an inflammatory disease? *Surgery* 134:329-335.

118. Charo, I.F., and Ransohoff, R.M. 2006. The many roles of chemokines and chemokine receptors in inflammation. *N Engl J Med* 354:610-621.

119. Geissmann, F., Manz, M.G., Jung, S., Sieweke, M.H., Merad, M., and Ley, K. 2011. Development of monocytes, macrophages, and dendritic cells. *Science* 327:656-661.

120. Ito, A., Suganami, T., Yamauchi, A., Degawa-Yamauchi, M., Tanaka, M., Kouyama, R., Kobayashi, Y., Nitta, N., Yasuda, K., Hirata, Y., et al. 2008. Role of CC chemokine receptor 2 in bone marrow cells in the recruitment of macrophages into obese adipose tissue. *J Biol Chem* 283:35715-35723.

121. Tamura, Y., Sugimoto, M., Murayama, T., Ueda, Y., Kanamori, H., Ono, K., Ariyasu, H., Akamizu, T., Kita, T., Yokode, M., et al. 2008. Inhibition of CCR2 ameliorates insulin resistance and hepatic steatosis in db/db mice. *Arterioscler Thromb Vasc Biol* 28:2195-2201.

122. Yang, S.J., IglayReger, H.B., Kadouh, H.C., and Bodary, P.F. 2009. Inhibition of the chemokine (C-C motif) ligand 2/chemokine (C-C motif) receptor 2 pathway attenuates hyperglycaemia and inflammation in a mouse model of hepatic steatosis and lipoatrophy. *Diabetologia* 52:972-981.

123. Gower, R.M., Wu, H., Foster, G.A., Devaraj, S., Jialal, I., Ballantyne, C.M., Knowlton, A.A., and Simon, S.I. 2011. CD11c/CD18 expression is upregulated on blood monocytes during hypertriglyceridemia and enhances adhesion to vascular cell adhesion molecule-1. *Arterioscler Thromb Vasc Biol* 31:160-166.

124. Wu, H., Perrard, X.D., Wang, Q., Perrard, J.L., Polsani, V.R., Jones, P.H., Smith, C.W., and Ballantyne, C.M. 2010. CD11c expression in adipose tissue and blood and its role in diet-induced obesity. *Arterioscler Thromb Vasc Biol* 30:186-192.

125. Ablamunits, V., Weisberg, S.P., Lemieux, J.E., Combs, T.P., and Klebanov, S. 2007. Reduced adiposity in ob/ob mice following total body irradiation and bone marrow transplantation. *Obesity (Silver Spring)* 15:1419-1429.

126. Boring, D., and Doninger, C. 1997. The need for balancing the regulation of pharmaceutical trademarks between the Food and Drug Administration and the Patent and Trademark Office. *Food Drug Law J* 52:109-116.

127. Peters, W., Dupuis, M., and Charo, I.F. 2000. A mechanism for the impaired IFN-gamma production in C-C chemokine receptor 2 (CCR2) knockout mice: role of CCR2 in linking the innate and adaptive immune responses. *J Immunol* 165:7072-7077.

128. Szymczak, W.A., and Deepe, G.S., Jr. 2009. The CCL7-CCL2-CCR2 axis regulates IL-4 production in lungs and fungal immunity. *J Immunol* 183:1964-1974.

129. Kuziel, W.A., Morgan, S.J., Dawson, T.C., Griffin, S., Smithies, O., Ley, K., and Maeda, N. 1997. Severe reduction in leukocyte adhesion and monocyte extravasation in mice deficient in CC chemokine receptor 2. *Proc Natl Acad Sci U S A* 94:12053-12058.

130. Sonoda, K.H., Yoshimura, T., Egashira, K., Charo, I.F., and Ishibashi, T. Neutrophil-dominant experimental autoimmune uveitis in CC-chemokine receptor 2 knockout mice. *Acta Ophthalmol*.

131. Chomarat, P., Banchereau, J., Davoust, J., and Palucka, A.K. 2000. IL-6 switches the differentiation of monocytes from dendritic cells to macrophages. *Nat Immunol* 1:510-514.

132. Obstfeld, A.E., Sugaru, E., Thearle, M., Francisco, A.M., Gayet, C., Ginsberg, H.N., Ables, E.V., and Ferrante, A.W., Jr. 2010. C-C chemokine receptor 2 (CCR2) regulates the hepatic recruitment of myeloid cells that promote obesity-induced hepatic steatosis. *Diabetes* 59:916-925.

133. el-Cheikh, M.C., and Borojevic, R. 1990. Extramedullar proliferation of eosinophil granulocytes in chronic schistosomiasis mansoni is mediated by a factor secreted by inflammatory macrophages. *Infect Immun* 58:816-821.

134. Radinger, M., Bossios, A., Sjostrand, M., Lu, Y., Malmhall, C., Dahlborn, A.K., Lee, J.J., and Lotvall, J. 2011. Local proliferation and mobilization of CCR3(+) CD34(+) eosinophil-lineage-committed cells in the lung. *Immunology* 132:144-154.

135. Struthers, M., and Pasternak, A. 2010. CCR2 antagonists. *Curr Top Med Chem* 10:1278-1298.

136. Kang, Y.S., Cha, J.J., Hyun, Y.Y., and Cha, D.R. 2011. Novel C-C chemokine receptor 2 antagonists in metabolic disease: a review of recent developments. *Expert Opin Investig Drugs* 20:745-756.

137. Weiss, R., Dziura, J., Burgert, T.S., Tamborlane, W.V., Taksali, S.E., Yeckel, C.W., Allen, K., Lopes, M., Savoye, M., Morrison, J., et al. 2004. Obesity and the metabolic syndrome in children and adolescents. *N Engl J Med* 350:2362-2374.

138. Olshansky, S.J., Passaro, D.J., Hershow, R.C., Layden, J., Carnes, B.A., Brody, J., Hayflick, L., Butler, R.N., Allison, D.B., and Ludwig, D.S. 2005. A potential decline in life expectancy in the United States in the 21st century. *N Engl J Med* 352:1138-1145.

139. Olefsky, J.M., and Glass, C.K. 2010. Macrophages, inflammation, and insulin resistance. *Annu Rev Physiol* 72:219-246.

140. Gregor, M.F., and Hotamisligil, G.S. 2011. Inflammatory mechanisms in obesity. *Annu Rev Immunol* 29:415-445.

141. Mathis, D., and Shoelson, S.E. 2011. Immunometabolism: an emerging frontier. *Nat Rev Immunol* 11:81.

142. Spranger, J., Kroke, A., Mohlig, M., Hoffmann, K., Bergmann, M.M., Ristow, M., Boeing, H., and Pfeiffer, A.F. 2003. Inflammatory cytokines and the risk to develop type 2 diabetes: results of the prospective population-based European Prospective Investigation into Cancer and Nutrition (EPIC)-Potsdam Study. *Diabetes* 52:812-817.

143. Woodruff, T.M., Nandakumar, K.S., and Tedesco, F. 2011. Inhibiting the C5-C5a receptor axis. *Mol Immunol* 48:1631-1642.

144. Wheat, W.H., Wetsel, R., Falus, A., Tack, B.F., and Strunk, R.C. 1987. The fifth component of complement (C5) in the mouse. Analysis of the molecular basis for deficiency. *J Exp Med* 165:1442-1447.

145. Ooi, Y.M., and Colten, H.R. 1979. Genetic defect in secretion of complement C5 in mice. *Nature* 282:207-208.

146. Wetsel, R.A., Fleischer, D.T., and Haviland, D.L. 1990. Deficiency of the murine fifth complement component (C5). A 2-base pair gene deletion in a 5'-exon. *J Biol Chem* 265:2435-2440.

147. Mastellos, D., Papadimitriou, J.C., Franchini, S., Tsonis, P.A., and Lambris, J.D. 2001. A novel role of complement: mice deficient in the fifth

component of complement (C5) exhibit impaired liver regeneration. *J Immunol* 166:2479-2486.

148. Lee, H.M., Wu, W., Wysoczynski, M., Liu, R., Zuba-Surma, E.K., Kucia, M., Ratajczak, J., and Ratajczak, M.Z. 2009. Impaired mobilization of hematopoietic stem/progenitor cells in C5-deficient mice supports the pivotal involvement of innate immunity in this process and reveals novel promobilization effects of granulocytes. *Leukemia* 23:2052-2062.

149. Ricklin, D., Hajishengallis, G., Yang, K., and Lambris, J.D. 2010. Complement: a key system for immune surveillance and homeostasis. *Nat Immunol* 11:785-797.

150. Ratajczak, M.Z., Lee, H., Wysoczynski, M., Wan, W., Marlicz, W., Laughlin, M.J., Kucia, M., Janowska-Wieczorek, A., and Ratajczak, J. 2010. Novel insight into stem cell mobilization-plasma sphingosine-1-phosphate is a major chemoattractant that directs the egress of hematopoietic stem progenitor cells from the bone marrow and its level in peripheral blood increases during mobilization due to activation of complement cascade/membrane attack complex. *Leukemia* 24:976-985.

151. Bhatia, M., Saluja, A.K., Singh, V.P., Frossard, J.L., Lee, H.S., Bhagat, L., Gerard, C., and Steer, M.L. 2001. Complement factor C5a exerts an anti-inflammatory effect in acute pancreatitis and associated lung injury. *Am J Physiol Gastrointest Liver Physiol* 280:G974-978.

152. Bruning, J.C., Michael, M.D., Winnay, J.N., Hayashi, T., Horsch, D., Accili, D., Goodyear, L.J., and Kahn, C.R. 1998. A muscle-specific insulin receptor knockout exhibits features of the metabolic syndrome of NIDDM without altering glucose tolerance. *Mol Cell* 2:559-569.

153. Bluher, M., Kahn, B.B., and Kahn, C.R. 2003. Extended longevity in mice lacking the insulin receptor in adipose tissue. *Science* 299:572-574.

154. Michael, M.D., Kulkarni, R.N., Postic, C., Previs, S.F., Shulman, G.I., Magnuson, M.A., and Kahn, C.R. 2000. Loss of insulin signaling in hepatocytes leads to severe insulin resistance and progressive hepatic dysfunction. *Mol Cell* 6:87-97.

155. Gerard, N.P., Hodges, M.K., Drazen, J.M., Weller, P.F., and Gerard, C. 1989. Characterization of a receptor for C5a anaphylatoxin on human eosinophils. *J Biol Chem* 264:1760-1766.

156. McCall, C.E., Bass, D.A., Cousart, S., and DeChatelet, L.R. 1979. Enhancement of hexose uptake in human polymorphonuclear leukocytes

by activated complement component C5a. *Proc Natl Acad Sci U S A* 76:5896-5900.

157. Paglialunga, S., Schrauwen, P., Roy, C., Moonen-Kornips, E., Lu, H., Hesselink, M.K., Deshaies, Y., Richard, D., and Cianflone, K. 2007. Reduced adipose tissue triglyceride synthesis and increased muscle fatty acid oxidation in C5L2 knockout mice. *J Endocrinol* 194:293-304.

158. Cui, W., Paglialunga, S., Kalant, D., Lu, H., Roy, C., Laplante, M., Deshaies, Y., and Cianflone, K. 2007. Acylation-stimulating protein/C5L2-neutralizing antibodies alter triglyceride metabolism in vitro and in vivo. *Am J Physiol Endocrinol Metab* 293:E1482-1491.

159. Flegal, K.M., Carroll, M.D., Kit, B.K., and Ogden, C.L. 2012. Prevalence of obesity and trends in the distribution of body mass index among US adults, 1999-2010. *JAMA* 307:491-497.

160. Flegal, K.M., Ogden, C.L., Yanovski, J.A., Freedman, D.S., Shepherd, J.A., Graubard, B.I., and Borrud, L.G. 2010. High adiposity and high body mass index-for-age in US children and adolescents overall and by race-ethnic group. *Am J Clin Nutr* 91:1020-1026.